Univerzita Karlova

3. lékařská fakulta

Dizertační práce

Praha, 2020 **MUDr. Matěj Patzelt**

Univerzita Karlova
3. lékařská fakulta

Dizertační práce

Zobrazování měkkých tkání pomocí mikro-CT

Imaging of Soft Tissues in Micro-CT

Školitel: Prof. MUDr. Jozef Rosina, Ph.D., MBA
Konzultant: MUDr. Jiří Kubeš, Ph.D.

Prohlášení:

Prohlašuji, že jsem závěrečnou práci zpracoval samostatně a že jsem řádně uvedl a citoval všechny použité prameny a literaturu. Současně prohlašuji, že práce nebyla využita k získání jiného nebo stejného titulu.

Souhlasím s trvalým uložením elektronické verze mé práce v databázi systému meziuniverzitního projektu Theses.cz za účelem soustavné kontroly podobnosti kvalifikačních prací. Prohlašuji, že odevzdaná tištěná verze práce a verze elektronická nahraná do Studijního informačního systému (SIS 3. LF UK) jsou totožné.

V Praze 2020 MUDr. Matěj Patzelt

Identifikační záznam:

PATZELT, Matěj. *Zobrazování měkkých tkání pomocí mikro-CT. [Imaging of Soft Tissues in Micro-CT]*. Praha, 2020. 99 stran, 5 příloh. Dizertační práce. Univerzita Karlova, 3. lékařská fakulta, Klinika plastické chirurgie 3. LF UK a FNKV, Ústav lékařské biofyziky a lékařské informatiky 3.LF UK 2020. Školitel prof. MUDr. Jozef Rosina, Ph.D., MBA.

Klíčová slova: mikro-CT, měkké tkáně, etanol, myš

Key words: micro-CT, soft tissues, ethanol, mouse

Poděkování:

Rád bych poděkoval mému školiteli prof. MUDr. Jozefu Rosinovi, Ph.D, MBA za perfektní vedení a pomoc při studiu a výzkumu.

Dále děkuji MUDr. Janě Mrzílkové, Ph.D a Ing. Janu Dudákovi, se kterými jsem výzkum prováděl ve Specializované laboratoři experimentálního zobrazování. Bez nich by žádný z prezentovaných článků a ani tato dizertační práce nevznikly.

Velký dík patří profesoru Josefu Stinglovi a doktorce Aleně Doubkové, kteří mě k vědě ve třetím ročníku studia všeobecného lékařství přivedli.

Poděkovat nesmím zapomenout také panu doktoru Vladimíru Musilovi a Ivance Žížalové.

Speciální díky náleží doktorce Lucii Zárubové, která je prý to nejlepší, co mě v životě potkalo.

Na závěr děkuji svojí rodině a přátelům za podporu během studia a hlavně během psaní této práce.

Obsah:

Úvod

Výpočetní tomografie (Computed Tomography, CT) je zobrazovací metoda, která využívá rentgenové záření k neinvazivnímu zobrazení vnitřní struktury zkoumaného objektu. Rozlišení výpočetní tomografie se pohybuje v řádech stovek mikrometrů. Největší využití CT našlo v humánní medicíně, kde v dnešní době patří mezi standardní zobrazovací vyšetření.

Mikrovýpočetní tomografie (Micro-Computed Tomography, Micro-CT, mikro-CT) pracuje na stejném principu jako klasická výpočetní tomografie. Rozdíl je v rozlišení, které je výrazně větší (v řádech jednotek mikrometru), a také ve velikosti zkoumaného objektu, která je naopak výrazně menší (v řádech jednotek centimetrů).

Mikro-CT je široce užíváno v průmyslu ke zkoumání kvality materiálů, dále také v archeologii ke studiu materiálů historických předmětů. V posledních letech si však našlo cestu i do biomedicínského výzkumu.

Mikro-CT umožňuje studium biologických vzorků s rozlišením srovnatelným s rozlišením světelného mikroskopu a to bez nutnosti prokrajování vzorků a tudíž jejich zničení. Díky této výhodě mohou být vzorky zkoumány opakovaně, v kombinaci několika různých metod. Ideálním postupem je studium makrostruktury vzorku, následně vyšetření v mikro-CT a dále např. vyšetření pomocí imunohistochemie, nebo klasické histologie pod světelným mikroskopem.

Při zobrazování předmětu v mikro-CT prochází rentgenové paprsky zkoumaným objektem a foton-senzitivní detektory následně detekují záření, které objektem prošlo. Během snímání jsou pořízeny stovky dvojrozměrných řezů z mnoha úhlů kolem objektu. Výsledkem snímání je dataset 2D řezů v jasně definovaných paralelních rovinách. Získaná data jsou uložena v počítači, kde je možné jednotlivé snímky prohlížet, dále je možné z nich vytvořit 3D rekonstrukci a provést post-produkci.

Vzhledem k principu fungování mikro-CT se nejlépe zobrazují struktury s vysokým protonovým číslem (kosti, zuby, apod.). Právě tato vlastnost je největší limitací mikro-CT při zobrazování měkkých tkání jako jsou svaly nebo nervy. Různé měkké

tkáně se v absorpci rentgenového záření příliš neliší, mají nízký vnitřní kontrast a tudíž je ve výsledném snímku nelze příliš rozlišit. Proto je nutné při zobrazování měkkých tkání v mikro-CT kontrast zvýšit. Nejjednodušší metodou je využití přirozeného kontrastu v rámci zkoumaného orgánu, například v plicích mezi dýchacími cestami a plicním parenchymem. Další možností jsou fixační činidla, jako je například jodid draselný nebo fosfowolframová kyselina. Pro zobrazení cévního řečiště je poté nutná aplikace intravaskulární kontrastní látky, nejčastěji jodu či nanočástic zlata. Žádná metoda však není dokonalá. Některé metody jsou příliš složité, jiné jsou extrémně drahé, nebo jsou pro živé tkáně naprosto nevhodné pro svoji toxicitu.

Tato komentovaná dizertační práce se zabývá problematikou zobrazení měkkých tkání v mikro-CT a klade si za cíl představit metodu zlepšení kontrastu měkkých tkání při zobrazování v mikro-CT.

1. Princip mikro-CT

Mikrovýpočetní tomografie pracuje na stejném principu jako klasická výpočetní tomografie, kterou v sedmdesátých letech dvacátého století představil Hounsfield (Hounsfield 1973; 1976; 1978). Samotné mikro-CT bylo představeno v osmdesátých letech jako reakce na potřebu zobrazování vzorků ve vyšším rozlišení (Feldkamp et al. 1984). Nynější mikro-CT jsou navržené k zobrazování objektů v řádech několika mikrometrů (Ritman 2004). K tomu je však nutné, aby zkoumaný objekt měl rozměry pouze v řádech centimetrů (Gregor et al. 2012). Základem přístroje je rentgenka, která emituje kuželovitý paprsek rentgenového záření, které pod různými úhly prochází zkoumaným objektem (Badea et al. 2008a). Fotosenzitivní detektory poté detekují záření, které nebylo absorbováno a objektem prošlo. Výsledkem je následně dataset stovek až tisíců dvojrozměrných projekcí, které jsou pomocí počítačového softwaru zpracovány a převedeny do podoby trojrozměrné tomografie, případně celého trojrozměrného objektu (Hutchinson et al. 2017b).

1.1. Rentgenové záření

Rentgenové záření je elektromagnetické ionizující záření o vlnových délkách v rozsahu 10^{-8} – 10^{-12}m. Vzniká přirozeně ve vesmíru, například z hvězd, nebo uměle v rentgenové lampě. Podle vlnové délky můžeme rentgenové záření dělit na měkké, které má nižší energii a vlnovou délku mezi 10^{-8} – 10^{-10}m, a tvrdé o vlnové délce 10^{-10} – 10^{-12}m, které má energii vyšší. Dále rentgenové záření dělíme podle vzniku na brzdné a charakteristické (Navrátil a Rosina 2019).

Brzdné rentgenové záření vzniká prudkým zabrzděním záporně nabitého elektronu, vylétajícího z katody, v okolí kladných atomových jader materiálu anody. Působením coulombických sil dochází ke změně trajektorie letu elektronů a zároveň ke snížení jejich kinetické energie. Změna kinetické energie elektronu se vyzáří ve formě fotonu rentgenového záření. Brzdné rentgenové záření má spojité spektrum, protože následkem různých interakcí elektronů s obaly atomů došlo ke ztrátě jejich energie a tudíž se do silového pole jádra se dostávají elektrony o různé energii (obr. 1). Energie brzdného záření závisí na energii letících elektronů, která je daná napětím mezi katodou a anodou v rentgenové lampě, čím vyšší je napětí, tím větší je energie rentgenového záření.

Charakteristické rentgenové záření vzniká při deexcitaci vybuzených elektronů anody do jejich původního stavu. Elektrony emitované z katody letí k anodě, na kterou dopadají, a předávají svoji energii elektronům v obalech atomů anody. Elektrony jsou díky předané energii buď excitovány, nebo ionizovány. Při sestupu elektronů do nižší energetické hladiny, ať už jako návrat excitovaného elektronu do základní hladiny, či jako zaplnění místa po chybějícím ionizovaném elektronu elektronem z vyšší energetické hladiny, dochází k vyzáření přebytečné energie ve formě fotonu rentgenového záření. Charakteristické rentgenové záření má čárové spektrum, které je dané stále stejným energetickým rozdílem mezi jednotlivými hladinami (obr. 1). Tento rozdíl určuje vlnovou délku záření, vzniká tedy pouze rentgenové záření o určitých vlnových délkách. Energie charakteristického záření závisí pouze na materiálu anody. Čím vyšší má materiál anody protonové číslo, tím je energie rentgenového záření vyšší.

Obr. 1: Energetické spektrum RTG záření

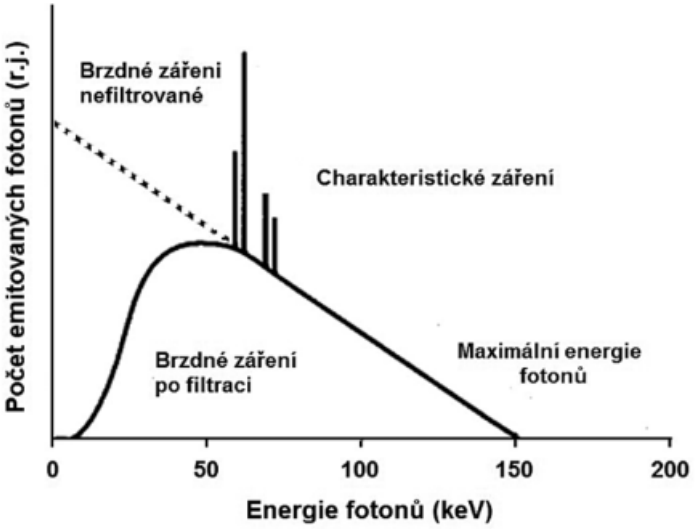

Zdroj: Navrátil a Rosina, 2019

1.2. Rentgenová lampa

Zdrojem rentgenového záření v mikro-CT je rentgenová lampa, neboli rentgenka, která je tvořená trubicí s vakuem, dále wolframovou katodou, která má tvar spirály a je zdrojem elektronů, a anodou. Anodu v mikro-CT nejčastěji tvoří terčík z wolframu s ohniskem o velikosti do 50 mikrometrů. Anoda pracuje s napětím v rozmezí 20-100 kV a proudem v rozmezí mezi 50-1000 mikroampérů (Clark a Badea 2014). Díky žhavícímu transformátoru se termoemisí uvolní z katody mrak elektronů, které jsou napětím mezi katodou a anodou přitahovány k anodě, na kterou dopadají, konkrétně na její dopadové ohnisko, které je skloněno o 10-19° ve směru letících elektronů. Díky tomuto sklonu má ploška (termické ohnisko), na kterou elektrony dopadají, tvar obdeníku, který je menší než dopadové ohnisko. Ploška, ze které vystupuje rentgenové záření, se nazývá optické ohnisko a je projekcí termického ohniska ve směru centrálního rentgenového paprsku. Centrální paprsek rentgenku opouští skrz okénko. Během tohoto procesu je anoda značně tepelně zatížená, a proto musí být náležitě chlazena. Anoda v mikro-CT je běžně chlazená vzduchem.

Obr. 2: Rentgenová lampa (A-anoda, K-katoda, O-okénko, CP-centrální paprsek, OO-optické okénko, TO-termické okénko)

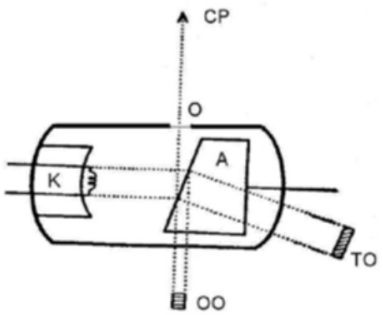

Zdroj: Navrátil a Rosina, 2019

1.3. Detektor

Klíčovou součástkou mikro-CT je detektor, který může být v současnosti dvojího typu.

Prvním, starším a více používaným typem, jsou detektory CCDs (Charge-Coupled Devices) a CMOS (Complementary Metal Oxide Semiconductor). Jedná se o scintilační detektory, které konvertují dopadající rentgenové záření na viditelné světlo, které je v polovodičové diodě následně transformováno na elektrický signál. Tento elektrický signál je úměrný celkové energii všech absorbovaných fotonů, proto jsou také zatížené vznikem velkého množství šumu, nicméně hlavním omezením je, že nedokážou určit jednotlivé vlnové délky rentgenového záření, které na ně dopadlo (Ritman 2004; Kim et al. 2013; Clark a Badea 2014).

Obr. 3 Schéma scintilačního detektoru

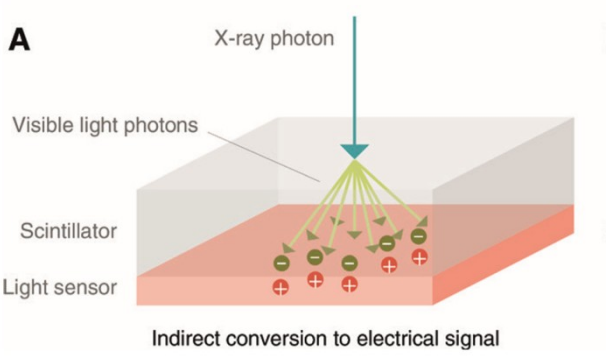

Zdroj: Willemink et al., 2018

Druhým typem detektorů jsou spektrální detektory PCXD (Photon Counting X-ray Detectors). Jedná se o přímé detektory, které mění ionizující záření přímo na elektrický signál. Principem je interakce dopadajícího fotonu ionizujícího záření na detekční element. Detektory jsou tedy schopné určit počet dopadajících fotonů za určitý časový interval. Výhodou těchto detektorů je redukce šumu a schopnost určit jednotlivé vlnové délky dopadajícího ionizujícího záření. Díky schopnosti odlišit jednotlivá kvanta dopadajícího záření dokážou tyto detektory přesněji určit vlastnosti

materiálu, kterým záření prošlo. Nevýhodou zůstává cena detektorů a také jejich omezená velikost (Ren et al. 2018; Dudak et al. 2015; Willemink et al. 2018).

Obr. 3 Schéma Photon-Counting detektoru

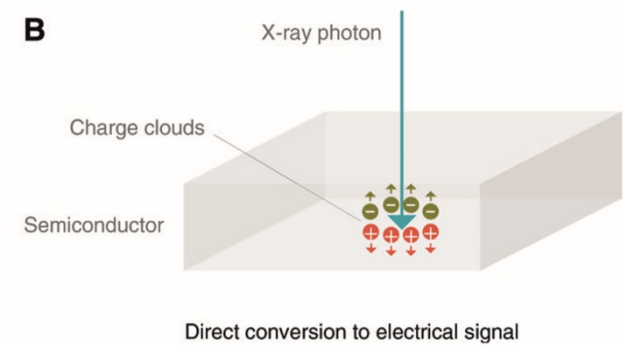

Zdroj: Willemink et al., 2018

1.4. Konstrukce mikro-CT

V současnosti existují dva typy konstrukce či geometrie pro systémy mikro-CT, a to buď systém s rotujícím vzorkem, nebo systém s rotující gantry.

První typ je široce využíván v systémech pro zobrazování ex-vivo vzorků, kde je gantry stacionární a vzorek rotuje kolem vlastní osy. Tento typ je nevhodný pro studium živých objektů, hlavně kvůli vertikálnímu uložení zkoumaného vzorku. Naopak u tohoto typu je jednodušší změnit vzdálenost vzorku od rentgenky a tím docílit změny zvětšení (Schambach et al. 2010).

Obr. 4 Schéma konstrukce mikro-CT se systémem rotujícího vzorku

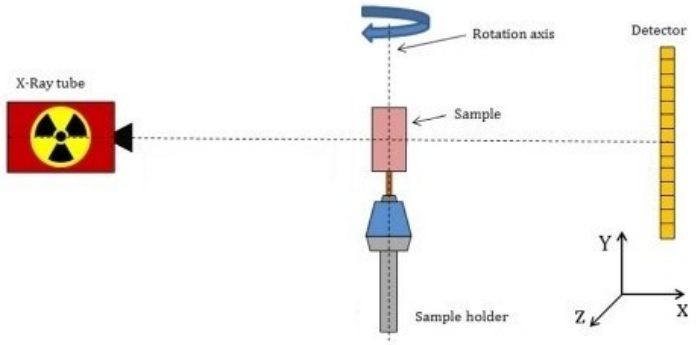

Zdroj: Autorem upravený obrázek z publikace Dudak et al., 2014

Druhý typ je využíván pro studium vzorků in-vivo, kde gantry rotuje kolem centrální osy, zatímco vzorek je stacionárně uložený mezi rentgenkou a detektorem. Tento typ je vhodný pro studium zvířat, která jsou umístěna v horizontální pozici. Změna zvětšení je v tomto případě složitější kvůli změně geometrie v gantry (Badea et al. 2005).

Obr. 5 Schéma konstrukce mikro-CT se systémem rotující gantry

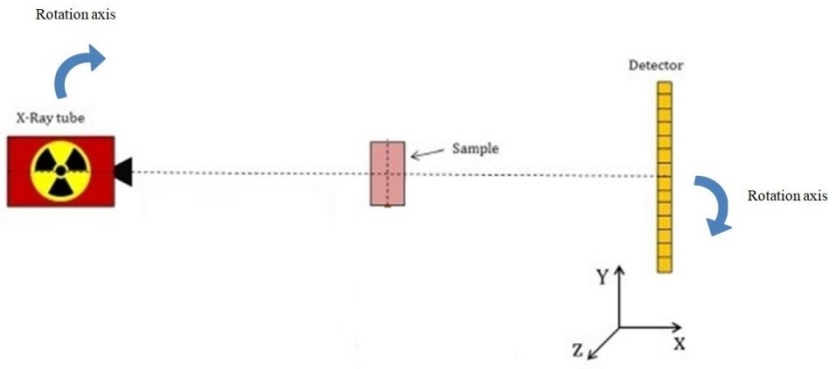

Zdroj: Autorem upravený obrázek z publikace Dudak et al., 2014

2. Přehled problematiky

Mikro-CT se záhy po svém uvedení začalo používat v průmyslu pro kontrolu kvality vyrobených materiálů. Jedná se hlavně o detekci mikrotrhlin, výpočtu porózity materiálů nebo analýzu polymerů (du Plessis et al. 2016; 2015; Maire a Withers 2014; Salvo et al. 2003). Dále si tato technologie našla cestu i do archeologie k nedestruktivní analýze vnitřní struktury artefaktů či k detekci vrstev nátěru na historických obrazech (SÉGuin 1990; Doi et al. 2013).

Nejširší využití však mikro-CT našlo v biomedicínském výzkumu. Vzhledem k principu technologie začal výzkum u mineralizovaných tkání – kostí a zubů. U těchto vzorků není třeba použít žádné kontrastní látky a je tedy možné je snímat nativně. Práce se zabývají hlavně anatomií kostí, hustotou kostní hmoty, remodelací a regenerací kostí, případně se soustřeďují na osteoporózu a léčbu fraktur (Chou et al. 2007; Kapadia et al. 1998; Ding et al. 1999; O'Neill et al. 2012; Borah et al. 2001). Ve výzkumu zubů je mikro-CT využíváno ještě více. Jedná se hlavně o výzkum zubních implantátů, zubních kanálků, vývoje zubů či zobrazení poruch alveolárního výběžku (Hutchinson et al. 2017a; Nakashima et al. 2018; Rani et al. 2018; Swain a Xue 2009).

Další výzkum se poté posunul k zobrazování vnitřních orgánů, a to ex-vivo i in-vivo.

Zobrazení měkkých tkání jakými jsou svaly, cévy, tuk nebo nervová tkáň v mikro-CT je však obtížné, protože na rozdíl od kostí či zubů, jsou složeny z prvků s nízkým atomovým číslem, a tudíž málo pohlcují rentgenové záření. Navíc rozdíl v míře pohlcování rentgenového záření je mezi jednotlivými strukturami měkkých tkání minimální a ve výsledných snímcích mezi nimi není dostatečný kontrast. Mají takzvaně nízký vnitřní kontrast. Proto je nutné pro jejich zobrazení použít kontrastní látky, a to buď ex-vivo, kdy je vzorek do kontrastní látky ponořen, nebo in-vivo, kdy je kontrastní látka vstříknuta do cévního systému experimentálního zvířete, nejčastěji laboratorní myši.

Kontrastní látky pro použití v mikro-CT jsou vyvíjeny od počátku využívání této technologie. Liší se různou afinitou k různým tkáním, různými metodami rozpouštění, cenou, toxicitou nebo také dobou nutné expozice a eliminace

(Descamps et al. 2014). Bez rozdílu zkoumané měkké tkáně by měla být ideální kontrastní látka snadno použitelná, dostupná a měla by rovnoměrně pronikat i tlustými vrstvami tkáně (Pauwels et al. 2013).

Nejpoužívanější kontrastní látky vychází z anorganického jodového základu, patří sem hlavně Lugolův roztok (I_2KI), který se velmi dobře váže na svalová vlákna a pojivové tkáně, dále pak nízkoosmolární Omnipaque™ (iohexol), která se využívá v humánní medicíně, nebo jód rozpuštěný v etanolu či metanolu (Gignac a Kley 2014; Jeffery et al. 2011). Další skupinou kontrastních látek jsou fosfowolframová kyselina a fosfomolybdenová kyselina, které v současnosti patří mezi nejpoužívanější kontrastní látky v pre-klinickém výzkumu (Mizutani a Suzuki 2012). Fosfowolframová kyselina je snadno dostupné a minimálně toxické činidlo, které však velmi pomalu penetruje tkáněmi. Pro dostatečnou penetraci vzorku, který má tloušťku 2-3mm je nutná inkubace minimálně přes noc (Chaffey 2001; Metscher 2009a). Fosfomolybdenová kyselina, která také pomalu penetruje tkáněmi, je málo toxická sloučenina, která výborně zvyšuje kontrast měkkých tkání, nicméně doba fixace se počítá na dny, až týdny. Nevýhodou těchto kyselin je značná změna objemu fixovaných vzorků, kdy dochází ke značnému zmenšování, a také jejich protokol fixace, který je složitý a vyžaduje zkušeného laboratorního pracovníka (Descamps et al. 2014; Balint et al. 2016).

Vysoce účinnými kontrastními látkami jsou také osmium tetraoxid a chlorid rtuťnatý, které jsou však vysoce toxické. Osmium tetraoxid je konvenční fixační činidlo pro elektronovou mikroskopii, principem fixace je navázání osmia na membránové lipidy buněk, avšak bez určité specifity. Je to navíc velice drahé činidlo, které špatně penetruje tkáněmi a nelze použít u vzorků, které byly fixovány v jakémkoliv alkoholovém roztoku (Johnson et al. 2006; Metscher 2009a; 2009b; Mizutani a Suzuki 2012).

Mezi intravaskulární kontrastní látky patří hlavně již zmíněné jodové látky, jako jsou Omnipaque™ či Fenestra™, které jsou však pro využití na zvířecím modelu nevhodné, protože v cévním systému cirkulují v dostatečné koncentraci pouze v řádech sekund až minut. Například v případě laboratorních myší jsou z cévního systému odvedeny v průběhu sekund (Lin et al. 2008). Další skupinou jsou intravaskulární kontrastní látky založené na nanočásticích kovů, například zlata nebo

bismutu. Mezi nejvyužívanější patři Aurovist™, který obsahuje nanočástice zlata, jeho velkou výhodou je schopnost projít celým kapilárním řečištěm ve velmi vysoké koncentraci, navíc zlato výborně pohlcuje rentgenové paprsky a tudíž jsou, i ze zkušenosti autora, výsledné angiografie vysoce detailní a přesné. Oproti jodovým kontrastním látkám je jeho retence v cévním systému laboratorních zvířat v řádech hodin až desítek hodin. Nevýhodou této kontrastní látky je jednak cena (Willekens et al. 2009), ale i výrazné potlačení signálu z ostatních tkání, tudíž nelze zkoumat cévní systém v topografických souvislostech. Všechny tyto látky jsou primárně určeny pro in-vivo studium cévního systému.

Cévní systém je možné v mikro-CT také zobrazit ex-vivo, a to pomocí pryskyřic a silikonů. Nejvhodnějším zástupcem je silikon Microfil™, který obsahuje částice olova. Microfil™ má nízkou viskozitu a volně prochází celým cévním systémem. Díky svým hydrofobním vlastnostem neprochází z cév do tkání (Ghanavati et al. 2014; Kwon et al. 1998a; 1998b; Bentley et al. 2002; Zagorchev et al. 2010). Díky obsahu olova jsou cévy dobře viditelné, nicméně jejich signál následně potlačuje zobrazení ostatních struktur. Alternativou je poté Neoprene latex™, který má obdobné vlastnosti, ale neobsahuje olovo (Oses et al. 2009). Při použití pryskyřice Biodur™ či Mercox™ je možné provést nástřik cévního systému zkoumaného vzorku a následně vytvořit korozivní preparát. Tento odlitek cévního systému je poté možné zkoumat v mikro-CT (Jirik et al. 2016). Nevýhodou je samozřejmě zničení původního vzorku.

Aplikace kontrastních látek je nyní nejvíce využívaná ve výzkumu kardiovaskulárního systému. Degenhardt a Wong studují vývoj kardiovaskulárního systému na myších embryích (Degenhardt et al. 2010; Wong et al. 2013). U dospělých jedinců se nejčastěji zkoumá ateroskleróza koronárních i periferních tepen – její rozvoj i léčebné možnosti (Clauss et al. 2006). Výzkum samotného srdce je závislý na gatovacím systému, kdy skenování probíhá v cyklech podle EKG. Díky kardio mikro-CT je možné sledovat ejekční frakci, jednotlivé objemy srdečních oddílů i jednotlivých cyklů, dále je možné zobrazit papilární svaly i remodelaci srdeční svaloviny po infarktu myokardu (Badea et al. 2005; Detombe et al. 2008; Drangova et al. 2007; Nahrendorf et al. 2007; Badea et al. 2008b). Výzkum cévního systému je realizován hlavně in-vivo vstříknutím kontrastní látky, od zkoumání ex-

vivo pomocí korozivních preparátů, které vznikají nástřikem cévního systému polymerem, např. Biodur™ nebo Microfil™, se již upouští (Clauss et al. 2006; Ghanavati et al. 2014).

Výzkum plic je v mnohém jednodušší než u ostatních měkkých tkání, protože lze využít přirozeného kontrastu mezi vzduchem v plicích a okolní tkání. Naopak in-vivo zobrazování plic je mnohem náročnější kvůli vysoké frekvenci dýchacích pohybů laboratorní myši. Když pomineme studium cévního systému plic, tak se výzkum soustředí hlavně na animální modely onemocnění plic, jako je emfyzém, plicní fibróza, chronická obstrukční plicní nemoc nebo tumory plic. Mikro-CT je zde vhodnou modalitou pro dlouhodobé studium vývoje onemocnění (Gammon et al. 2014; Vande Velde et al. 2016; Shofer et al. 2007; Ford et al. 2020). Parameswaran používá impregnaci stříbrem, aby zobrazil alveoly a jejich tenkou stěnu, následně tak kvantifikoval dechový objem alveolů (Parameswaran et al. 2009). Zajímavostí je použití Xenonu jako in-vivo inhalační kontrastní látky k zobrazení vnitřní struktury plic hlodavců (Lam et al. 2007). Plíce jsou také zkoumané z hlediska srovnání s klasickou histologií, kdy se zavedl nový termín – virtuální histologie. Díky dobře zvolené kontrastní látce, nejčastěji se jedná o fosfomolybdenovou kyselinu, a metodě fázového kontrastu snímání v mikro-CT se daří dosáhnout zobrazení přesnějších anatomických struktur než u konvenční histologie (Albers et al. 2018).

V současné době se výzkum centrálního nervového systému (CNS) těší velké popularitě. Pro samotné zobrazení struktur CNS se běžně používá magnetická rezonance (MRI), případně mikro-magnetická rezonance (mikro-MRI) (Kovacevic et al. 2005). Její výhoda spočívá v mnohem lepším rozlišení bílé a šedé hmoty mozkové, nicméně i mikro-CT nachází v tomto odvětví výzkumu své uplatnění, a to zejména díky větší dostupnosti a nižší pořizovací ceně i provozním nákladům. Nejčastěji se jedná o studium tumorů mozku na animálních modelech, hlavně gliomů (Engelhorn et al. 2009; de Crespigny et al. 2008). 3D zobrazení zdravého mozku animálního modelu provádí například Zikmund (Zikmund et al. 2018) nebo Takeda (Takeda et al. 2013). Tomografické řezy mozkem myši porovnává s histologickými řezy Saito (Saito a Murase 2012). Další studie se zaměřují na detekci ischémie v mozku animálního modelu (Erjavec 2013; Hayasaka et al. 2012). Řezy lidského mozku fixovaného v 10% formaldehydu zkoumá Mizutani. Podařilo se mu zobrazit

kapilární síť a také pyramidovou vrstvu neokortexu (Mizutani et al. 2008). Girard a Choi využívají mikro-CT ke zkoumání cévní mozkové malformace na animálním modelu (Girard et al. 2016; Choi et al. 2017). Mikro-CT se také využívá pro výzkum v oblasti periferního nervového systému, například Hopkins studoval regeneraci periferních nervů na animálním modelu na titanových bioimplantabilních vodičích. Následně v mikro-CT analyzoval růst poraněných periferních nervů podél těchto vodičů (Hopkins et al. 2015).

Zobrazení parenchymatózních orgánů jako jsou ledviny, játra nebo slezina se stalo rutinní záležitostí. Shirai například zobrazuje vnitřní strukturu myších ledvin fixovaných v etanolu za použití snímání pomocí fázového kontrastu (Shirai et al. 2014). Perrien zase pomocí microfilu zkoumá volumometrii cévního systému ledviny myši (Perrien et al. 2016). Missbach-Guenter se zabývají výše popsanou virtuální histologií pomocí mikro-CT, kdy myší ledviny fixují ve fosfowolframové kyselině a vytvářejí sérii řezů, která svou kvalitou snese srovnání s konvenční histologií (Missbach-Guentner et al. 2018).

Kromě kontrastních látek je možné zlepšit zobrazení měkkých tkání v mikro-CT také pomocí metody fázového kontrastu. Rentgenové záření je elektromagnetické vlnění, u kterého při průchodu zkoumaným objektem dochází ke změně jeho amplitudy a k fázovému posunu vlnění. A právě tento fázový posun můžeme detektovat a následně vyhodnocovat. Fázový posun má až 1000x větší senzitivitu než absorpce rentgenového záření nízkoprotonovými prvky (Takeda et al. 2013; 1995; 2000).

Kromě laboratorního a pre-klinického výzkum se mikro-CT také využívá v klinickém výzkumu. V ortopedii se například zkoumají explantované jamky z náhrad ramenního kloubu, kde se sleduje oděr materiálu (Kurdziel et al. 2018). Zubní lékařství využívá mikro-CT ke zhodnocení kvality kostí pro implantaci zubních implantátů (Vasconcelos et al. 2016). V chirurgii prsní žlázy se testuje zavedení mikro-CT k peroperačnímu zhodnocení tumorů po prs záchovných operacích (Sarraj et al. 2015; Tang et al. 2013; 2016). V soudním lékařství našlo využití v zobrazení střelných a bodných ran (Rutty et al. 2013; Fais et al. 2015). Možnosti využití mikro-CT v klinické praxi se s klesající cenou přístroje a naopak se zvyšujícím rozlišením a dostupností kontrastních látek neustále rozšiřují.

3. Cíle dizertační práce

Cílem dizertační práce je vytvořit levnou a jednoduchou metodu ex-vivo fixace měkkých tkání pro zobrazení v modifikovaném mikro-CT MARS (Medipix All Resolution System).

Jednotlivé dílčí cíle jsou následující:

1. modifikovat přístroj mikro-CT MARS
2. porovnat různé typy fixace srdce a plic animálního modelu v etanolu jako kontrastního činidla pro zobrazení v mikro-CT
3. zobrazit vnitřní strukturu zdravého mozku animálního modelu fixovaného ex-vivo v etanolu v mikro-CT a popsat zobrazené struktury

4. Metodika

4.1. Modifikovaný mikro-CT přístroj MARS

Výzkum byl prováděn na přístroji mikro-CT Medipix All Resolution System (MARS), který byl vyvinut Univerzitou v Canterbury na Novém Zélandu. Pro potřeby výzkumu byl však přístroj výrazně modifikován.

Konstrukce přístroje zůstala stejná, jedná se o typ, kde jsou detektor a rentgenka umístěny v jedné gantry, která rotuje kolem stacionárního vzorku.

Původní rentgenka byla nahrazena rentgenovou lampou KEVEX^{TM} PXS-11 s provozním napětím 40-70 kV a s 30 μm ohniskem.

Mikro-CT bylo osazeno novým PCXD detektorem Timepix Quad s rozměry 2,8 x 2,8 cm, který je složen ze čtyř čipů o celkové ploše 512 x 512 pixelů. Takto modifikované mikro-CT dosahuje prostorového rozlišení 30 μm.

Konstrukce gantry umožňuje snímat objekty, které jsou v dlouhé ose delší než 2,8 cm a to tím, že se vzorek snímá např. ve třech sub-akvizicích, kdy se vzorek posune o délku detektoru a výsledné sub-akvizice se poté spojí do jednoho snímku.

Zvětšení je realizováno změnou vzdálenosti rentgenky od vzorku a dosahuje od 1,25 k 2x zvětšení.

Přístroj je schopný pořizovat jednak tomografie s následnou 3D rekonstrukcí, ale také takzvané mikroradiografie. Jedná se o 2D sumační projekci, jejíchž pořízení trvá v řádech sekund. Mikroradiografie je vhodná jako prvotní sken zkoumaného objektu k určení například oblasti zájmu (Region of Interest, ROI).

Obr. 6 Fotografie modifikovaného mikro-CT MARS

Zdroj: Dudak et al., 2014

4.2. Skladba dizertační práce

Dizertační práce vychází z pěti publikovaných impaktovaných monotematicky zaměřených publikací. První tři publikace jsou technického rázu a vznikly pod „taktovkou“ inženýrů z Ústavu technické a experimentální fyziky, České vysoké učení technické (ÚTEF ČVUT) v Praze a Fakulty biomedicínského inženýrství, České vysoké učení technické (FBMI ČVUT).

Zbylé dvě publikace se zabývají zkoumáním biologických vzorků a vznikly primárně pod vedením pracovníků 3. lékařské fakulty Univerzity Karlovy (3. LF UK).

Výsledkem úzké spolupráce lékařů a inženýrů je soubor vědeckých prací, které zahrnují modifikaci původního mikro-CT přístroje, vývoj držáků pro vzorky a následně výzkum a vývoj nových protokolů pro zobrazování měkkých tkání v mikro-CT.

5. Publikace

Kapitola shrnuje pět impaktovaných publikací, na kterých autor pracoval a je uveden jako spoluautor, nebo je prvním autorem. Ke každé publikaci je sepsán komentář shrnující klíčové body publikace. Originály článků jsou přiloženy.

5.1. X-ray micro-CT scanner for small animal imaging based on Timepix detector technology

Citace: DUDÁK, Jan; ŽEMLIČKA, Jan; KREJČÍ, František; POLANSKÝ, Štěpán; JAKUBEK, Jan; MRZÍLKOVÁ, Jana; **PATZELT, Matěj;** TRNKA, Jan. X-ray micro-CT scanner for small animal imaging based on Timepix detector technology. *Nuclear Instruments & Methods in Physics Research Section A - Accelerators Spectrometers Detectors and Associated Equipment*. 2015, **774**(11), 81-86. ISSN 0168-9002. DOI: 10.1016/j.nima.2014.10.076. **IF: 1.316/2013**.

5.1.1. Úvod a metodika

Cílem publikace bylo přepracovat a upravit originální mikro-CT MARS a vybavit ho detektorem Timepix Quad a otestovat jeho schopnost snímat a zobrazit měkké tkáně. Původní mikro-CT MARS bylo nově osazeno rentgenkou KEVEX^{TM} PXS-11 s provozním napětím 40-70 kV a s 30 μm ohniskem a polovodičovým photon counting (foton-počítajícím) detektorem Timepix Quad s rozměry 2,8 x 2,8cm, který je složen ze čtyř čipů o celkové ploše 512 x 512 pixelů. Systém byl otestovaný na plastovém fantomu, který simuloval měkké tkáně, skládal se ze čtyř dutin, první byla naplněna vodou, ta simulovala svalovou tkáň, další byla naplněná voskem, pro simulaci nervové tkáně, třetí byla naplněná olejem, který simuloval tukovou tkáň, čtvrtá byla naplněná vzduchem. Poté byl přístroj testován na reálných vzorcích, a to na vzorku hlavy hada a na čili papričce. V rámci studie byly zavedeny dva typy snímání. Prvním byla takzvaná mikroradiografie, což je prostý 2D snímek. Vzniká jako sumační snímek z jedné projekce. Jedná se o velice rychlé snímání, které umožňuje rychlou inspekci daného objektu a následně rozhodnutí o oblasti zájmu pro

druhý typ snímání – tomografii s následnou 3D rekonstrukcí, která je časově mnohem náročnější.

5.1.2. Výsledky, diskuze a závěr

Úspěšně se podařilo přebudovat mikro-CT MARS a osadit ho novými komponenty, zejména foton-počítajícím detektorem Timepix. Takto sestavené mikro-CT disponuje rozlišením cca 30 μm. Přístroj byl následně úspěšně otestován pro zobrazování měkkých tkání, nejdříve na fantomu a poté na reálných měkkých tkáních. Nevýhodou modifikovaného mikro-CT MARS jsou malé rozměry Timepix Quad detektoru. Pro velké vzorky, které rozměry přesahují rozměry detektoru, byl proto vytvořen systém, kdy gantry umožňuje posunutí vzorku o rozměr detektoru. Vzorek je tak snímán postupně v několika subakvizicích, které jsou následně spojeny v jeden objekt. Tento přístup lze aplikovat při vytváření 2D snímků (mikroradiografií), tak i u klasických tomografií.

Nuclear Instruments and Methods in Physics Research A 773 (2015) 81–86

Contents lists available at ScienceDirect

Nuclear Instruments and Methods in Physics Research A

journal homepage: www.elsevier.com/locate/nima

X-ray micro-CT scanner for small animal imaging based on Timepix detector technology

Jan Dudak [a,b,*], Jan Zemlicka [a], Frantisek Krejci [a], Stepan Polansky [a], Jan Jakubek [a], Jana Mrzilkova [c], Matej Patzelt [c], Jan Trnka [c]

[a] Institute of Experimental and Applied Physics, Czech Technical University in Prague, Horska 3a/22, 128 00 Prague 2, Czech Republic
[b] Faculty of Biomedical Engineering, Czech Technical University in Prague, Nam. Sitna 3105, 272 00 Kladno, Czech Republic
[c] Third Faculty of Medicine, Charles University in Prague, Ruska 87, 100 00 Prague, Czech Republic

ARTICLE INFO

Article history:
Received 7 August 2014
Received in revised form
23 October 2014
Accepted 29 October 2014
Available online 13 November 2014

Keywords:
Computerized tomography
Hybrid detector
Timepix
Small animal imaging

ABSTRACT

We describe a newly developed compact micro-CT scanner with rotating gantry equipped with a Timepix Quad hybrid pixel semiconductor detector and a micro-focus X-ray tube providing spatial resolution down to 30 μm. The resolving power of the device in relation to soft tissue sensitivity is demonstrated using a tissue-equivalent phantom and different types of biological samples. The results demonstrate that the use of noiseless particle counting detectors is a promising way to achieve sufficient soft tissue contrast even without any contrast agents.

1. Introduction

X-ray radiography is a noninvasive imaging technique for visualization of internal structures of investigated samples. The technique utilizes intensity changes of X-ray beam transmitted through the sample detected by an appropriate detecting unit. Using a large set of projections acquired at different angles and dedicated mathematical algorithms, it is furthermore possible to produce a 3D voxel-based model of the scanned sample (computed tomography) [1].

The main limitation of conventional X-ray micro-radiography and computed micro-tomography is poor soft tissue contrast caused by low X-ray attenuation and low intrinsic contrast of investigated structures. This limitation is conventionally solved by the use of contrast agents improving visibility of treated anatomical structures. The other possibility is based on the use of a new generation of noiseless particle counting detectors.

The highest spatial resolution and contrast is provided by synchrotron radiation [2], but it requires large scale instrumentation and preparation. On the other hand, table top systems based on X-ray tubes provide wide, easy and cost-effective access and therefore their use is much more common. Modern high-quality micro- and nano-focus X-ray tubes enable measurement with high contrast and spatial resolution at micrometer scale in table-top laboratory-based systems [3–5]. The availability of compact X-ray micro-CT systems has consequently enabled greater applications in different fields such as medicine, biology, aerospace, cultural heritage, geology, etc.

1.1. Limitations of current X-ray imaging systems

X-ray imaging techniques are routinely used for imaging of high density structures with significant X-ray attenuation. In the case of low density materials such as biological soft tissue, however, effective visualization with X-rays is complicated due to low absorption and low intrinsic contrast of investigated structures [3]. This fact significantly limits the applicability of X-ray radiography in biology and biomedical research, because the technique can provide sufficient image quality just for skeletal topology. For reliable visualization of soft tissue, the application of a contrast agent with affinity to selected structures is consequently necessary [5–7]. Even though this approach can improve visualization of various organ structures, the application of contrast agents is in many cases connected with undesirable effects (e.g. toxicity) and often is not compatible with in-vivo imaging [6]. Therefore the improvement of imaging capabilities of existing technique remains a major instrumental challenge.

* Corresponding author at: Institute of Experimental and Applied Physics, Czech Technical University in Prague, Horska 3a/22, 128 00 Prague 2, Czech Republic. Tel.: +420 224 359 179.
E-mail address: jan.dudak@utef.cvut.cz (J. Dudak).

http://dx.doi.org/10.1016/j.nima.2014.10.076
0168-9002/

1.2. High-contrast radiography with counting detectors

A feasible way to overcome low intrinsic contrast of soft tissue structures is the use of photon counting pixel devices such as the hybrid semiconductor detectors Medipix [8]. The detectors work in noise-free particle counting mode, enabling complete suppression of noise (dark-current, leakage currents, read-out noise, etc.), which is a limiting factor for dynamic range of conventional imaging devices such as CCD and flat panels. As a result, particle counting detectors provide virtually unlimited dynamic range (in practice limited just by the number of detected particles) [9]. The other significant advantage of noiseless quantum-counting detectors in relation to soft tissue contrast is the use of direct-conversion sensor materials with peak sensitivity for low X-ray energies (3–35 keV range for 300 μm thick silicon sensors). These important features make hybrid semiconductor detectors a powerful tool for detecting even subtle changes in the intensity of radiation transmitted through faintly absorbing materials [9].

In this paper, we present the performance of a newly assembled micro-CT scanner for small animal imaging equipped with the hybrid semiconductor pixel detector Timepix. The system is based on the mechanics with a rotating gantry of the MARS CT system [10] but newly equipped with a micro-focus X-ray tube and a Timepix Quad detector [11]. For the newly assembled system, a dedicated control, acquisition and CT reconstruction software was also developed. The CT-system was tested in terms of spatial resolution and soft tissue contrast using a tissue equivalent phantom and different types of biological samples.

2. Materials and methods

2.1. Original MARS scanner

The mechanics of presented device is based on the original MARS CT System design (Medipix All Resolution System developed by the University of Canterbury, New Zealand [10]). The gantry is built in the same way as that of conventional medical CTs utilizing a rotating gantry holding the X-ray tube and the detector and a separate fixed sample holder mounted in the gantry's central axis (see Figs. 1 and 2). The gantry construction allows changing fluently geometrical magnification of the imaging system within the range from 1.25 to 2 (see Fig. 1). The original system was equipped with a conventional X-ray tube with a reflecting anode providing high intensity output required for fast scanning of biological samples. On the other hand, the spatial resolution provided by that configuration was 53 μm and 204 μm in horizontal and vertical direction, respectively (resolution given in FWHM of the Edge response function, measured with magnification factor of 2). Inconvenient resolution anisotropy due to an ellipsoidal shape of the X-ray spot together with its large size therefore significantly limited the imaging performance for small-animal imaging.

2.2. Redesigned system

To improve the imaging performance of the CT system, the original X-ray tube was replaced by a new micro-focus X-ray tube KEVEX^{TM} PXS-11 (operating voltage 40–70 kV) characterized by a 30 μm focal spot (FWHM) at 70 kV. This replacement enables fully utilizing the high granularity of pixel detectors (55 pixel pitch in the case of the used Timepix detector).

As an imager we have installed a Timepix Quad detector [8]. The detector consists of four Timepix read-out chips bump-bonded to a single common sensor (300 μm silicon) read out by an array of 512 by 512 pixels of full dimensions 2.8 cm × 2.8 cm and total sensitive area of 7.84 cm^2. The Timepix detector can be operated as a photon counter or as a fully spectroscopic device. The spectroscopic mode (TOT mode – Time over threshold) opens possibility of using the technique of energy sensitive radiography [12]. In the assembled system, the detector communicates with the PC via a newly installed FITPix interface [13] and it is controlled by the Pixelman software [14]. For remote operation of stepper motors, a dedicated Java plugin for Pixelman was developed. The application of this in-house developed read-out electronics and software enables full control over the detector settings (equalization procedures, DACs control) and data acquisition including advanced scripting tools for various scanning regimes. The application of the Pixelman software furthermore enables also direct application of previously developed tools, e.g. for beam hardening effect correction [15] and tomographic reconstruction.

Another important reason for switching from the original MARS Medipix3 camera to the newly installed Timepix-based imager is also exploiting the newly developed technology for construction of a large-area hybrid pixel detector with full area sensitivity (the architecture is based on Timepix chips) [16]. The sensitive area of a Medpix3 MARS camera is limited by the QUAD configuration utilizing 2 × 2 chips. The field of view provided by this detector configuration is in many cases not satisfactory for tomographic measurement of larger biological samples. Especially if a magnifying geometry is used, mechanical shift of detector

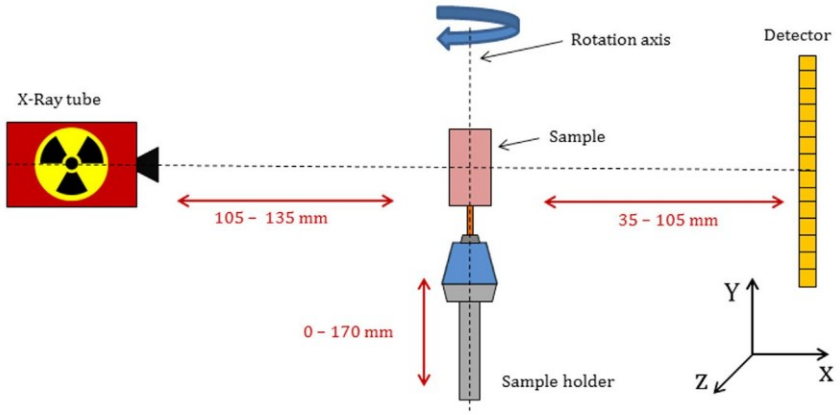

Fig. 1. Schematic drawing of the imaging geometry of the presented system showing the adjustability and ranges of various system components. Besides the indicated movements, the detector can be translated in the *Z* axis (perpendicular to the scheme plane) enabling acquiring of radiograms and CT scans of samples larger than the sensitive area of the detector.

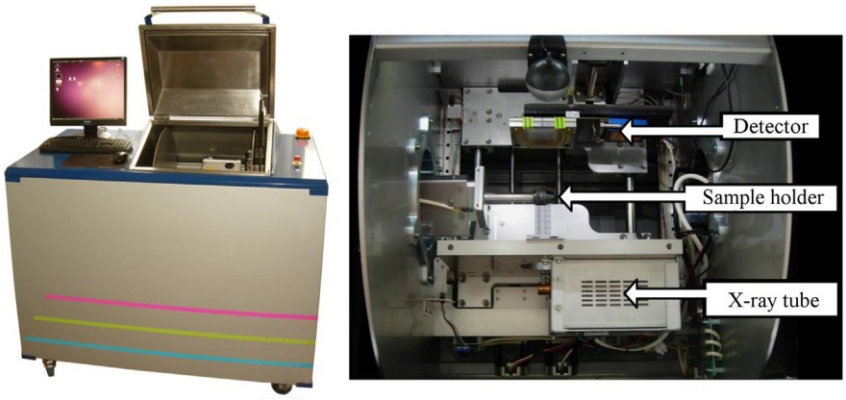

Fig. 2. Redesigned MARS CT scanner with opened gantry (left), detailed view of the gantry with the new micro-focus X-ray tube KEVEXTM PXS-11 and the Timepix Quad detector newly installed (right).

during measurement is consequently necessary. The replacement with Timepix detector technology therefore provides the possibility to enlarge the field-of view in the new micro-CT system.

2.3. Data acquisition and processing

The new system is capable of acquiring high quality 2D radiographic projections as well as a full tomographic dataset with enhanced soft tissue contrast. Before further processing, a beam hardening correction is applied to the data [15]. The BH correction transforms the image information from signal/intensity to signal/thickness dependence. The result of BH correction is the linearization of the acquired information and reduction of inaccuracy caused by different responses of individual pixels to the radiation. After application of the BH correction the following particular processing depends on the data type (tomographic reconstruction, merging tiles).

2.3.1. 2D projection micro-radiography

While the 3D voxel model provides more complex information about investigated object, the 2D projection imaging has many advantages with practical simplicity. Acquisition of a single radiographic projection is in comparison with the computed tomography much simpler, faster and therefore suitable for a first rapid inspection of sample. In the case of some purely soft tissue samples it is very difficult to measure a tomographic dataset because of the sample instability and therefore the fast projection is the only practical way of radiographic imaging.

In single projection mode the unique features of the Timepix detector (unlimited dynamic range, noise-free operation) are highly helpful. The acquisition time is limited only by the stability of the sample and required contrast. Conventional acquisition time for sufficient image statistics is within the range from a few seconds to tens of seconds.

Moreover the gantry construction allows imaging of oversized samples by scanning with the detector producing multiple sub-acquisitions of the sample. Obtained sub-acquisitions are latermerged in a single image. This approach significantly increases the effective field of view of the imaging system. Fig. 3 presents two X-ray projections of a juvenile python head acquired at different angles with magnification factor of 2 acquired in six sub-acquisitions providing an effective area of the detector 970 by 1250 pixels (X-ray tube settings: 60 kV, 90 μA, 20 s per sub-acquisition).

Fig. 3. X-ray radiography of a head of a newborn python (*Python molurus bivittatus*) fixed in ethanol. Both projection images were assembled from six sub-acquisitions for total resolution of 970×1250 pixels and full sensitive area $5.3 \times 9.8\ \mathrm{cm}^2$. Nonlinear intensity transfer function is used to further enhance the image contrast.

2.3.2. Computed micro-tomography

Typical dataset for a tomography consists of 180 projections acquired with discrete 1° steps. Acquisition time is 5–10 s per each projection, giving a total acquisition time 15–30 min. In the case of larger samples exceeding the detector size, multiple sub-acquisition operation mode is also possible for tomographic measurements.

After data preprocessing the tomographic reconstruction is computed using an in-house developed OSEM (ordered subsets estimation maximization) based iterative algorithm implemented with parallel beam geometry. Even though, our algorithm was originally designed to be used with small field of view given by a single Medipix chip ($14 \times 14\ \mathrm{mm}^2$) and long source-to-detector distance (SSD), sufficient results can be achieved also for geometry of the presented device. The beam convergence of the CT devices caused by the larger size of the used detector and short SDD (140–240 mm, see Fig. 1) will be taken into account in the upcoming version of the reconstruction software which is under development.

The reconstructed 3D model is then visualized using false colors to highlight different materials within the sample according to their different densities.

3. Results

3.1. Spatial resolution

The spatial resolution of the redesigned device was evaluated using imaging of thin iron edge measured with different

geometrical magnifications at X-ray tube accelerating voltage of 55 kV. The spatial resolution was estimated from measured Edge response function by the oversampling algorithm described in [17]. The dependence of the spatial resolution on the geometrical magnification is plotted in Fig. 4. The best achievable spatial resolution is 28 μm with the magnification factor of 2. The result indicates that the actual focal spot used for X-ray tube settings is smaller than the nominal value given by the manufacturer at the maximal tube output power.

3.2. Tissue-equivalent phantom

In order to test the soft tissue sensitivity of the presented system we used a tissue equivalent phantom. The phantom was made of a PMMA cylinder (10 mm diameter) with 4 parallel cavities drilled in the cylinder (see Fig. 5). The cavities were filled by soft-tissue equivalent materials – water (muscle substitute), wax (neural tissue substitute), oil (fat substitute) and air [18,19]. The phantom as well as all other samples presented in this work was measured in absorption Medipix photon counting mode. The results of tomographic reconstruction of the phantom are shown in Fig. 5. The reconstructed 3D model is visualized using a false colors coding to highlight different materials within the sample according to their different densities. The phantom was not created with a defined precision and therefore it is not possible to use it as a geometrical standard. Nevertheless the tomographic reconstruction of the phantom clearly demonstrates the ability to distinguish between very similar materials just based on slight differences in their X-ray attenuation.

The ability to segregate different soft tissue equivalent materials is quantitatively shown in Fig. 6. Fig. 6 presents a histogram of relative densities of five square ROIs within the reconstructed volume as depicted in the right part of the figure. The densities within the volume (horizontal axis) are relative to the mean density of the ROI covering the PMMA area. Each individual contribution of the histogram was fit by a Gaussian distribution and as can be seen it exceeds by far the FWHM criterion. Parameters of the Gaussian fit are shown too.

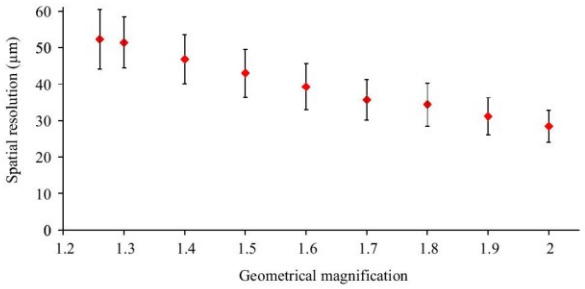

Fig. 4. Dependence of the spatial resolution in projection images (FWHM of the Edge response function) of the micro-CT system on the adjusted geometrical magnification.

3.3. Complex biological samples

The performance of the micro-CT device was tested also with real biological samples. The tomographic reconstruction of a head of a juvenile python (the same sample as in Fig. 3) is shown in the upper part of Fig. 7. The sample was scanned in three sub-acquisitions. From the presented images it can be seen that the presented device is capable of visualizing complex biological samples composed of different types of tissue, including very soft parts. The acquired 3D model consequently enables visualization of internal skeletal morphology together with detailed rendering of soft tissue structures. The bottom part of Fig. 7 presents the tomographic reconstruction of a fresh chili pepper as an example of sample absolutely missing any hard structures. The pepper was scanned in two sub-acquisitions mode.

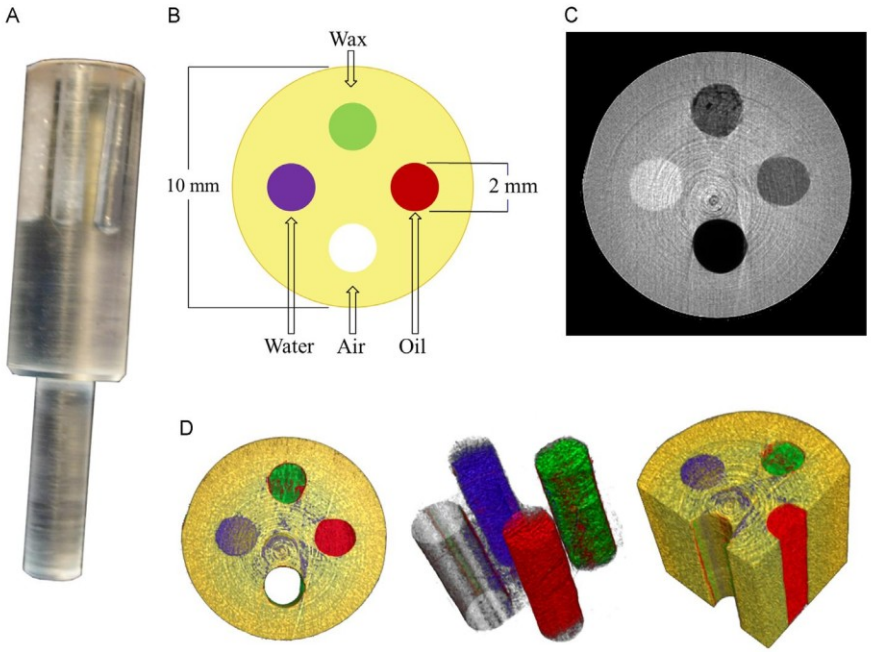

Fig. 5. Photo (A) of a PMMA phantom with soft tissue equivalent materials (wax, water, oil, air) used for the evaluation of the micro-CT sensitivity, schematic drawing of the phantom cross-section layout (B), example of a reconstructed slice (C), and examples of volume rendering of the reconstructed model using false colors visualization displaying wax (green), oil (red), water (purple) and air (empty space) (D). Imaging parameters: tube voltage 60 kV, current 110 μA, and magnification factor of 1.8. Acquisition time per projection 20 s. (For interpretation of the references to color in this figure legend, the reader is referred to the web version of this article.)

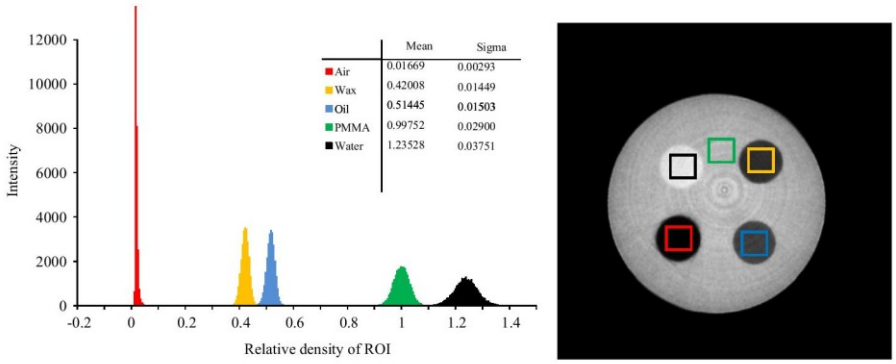

Fig. 6. Histogram of relative densities distribution of five square ROIs within the 3D voxel model of PMMA tissue-equivalent phantom (left). Density values are relative to the density of PMMA. Mean and sigma values of Gaussian fit of all peaks are shown. One of tested tomographic slices with ROIs signed (right).

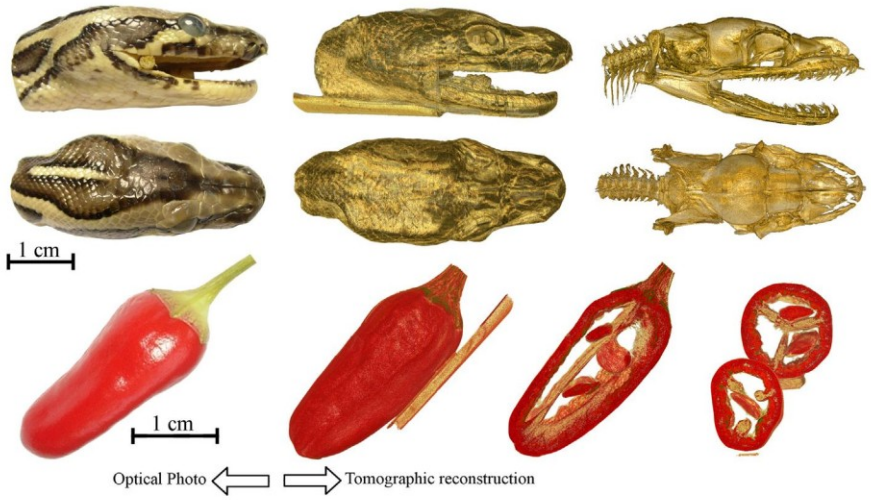

Fig. 7. Examples of tomographic reconstruction of different biological samples: a newborn python head (top part) and chili pepper (bottom part). The left part of the image shows optical photos of the samples, the right part presents visualizations of acquired tomographic reconstructions. Data acquired by the redesigned CT scanner equipped with a Timepix Quad imager. Acquisition parameters: tube voltage 60 kV, current 90 μA, and magnification factor of 2. Acquisition time per projection was 10 s and 5 s for the python and the pepper respectively.

4. Conclusions

We have successfully redesigned a micro-CT system for imaging of biomedical samples providing high sensitivity for visualization of even soft tissue samples. The system is newly based on implementation of the Timepix Quad hybrid pixel semiconductor detector, micro-focus X-ray tube and mechanics with rotating gantry originally developed for the MARS system. For the newly assembled system, dedicated control, acquisition and CT reconstruction software enabling full control over the performance of the CT device was developed. The current device provides spatial resolution better than 30 μm. The pilot measurements with a tissue-equivalent phantom proved that the redesigned CT system is suitable for soft tissue imaging with no need of special sample preparation. The enhanced soft tissue sensitivity together with high spatial resolution makes the new scanner a powerful and flexible tool for study of anatomy and morphology of small animals.

In the next work, we will optimize the scanning protocols with the aim to find optimal acquisition parameters for different types of samples and we will use the spectroscopic properties of Timepix detector to produce energy sensitive tomographic measurements. Since all data presented in this work were acquired in Medipix photon counting mode the application of the spectral Time-over-threshold mode promises to further improve the future results. The Timepix detector has been already demonstrated to be a suitable tool for energy sensitive radiography of soft materials [20]. We will further develop the method with the aim to find applications of energy sensitive radiography and tomography in biology and biomedical research.

Acknowledgments

Work was supported by Grant NAKI DF12P01OVV048 and by Project CZ.1.05/3.1.00/14.0301 of the EU funding program Research and Development for Innovation of the Czech Republic. The animal samples were kindly provided by P. Frydlova, O. Simkova and D. Frynta from Department of Zoology, Faculty of Science, Charles University in Prague, Czech Republic. Research was carried out in the frame of Medipix collaboration. Volume rendering and false color visualizations of tomographic voxel models were created using the Voreeen VE software [21].

References

[1] E.N. Landis, D.T. Keane, Materials Characterization 61 (12) (2010) 1305.
[2] P.J. Withers, Materials Today 10 (12) (2007) 26.

[3] R. Mizutani, Y. Suzuki, Micron 43 (2–3) (2012) 104.
[4] H. Li, et al., Progress in Natural Science 18 (5) (2008) 513.
[5] S.J. Schambach, et al., Methods 50 (1) (2010) 2.
[6] B.D. Metscher, BMC Physiology 9 (2009) 11.
[7] N.S. Jeffery, et al., Journal of Biomechanics 44 (1) (2011) 189.
[8] Medipix collaboration website at ⟨http://medipix.web.cern.ch/MEDIPIX/⟩ (2014).
[9] P.M. Frallicciardi, et al., Nuclear Instruments and Methods in Physics Research Section A 607 (1) (2009) 221.
[10] M.F. Walsh, et al., Journal of Instrumentation 6 (1) (2011) C01095.
[11] X. Llopart, et al., Nuclear Instruments and Methods in Physics Research Section A 581 (1–2) (2007) 485.
[12] J. Jakubek, Journal of Instrumentation 4 (2009) P03013.
[13] V. Kraus, et al., Journal of Instrumentation 6 (2011) C01079.
[14] D. Turecek, et al., Journal of Instrumentation 6 (2011) C01046.
[15] D. Vavrik, J. Jakubek, Nuclear Instruments and Methods in Physics Research Section A 607 (1) (2009) 212.
[16] J. Jakubek, et al., Journal of Instrumentation 9 (2014) C04018.
[17] J. Jakubek, et al., Nuclear Instruments and Methods in Physics Research Section A 509 (1–3) (2003) 294.
[18] W. Geraldelli, et al., IEEE Transactions on Nuclear Science NS-60 (2) (2013) 566.
[19] C.C. Ferreira, et al., Nuclear Instruments and Methods in Physics Research Section B 268 (16) (2010) 2515.
[20] J. Jakubek, Nuclear Instruments and Methods in Physics Research Section A 607 (1) (2009) 192.
[21] J. Meyer-Spradow, et al., IEEE Computer Graphics and Applications 29 (6) (2009) 6.

5.2. Evaluation of sample holders designed for long lasting X-ray micro-tomographic scans of ex-vivo soft tissue samples

Citace: DUDÁK, Jan; ŽEMLIČKA, Jan; KREJČÍ, František; KARCH, Jakub; **PATZELT, Matěj;** ZACH, PETR; SÝKORA, VIKTOR, MRZÍLKOVÁ, Jana. Evaluation of sample holders designed for long-lasting X-ray micro-tomographic scans of ex-vivo soft tissue samples. *Journal of Instrumentation* 2016, **11**(03), C03005-C03005. ISSN 1748-0221. DOI: 10.1088/1748-0221/11/03/C03005. **IF: 1.399/2015**.

5.2.1. Úvod a metodika

Snímání měkkých tkání v mikro-CT za účelem tomografického zobrazení s vysokým rozlišením trvá dle velikosti vzorku desítky minut. Během této doby musí být vzorek dobře zafixován, aby nedošlo ke vzniku artefaktů. Zároveň se však vzorek během snímání zahřívá, vypařuje se a mění objem a tvar. Cílem této práce bylo vytvořit držáky na vzorky pro mikro-CT MARS, které by udržely dostatečnou vlhkost kolem snímaného vzorku, tak aby nedošlo k jeho strukturálním změnám během snímání. Pro tyto účely byl vyvinut držák z injekční stříkačky, jejíž vnitřní prostor byl částečně rozdělen na dva, ve větším prostoru byl umístěn vzorek, menší sloužil jako rezervoár tekutiny, v tomto případě etanolu. Ten se postupně během snímání vypařoval a udržoval vnitřní atmosféru s dostatečnou vlhkostí. Účinnost navrženého držáku byla ověřena sérií testů, kdy se vzorek umístil do výše představeného držáku a snímal po dobu 60 minut, stejný typ vzorku se poté snímal v původním otevřeném držáku a výsledky byly porovnány. Pro pořizování 2D snímků byl vytvořen speciální držák, který umožňuje snímat jednu projekci na vzorky o velikosti až 40x150 mm.

5.2.2. Výsledky, diskuze a závěr

Snímání vzorku plic laboratorních myší jasně ukázalo snížené zmenšování vzorku v dvojkomorovém držáku v porovnání s otevřeným držákem. Kromě srovnání tvaru a zmenšování objemu vzorku bylo také provedeno srovnání kvality výsledných tomografií. V případě otevřeného držáku se na tomografiích vyskytlo větší množství arfetaktů, jako například rozmazané okraje nebo pruhy. Vytvořený držák je vhodný pro udržení stability vzorku během snímání v mikro-CT po dobu desítek minut.

Jinst

PUBLISHED BY IOP PUBLISHING FOR SISSA MEDIALAB

RECEIVED: *September 30, 2015*
REVISED: *December 29, 2015*
ACCEPTED: *January 18, 2016*
PUBLISHED: *March 2, 2016*

17TH INTERNATIONAL WORKSHOP ON RADIATION IMAGING DETECTORS
28 JUNE – 2 JULY 2015,
DESY, HAMBURG, GERMANY

Evaluation of sample holders designed for long-lasting X-ray micro-tomographic scans of ex-vivo soft tissue samples

J. Dudak,[a,b,1] **J. Zemlicka,**[a] **F. Krejci,**[a] **J. Karch,**[a,b] **M. Patzelt,**[c] **P. Zach,**[c] **V. Sykora**[d] **and J. Mrzilkova**[c]

[a] *Institute of Experimental and Applied Physics, Czech Technical University in Prague, Horska 3a/22, 128 00 Prague, Czech Republic*
[b] *Faculty of Biomedical Engineering, Czech Technical University in Prague, Namesti Sitna 3105, 272 01Kladno, Czech Republic*
[c] *Third Faculty of Medicine, Charles University in Prague, Ruska 87, 100 00 Prague, Czech Republic*
[d] *First Faculty of Medicine, Charles University in Prague, Katerinska 32, 121 08 Prague, Czech Republic*

E-mail: jan.dudak@utef.cvut.cz

ABSTRACT: X-ray microradiography and microtomography are imaging techniques with increasing applicability in the field of biomedical and preclinical research. Application of hybrid pixel detector Timepix enables to obtain very high contrast of low attenuating materials such as soft biological tissue. However X-ray imaging of ex-vivo soft tissue samples is a difficult task due to its structural instability. Ex-vivo biological tissue is prone to fast drying-out which is connected with undesired changes of sample size and shape producing later on artefacts within the tomographic reconstruction. In this work we present the optimization of our Timepix equipped micro-CT system aiming to maintain soft tissue sample in stable condition. Thanks to the suggested approach higher contrast of tomographic reconstructions can be achieved while also large samples that require detector scanning can be easily measured.

KEYWORDS: Computerized Tomography (CT) and Computed Radiography (CR); Pixelated detectors and associated VLSI electronics; Hybrid detectors

[1]Corresponding author.

doi:10.1088/1748-0221/11/03/C03005

Contents

2016 JINST 11 C03005

1 Introduction

Microradiography and microtomography are imaging techniques utilizing the illumination of the investigated object by the X-rays to measure the intensity of the transmitted beam behind the object. While the microradiography is usually performed in a single acquisition and provides a single 2D image of the investigated object, the tomographic approach requires the acquisition of a large set of projections under different angles that after dedicated mathematical processing produces a 3D voxel-based model of the scanned object.

As the X-ray imaging systems are becoming compact and easily available its applications in the field of biomedical and preclinical research have constantly increasing tendency [1]. The state-of-the-art laboratory micro-CT systems provide high and isotropic spatial resolution in order of micrometres or tens of micrometres in case of ex-vivo or in-vivo imaging, respectively [2, 3].

X-ray radiography has been traditionally used for imaging of hard structures such as skeletal system while its applicability for soft tissue imaging was limited due to intrinsic low attenuation contrast. Nevertheless thanks to availability of a number of contrast agents the soft tissue X-ray imaging have become a powerful tool in medical diagnosis and in the field of high resolution pre-clinical imaging as well.

Although the invention of contrast agents successfully enhance the contrast of particular types or structures within soft tissue, various different problems complicating the X-ray imaging of ex-vivo soft-tissue samples still remain. Ex-vivo soft tissue is highly sensitive and unstable. It easily dries out, shrinks and undergoes structural and shape changes. Consequently, the acquisition of dataset of ex-vivo tissue samples in high resolution tomography (a time consuming process from minutes up to hours) is very challenging. To keep the sample in stable conditions, it is necessary to prevent and slow down any degradation of the sample during the scan to eliminate different artefacts otherwise

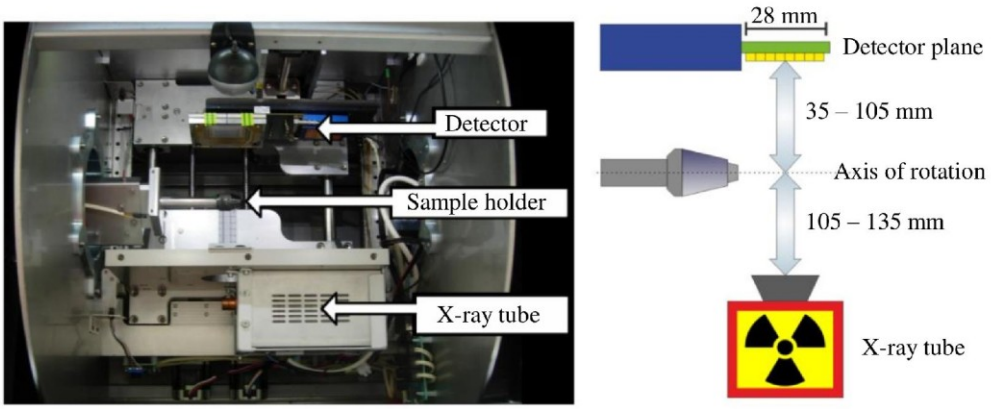

Figure 1. The gantry of the described micro-CT system holding the source and detector. The gantry rotates around horizontal axis with the sample in its center (left). Scheme describing the imaging geometry of the system (right).

appearing in the tomographic reconstruction. In this work, we present an extension of Micro-CT scanner utilizing Timepix detector technology [6] enabling efficient scanning of unstable soft-tissue samples. The new development is based on construction of devoted sample holders that maintain stable and saturated humidity around sample. The suggested approach minimizes undesirable tissue changes and enables obtaining higher contrast of obtained data with the possibility of longer acquisition times.

2 Materials and methods

2.1 Hybrid pixel semiconductor detector Timepix

Timepix detectors are hybrid pixel devices developed in frame of the Medipix collaboration at CERN [7]. The Timepix detector is composed of a monolithic semiconductor sensor layer bump-bonded to a CMOS-based pixelated read-out chip. The basic assembly provides the sensitive area of 1.4 by 1.4 cm^2 consisting of a square array of 256 by 256 pixels with 55 μm pixel pitch [8]. Although several different sensor materials are available, the most common sensor material is still 300 μm thick silicon.

The detector works in photon-counting noise-free mode. Each pixel works as an individual digital counter of incoming photons without presence of any noise (dark and leakage currents, read-out noise) that normally degrades the quality of radiographies acquired using conventional imaging detectors. Therefore, Timepix type detectors are able to acquire radiographies with virtually unlimited dynamic range (practical limit is given just by the number of detected photons) resulting in high contrast-to-noise ratio (CNR). The extremely wide dynamic range makes from Timepix technology a powerful tool even for X-ray imaging of objects with intrinsic low absorption and poor contrast [9].

The weakness of Timepix devices in the imaging field used to be their limited size (sensitive area just 2 cm^2). Recently this limitation was successfully overcome by the WidePIX® enabling to build large area Timepix devices fully comparable with conventional imaging detectors [10].

2016 JINST 11 C03005

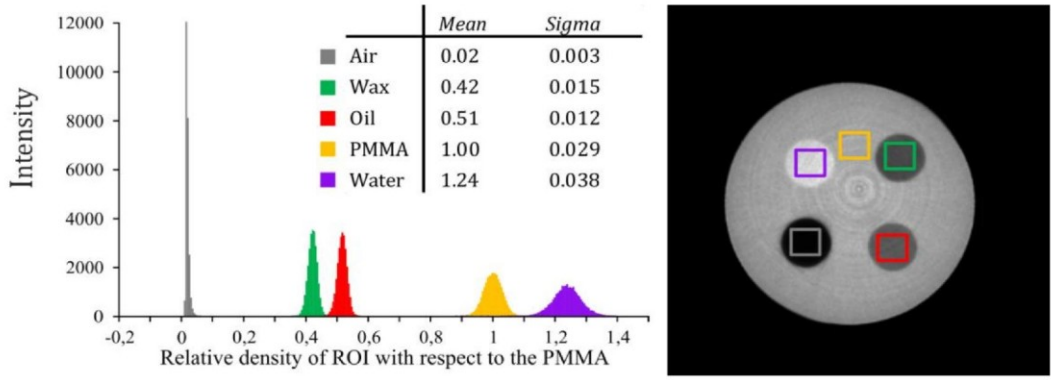

Figure 2. Demonstration of the contrast within the reconstructed CT slice between different soft tissue-equivalent materials achieved with the Timepix detector equipped micro-CT system. All selected ROIs (marked in the reconstructed slice in the right part of the figure) are clearly distinguishable. Mean and sigma values of Gaussian fit of all respective peaks are shown in the table. The relative density of each ROI was calculated with respect to the density of PMMA area in the reconstructed volume. Acquisition parameters: tube voltage 60 kV, current 110 μA, 180 projections, ca. $1.2 \cdot 10^5$ and $2 \cdot 10^4$ counts per pixel in open beam and behind the object respectively [6].

2.2 Small animal imaging Micro-CT scanner

The mechanics of the Micro-CT scanner were originally designed and developed by the University of Canterbury, New Zealand, as MARS (Medipix All Resolution System) [11]. The construction of the system was designed to be used for small animal imaging. The sample holder is fixed steadily in the horizontally oriented rotation axis while the gantry holding the X-ray tube and the detector rotates around it and acquires data (see figure 1). As the sample is placed stock-still on the horizontal sample holder, the risk of artefact occurance due to unstability of sample parts during the scan is minimised.

Compared to the original design, the presented device is equipped with Timepix Quad detector (512×512 pixels, sensitive area 2.8×2.8 cm^2) with a silicon sensor and the micro-focus X-ray tube KEVEX^{TM} PXS-11. The detector communicates with PC via FITPix interface [12].

The basic evaluation of the modified system performance for imaging of biomedical samples was already published in [6]. After performed hardware modification the highest achievable spatial resolution of the system is ca. 28 μm [6]. Furthermore the system was tested by means of soft tissue resolving ability using a tissue-equivalent phantom. The phantom was built of PMMA and contained four cavities filled by water, oil, wax and air to substitute muscle, fat, neural tissue and body cavities respectively. Figure 2 shows a chart proving that the Timepix detector is capable to clearly distinguish all phantom materials (figure 2 left) and an example of slice of reconstructed volume (figure 2 right) [6].

2.3 System control, data acquisition and processing

The whole system is operated using the Pixelman software [13]. A dedicated plugin with well-arranged GUI for remote control of gantry and its compartments was created. Beside the mechanical positioning of the system Pixelman performs data acquisition and allows the operator to adjust all acquisition parameters. The automated data acquisitions such as tomographic scan are performed

2016 JINST 11 C03005

via the Python scripting plug-in dedicated for creating custom user algorithms using the Pixelman function libraries.

A tomographic dataset consists typically of 180–360 individual projections acquired in equally-spaced gantry angles. Typical acquisition time per projection ensuring the sufficient contrast and low noise level lies within the range from ones to tens of seconds. The acquisition time of overall dataset is at least few minutes but preferably longer (tens of minutes or even hours) to exploit the capability of Timepix detector to acquire data with wide dynamic range. Pixelman is also featured by additional plug-ins for data pre-processing and corrections. For imaging purposes the most important plug-ins are flat-field correction and beam hardening (BH) correction. The algorithm of BH correction utilized by Pixelman was developed specifically for hybrid pixel detectors [14]. The correction is based on the acquisition of a set of well-defined absorbers of different thicknesses (typically aluminium foils) that are used to fit a polynomial function for each individual pixel. The obtained function characterizes the per-pixel detector response to the radiation under given imaging geometry, source parameters and absorber thickness. As the behaviour of each pixel under changing conditions is observed the bad pixels are recognizes and interpolated. This approach decreases the uncertainty of pixel response behind the object compared to the flat-field correction which uses calibration by the open beam only. Furthermore the correction results in data linearization as the data is transformed from intensity to equivalent thickness of the calibration material.

The standard data pre-processing consists of performing the BH-correction of all projections. In case of scanning of objects exceeding the field of view (see section 3.2) the individual sub-acquisitions must be merged together before further processing. Since the data after performing the referred BH correction is linear it can be directly used for tomographic reconstruction. The tomographic reconstruction is calculated using in-house developed OSEM based (Ordered Subsets Expectation Maximization) iterative algorithm.

3 Results

The ability to resolve reasonable contrast within the soft tissue was previously tested and proven using a tissue-equivalent phantom (see figure 2). As the scanning of real biomedical samples is, however, more complicated due to their instability requiring careful handling and keeping them under stable conditions. Tools developed with the aim to optimize acquisition of soft tissue samples are described in the following section.

3.1 Adjustable sample holders for native soft tissue samples

As there has been a large variety of sizes and shapes of objects being scanned with the scanner, a set of different sample holders was developed to optimally fulfill needs of experiments. The developed system of sample holders consists of an adjustable adapter base enabling precise centering of the sample in range +/− 5 mm in two perpendicular axes and set of adapters for different sample types (shown in figure 3). Thin-walled (0.3 mm thickness) cylindrical polypropylene containers of different diameters (5–28 mm) are dedicated for scanning ex-vivo biological tissue samples (see figure 3 A). The containers were designed to keep soft tissue samples in stable conditions, to eliminate drying-out and to support the sample. The container contains two semi-separated

2016 JINST 11 C03005

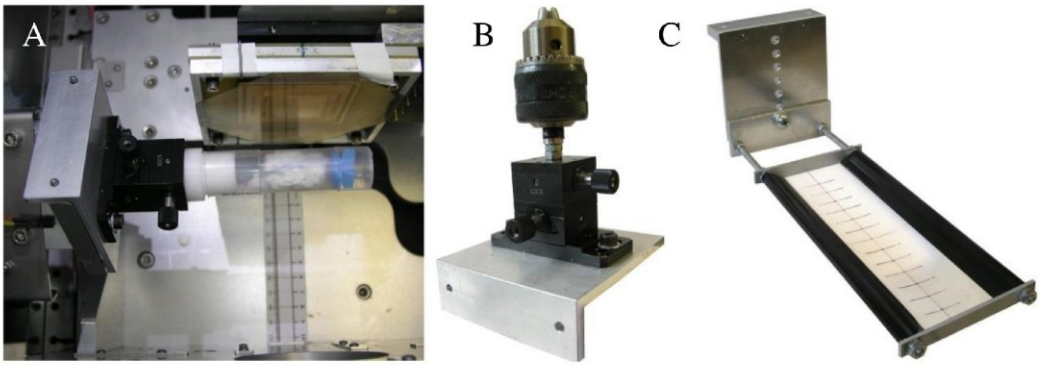

Figure 3. A) Double-compartment polypropylene container with liquid reservoir for scanning soft tissue samples placed in the gantry; B) adjustable adapter base of the developed sample holder allowing precise centering of the sample with a chuck mounted for holding rigid samples and phantoms; C) sample bed for quick 2D inspection of large samples enabling to gain magnification up to the factor of 3.2.

compartments — the first for the sample and the second as a liquid reservoir (i.e. ethanol) to keep the inner atmosphere saturated by humidity.

Eventually a sample holder dedicated for 2D radiography of large objects was designed. A large bed of the holder is dedicated for fast inspection of samples and can carry objects up to the size of 40 mm × 150 mm (figure 3). As the single projection scan does not require the sample placed in the rotation axis the sample holder can be set to eccentric position and gain the higher magnification factor up to the value of 3.2. The adapter base can hold a chuck as well (figure 3 B). The chuck is a preferable choice for rigid type of samples such as bones or for fastening various phantoms dedicated for system calibration.

3.1.1 Evaluation of sample stability improvement

Keeping the sample in closed atmosphere saturated by humidity significantly improves its stability. Picking the proper size of the container moreover supports the sample mechanically. The efficiency of using double-compartment sample containers with liquid reservoir was evaluated by observing the amount of changes within the sample during a 60 minutes lasting tomographic scan.

To evaluate the effectiveness of the sample environment stabilization, the same type of sample was scanned under identical conditions with the developed 2-chamber container and the original opened sample holder. Differences of relevant projections acquired at the beginning and the end of both tomographic scans are calculated (as a difference of respective images) and results are shown in figure 4. The amount of difference visible in the right part of the figure demonstrates that the shrinkage of sample scanned in the container with water reservoir is significantly smaller. Figure 5 shows the improvement of quality in reconstructed tomographic slices from the same datasets as presented in figure 4. Both samples were scanned and processed in the same way. While the slice in the left part of figure 5 suffers of a number of artifacts as blurring, streaks on the edges or germination of structures within the slice, the reconstruction on the right side of the figure does not exert any of these imperfections. From the sharply reconstructed cross-section of the sample holder it is clear that imaging geometry and reconstruction parameters were adjusted properly for both datasets.

2016 JINST 11 C03005

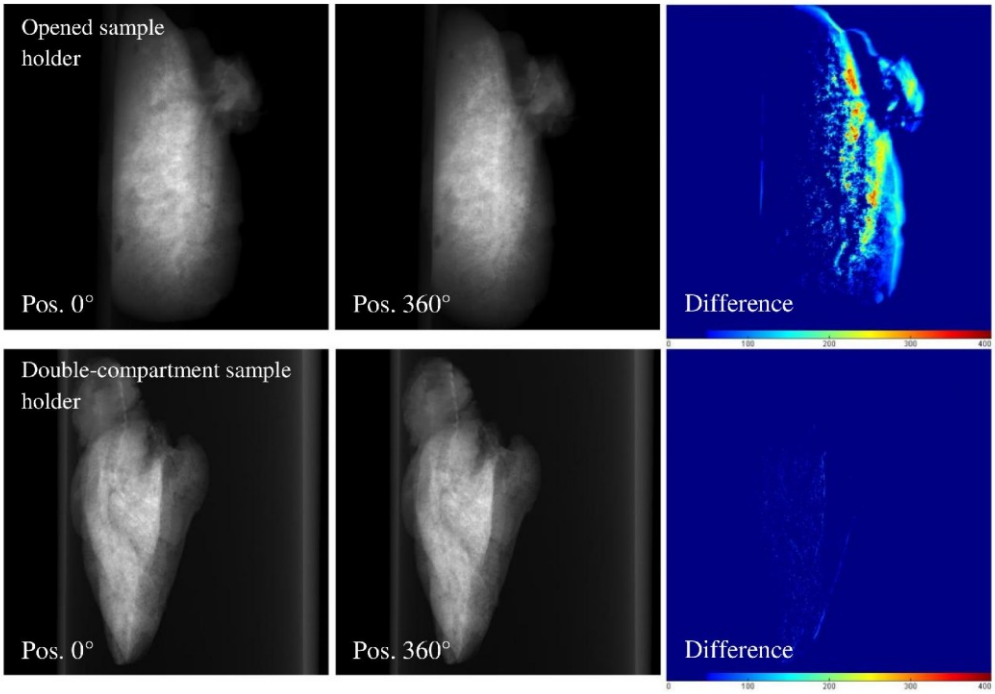

Figure 4. Demonstration of improvement of soft tissue sample stability with developed sample container. Top row shows the first and last projection of a sample (mouse lungs) scanned on the uncovered sample bed. Bottom row shows the first and last projection of different sample of the same type scanned in the double-compartment container. The time delay between projections at 0 and 360 degree positions is ca. 60 minutes. The differences of relevant projections clearly show the improvement of sample stability using suggested approach. Both difference images have the same intensity scale. Acquisition parameters: tube voltage 60 kV, current 140 μA, 360 projections, ca. $1 \cdot 10^5$ and $1.4 \cdot 10^4$ counts per pixel in open beam and behind the object respectively. Used magnification factor was 1.25, FOV 2.2×2.2 cm.

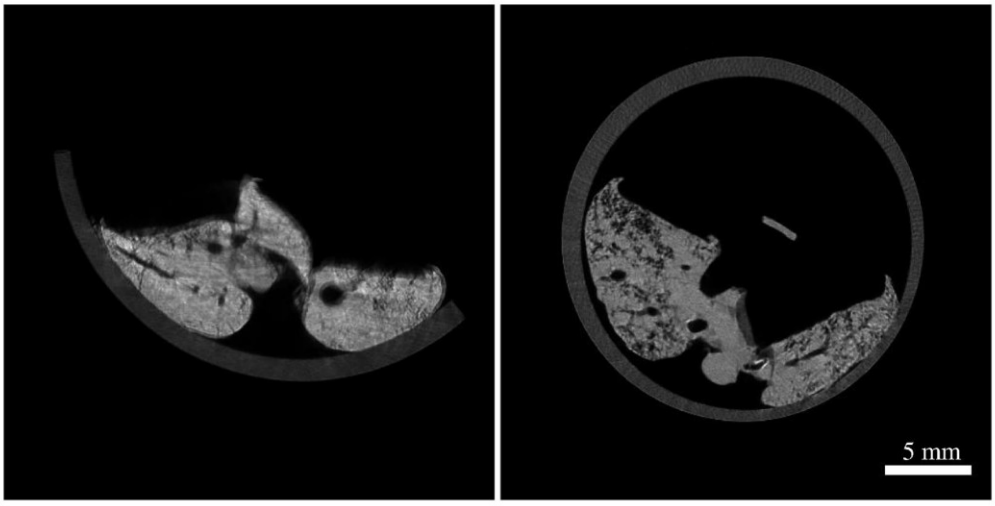

Figure 5. Comparison of tomographic slices of ex-vivo mouse lungs reconstructed from projections demonstrated in figure 4. Samples were scanned using an open holder (left) and using the developed double-compartment holder with water reservoir (right).

2016 JINST 11 C03005

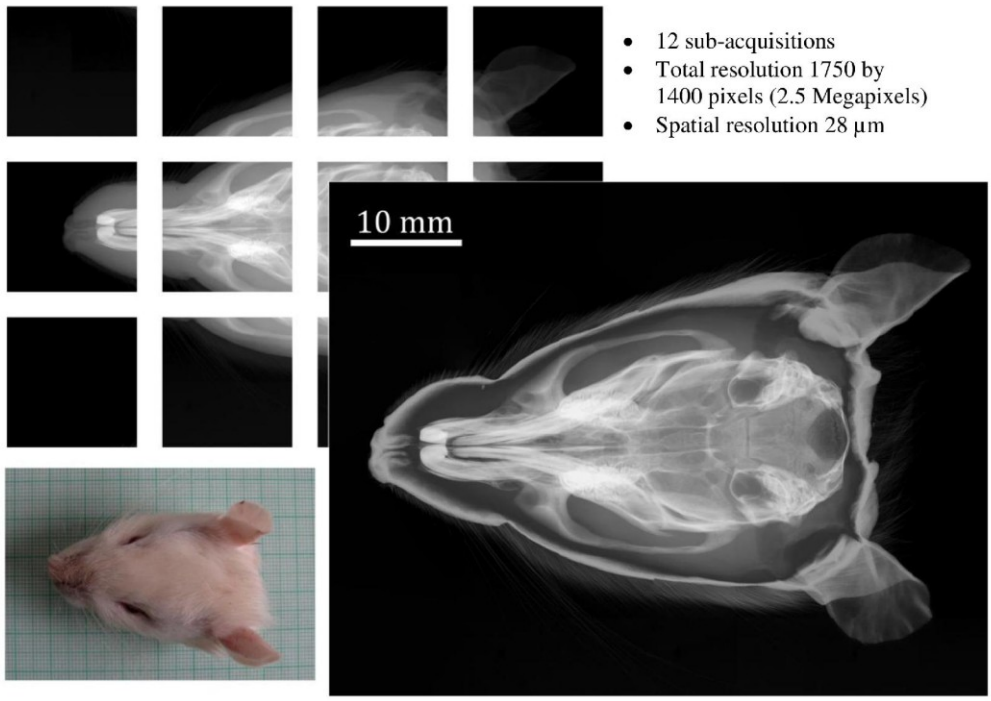

Figure 6. Laboratory rat head scanned using the tiling approach virtually enlarging the detector sensitive area. The sample is acquired in multiple sub-acquisitions which are later registered and merged into single image. Acquisition parameters: tube voltage 70 kV, current 100 μA, acquisition time 90 s per projection, ca. $4.5 \cdot 10^5$ and $1 \cdot 10^4$ counts per pixel in open beam and behind the object respectively.

3.2 Tiling approach for scanning large objects

Although the Quad configuration provides four times larger sensitive area compared to the basic Timepix assembly, for some applications the detector coverage (2.2×2.2 cm^2) is still not sufficient. Consequently, when the object projection exceeds the field of view, it is necessary to virtually enlarge the detector sensitive area. This can be accomplished by the gantry mechanics that allow shifting of the detector and/or the sample. Using the tiling approach a large object is scanned in multiple sub-acquisitions which are later registered and merged into a single image (see figure 6).

The tiling approach is suitable both for quick 2D projection inspection of the object as well as for acquisition of tomographic datasets. The inevitable drawback of the sample scannig lies in the total acquisition time prolongation making the sample environment stabilization (especially the humidity control) essential.

4 Conclusions

In this contribution, we presented the approach for imaging unstable ex-vivo soft tissue samples by means of X-ray micro-radiography and micro-CT. The proposed approach based on the developed 2-chamber sample container successfully supresses undesirable sample deformations caused by the sample drying. We have demonstrated that using this approach it is possible to keep soft-tissue samples stable for tens of minutes or even longer, which allows acquisition of standard tomographic datasets free of artefacts caused by sample distortion.

2016 JINST 11 C03005

Even though due to detector dimensions the system is preferably suitable for samples with dimension up 22 mm in diameter, the sensitive area can be effectively increased by the detector/sample shifting and acquiring multiple sub-acquisitions. In the future, the Quad detector configuration will be replaced by the large area detector built using WidePIX® technology to enable rapid scanning of larger objects.

Acknowledgments

The research was carried out in frame of the Medipix collaboration and was supported by the grant TA04011329 Advanced techniques of X-ray radiography for life sciences and industry of Technology Agency of The Czech Republic.

References

[1] S.J. Schambach et al., *Application of micro-CT in small animal imaging*, *Methods* **50** (2010) 2.

[2] A. Sharir et al., *High resolution 3D imaging of ex-vivo biological samples by micro CT*, *J. Vis. Exp.* **52** (2011) 2688.

[3] S. Sasov et al., *4D time-resolved in-vivo microtomography*, *IEEE Int. Symp. Biomed. Imaging* (2009) 582.

[4] X. Li et al., *Contrast agents for preclinical targeted X-ray imaging*, *Adv. Drug Delivery Rev.* **76** (2014) 116.

[5] R. Mizutani and Y. Suzuki, *X-ray microtomography in biology*, *Micron* **43** (2012) 104.

[6] J. Dudak et al., *X-ray micro-CT for small animal imaging based on Timepix detector technology*, *Nucl. Instrum. Meth.* **A 773** (2015) 81.

[7] Medipix Collaboration Website, http://medipix.web.cern.ch/.

[8] X. Llopart et al., *Timepix, a 65k programmable pixel readout chip for arrival time, energy and/or photon counting measurements*, *Nucl. Instrum. Meth.* **A 581** (2007) 485.

[9] J. Jakubek, *Semiconductor Pixel detectors and their applications in life sciences*, 2009 *JINST* **4** P03013.

[10] J. Jakubek et al., *Large area pixel detector WidePIX with full area sensitivity composed of 100 Timepix assemblies with edgeless sensors*, 2014 *JINST* **9** C04018.

[11] M.F. Walsh et al., *First CT using Medipix3 and the MARS-CT-3 spectral scanner*, 2011 *JINST* **6** C01095.

[12] V. Kraus et al., *FITPix — fast interface for Timepix pixel detectors*, 2011 *JINST* **6** C01079.

[13] D. Turecek et al., *Pixelman: a multi-platform data acquisition and processing software package for Medipix2, Timepix and Medipix3 detectors*, 2011 *JINST* **6** C01046.

[14] J. Jakubek, *Data processing and image reconstruction methods for pixel detectors*, *Nucl. Instrum. Meth.* **A 576** (2007) 223.

2016 JINST 11 C03005

5.3. High-contrast X-ray microradiography and micro-CT of ex-vivo soft tissue murine organs utilizing ethanol fixation and large area photon-counting detector

Citace: DUDÁK, Jan; ŽEMLIČKA, Jan; KARCH, Jakub; **PATZELT, Matěj;** MRZÍLKOVÁ, Jana; ZACH, Petr; HERMANOVÁ, Zuzana; KVACEK, Jiří; KREJČÍ, František. High-contrast X-ray microradiography and micro-CT of ex-vivo soft tissue murine organs utilizing ethanol fixation and large area photon-counting detektor. *Scientific Reports.* 2016, **6**, e30385;1-9. ISSN 2045-2322. DOI: 10.1038/srep30385 **IF: 5.228/2015**.

5.3.1. Úvod a metodika

Zobrazování měkkých tkání v mikro-CT vyžaduje ve většině případů použití kontrastní látky. Tyto látky jsou však často velmi nákladné, náročné na použití, toxické a také ve většině případů poškodí vzorek, tak, že jej nelze znovu použít v jiné vyšetřovací metodě. Cílem této práce bylo otestovat nově vytvořenou metodu etanolové fixace měkkých tkání pro zobrazení v mikro-CT osazeném foton-počítajícím detektorem a zjistit optimální nastavení přístroje pro snímání těchto vzorků. V práci byly použity orgány geneticky upravených myší C57BL/6J – srdce, plíce, mozek, játra a ledviny, které byly fixovány v 50%, 97% etanolu a ve vzestupné řadě koncentrací (50-97%) etanolu. Vzorky byly následně snímány po 24, 72, 168 a 336 hodinách. Vzniklé snímky byly následně porovnány se snímky nativních orgánů.

5.3.2. Výsledky, diskuze a závěr

Všechny vzorky fixované v etanolu vykázaly zvýšení kontrastu v porovnání s nativními vzorky. Díky účinnému zpevnění vzorků a rychlému vypařování etanol umožňuje stabilizaci vnitřní struktury vzorků a tím komory, cévy, bronchy, kalichy a další dutiny nekolabují a vyplňují se vzduchem. Díky tomu bylo možné detekovat přirozený kontrast mezi vzduchem a tkání. Z předběžných snímání vyšlo, že k největšímu zvýšení kontrastu došlo u fixace ve vzestupné řadě koncentrací etanolu po dobu 168 hodin. Metodika, porovnání časů fixace a koncentrací jsou popsány dále.

SCIENTIFIC REPORTS

OPEN

Received: 11 April 2016
Accepted: 30 June 2016
Published: 27 July 2016

High-contrast X-ray micro-radiography and micro-CT of ex-vivo soft tissue murine organs utilizing ethanol fixation and large area photon-counting detector

Jan Dudak[1,2], Jan Zemlicka[1], Jakub Karch[1,2], Matej Patzelt[3], Jana Mrzilkova[3], Petr Zach[3], Zuzana Hermanova[4], Jiri Kvacek[4] & Frantisek Krejci[1]

Using dedicated contrast agents high-quality X-ray imaging of soft tissue structures with isotropic micrometre resolution has become feasible. This technique is frequently titled as virtual histology as it allows production of slices of tissue without destroying the sample. The use of contrast agents is, however, often an irreversible time-consuming procedure and despite the non-destructive principle of X-ray imaging, the sample is usually no longer usable for other research methods. In this work we present the application of recently developed large-area photon counting detector for high resolution X-ray micro-radiography and micro-tomography of whole *ex-vivo* ethanol-preserved mouse organs. The photon counting detectors provide dark-current-free quantum-counting operation enabling acquisition of data with virtually unlimited contrast-to-noise ratio (CNR). Thanks to the very high CNR even ethanol-only preserved soft-tissue samples without addition of any contrast agent can be visualized in great detail. As ethanol preservation is one of the standard steps of tissue fixation for histology, the presented method can open a way for widespread use of micro-CT with all its advantages for routine 3D non-destructive soft-tissue visualisation.

Study of micro- and macroscopic structure of biological tissue provides essential information required both in medical diagnostics and research. Existing techniques for observation of tissue morphology, morphometry and phenotyping at the microscopic scale rely on histology[1]. Conventional histology, however, requires time consuming, complicated and destructive sample preparation protocols. The sample processing typically consists of different types of tissue dehydration, fixation, staining and resin-embedding followed by precise slicing and mounting on glass slides. Individual sample slices are then observed using a microscope, images are digitalized, evaluated and stored. Spatial resolution within the slice is basically given by the wavelength of used light. Improving further the spatial resolution requires the use of electron microscopy[1]. As each tissue sample is processed into a set of slices, the histology provides a sort of 3D information about the studied sample. Nevertheless, the spatial resolution of the obtained data set is highly anisotropic since the thickness of slices (affecting the resolution in the Z axis) is much larger than the spatial resolution within a single slice (XY plane). The assembling of the volumetric information from the set of 2D slices is, moreover, a complicated time consuming procedure prone to different artefacts[2].

Volumetric methods in conventional histology

A histological method producing true volumetric information was introduced as High Resolution Episcopic 3D Microscopy (HREM) or Surface Imaging Microscopy (SIM). HREM and SIM have much in common with

[1]Institute of Experimental and Applied Physics, Czech Technical University in Prague, Horska 3a/22, 128 00 Prague, Czech Republic. [2]Faculty of Biomedical Engineering, Czech Technical University in Prague, Namesti Sitna 3105, 272 01 Kladno, Czech Republic. [3]Third Faculty of Medicine, Charles University in Prague, Ruska 87, 100 00 Prague, Czech Republic. [4]National Museum, Vaclavske namesti 68, 115 79 Prague, Czech Republic. Correspondence and requests for materials should be addressed to F.K. (email: frantisek.krejci@utef.cvut.cz)

conventional histology, but utilizing a different scanning approach isotropic spatial resolution down to 0.5 μm can be achieved[2–5]. A significant drawback of these methods is, however, that they destroy the sample completely. On the contrary, in the case of conventional histology glass slides with sample slices can be stored and used repeatedly (for microscopy or more importantly for other techniques). In general, the optical-based methods can provide ultimate spatial resolution and contrast down to the cellular level, they can render 3D information about the investigated sample, but these techniques are destructive to the sample.

Virtual histology by means of X-ray imaging techniques

With the rapid development of technology in the field of X-ray imaging, high resolution information about the inner structures of objects can be obtained even non-destructively. The spatial resolution of X-ray micro-tomography systems is becoming almost comparable to conventional histology (tens of nanometres in the case of synchrotron radiation sources and micrometre level in the case of laboratory-scale devices[6,7]). Computed tomography, furthermore, produces a virtual 3D voxel-based model of the sample with isotropic spatial resolution. The reconstructed volume can be rendered and sliced in any required plane giving much more freedom in sample observation and data evaluation than conventional histology. Thanks to the non-destructive approach of the method, samples remain intact and still fully usable for further investigation procedures.

In spite of the high spatial resolution provided by X-ray micro-radiography and micro-CT, visualisation of soft tissue remains a challenging task due to the very low intrinsic attenuation contrast between the investigated structures. Consequently, for imaging of soft tissue with X-rays the application of a high-Z contrast agent is usually necessary[8–15]. To obtain a specific affinity of dedicated contrast agents to various tissue structures, a proper sample preparation protocol must be then followed. These contrast staining procedures are, however, elaborate, often time consuming (up to several days) and irreversible which prevents the use of a sample for other research methods.

Photon counting detector technology

The steady progress in miniaturization of front-end electronics in the last decades has opened the possibility for development of semiconductor pixel X-ray detectors with sophisticated digital per-pixel signal processing functionality enabling detection by so-called photon counting. Several different photon counting imaging detectors (PCD) have been developed in the last decade which are today commercially available (Medipix and Timepix[16], PILATUS[17] and Eiger[18], XPAD[19] and PiXirad[20]). These detectors operate typically in dark-current-free mode in which the signal generated by each incoming X-ray photon is processed at the pixel level individually including pre-amplification, comparison with the pre-adjusted amplitude threshold (set above the pixel intrinsic noise) and digital counting. As a result of this signal processing, these detectors are practically noiseless and the obtained contrast-to-noise ratio in X-ray radiographs and CT scans is limited only by the number of detected X-ray photons. Consequently, when applied for X-ray absorption radiography, even structures showing low difference in attenuation (e.g. soft tissue) can be visualised with high CNR compared to conventional imaging detectors utilizing scintillating sensors and charge-coupled detection instead of photon counting[21].

Despite the significant progress in imaging parameters provided by the photon counting technology a crucial limitation in the practical use of these devices for imaging has been the small sensitive area of only few square centimetres. This technological barrier has been fully overcome by the development of large-area photon counting semiconductor detectors such as the WidePIX device[22] consisting of a matrix array of Timepix chips equipped with edgeless sensors tightly placed side by side using customized tiling technique. The assembled detector matrix array has practically no gaps between chips resulting in a fully sensitive area of up to $14.3 \times 14.3\,cm^2$ (array of 100 Timepix chips). Such large-area semiconductor pixel detectors combined with modern table-top sources (e.g. micro-focus X-ray tubes) open the way for extended and new applications in X-ray imaging.

In this work we demonstrate performance of this recently developed large area hybrid pixel photon counting detector for high resolution X-ray microradiography and micro-tomography of *ex-vivo* ethanol-only preserved murine organs. The effect of *ex-vivo* soft tissue contrast enhancement after ethanol-preservation has been demonstrated in studies related to phase contrast X-ray imaging[23,24]. However, in the case of techniques based on X-ray absorption, ethanol is generally used as a soft tissue fixative and the sample needs to be further stained by a contrast agent (Lugol solution, phosphotungstic acid, osmium tetroxide, etc.)[8–14]. The presented experimental measurements demonstrate that using the PCD it is possible to visualize fine structures in ethanol-preserved mouse tissue samples even without use of any further contrast staining. The approach, furthermore, preserves the sample for standard imaging techniques, such as histology. The presented approach, therefore, radically simplifies the soft-tissue sample processing protocol for X-ray micro-radiography and micro-CT and opens the way for widespread use of these techniques for routine 3D non-destructive *ex-vivo* soft tissue visualisation.

Results

Compared to water, ethanol evaporates more effectively promptly leaving all kinds of cavities such as ventricles, vessels, alveoli, bronchi etc. Structures normally filled by liquid, therefore, become hollow and produce detectable absorption contrast. Since ethanol stiffens the tissue, investigated organ samples can easily withstand time consuming tomographic scans (from tens of minutes up to hours) without significant changes of the tissue shape and inner structure. The demonstration of the observed contrast improvement of the ethanol preserved tissue sample compared to the native sample is shown in Fig. 1. Microradiography of the native heart kept in saline (Fig. 1A) provides minimal contrast of inner structures as ventricles and veins are still filled by blood or saline having almost the same attenuation properties as the surrounding heart muscle tissue. On the other hand, in the case of ethanol preserved hearts (Fig. 1B–D) the microradiography reveals numerous details of sample inner structures. In all tested samples the gained contrast developed during first days of fixation, as ethanol penetrated the tissue,

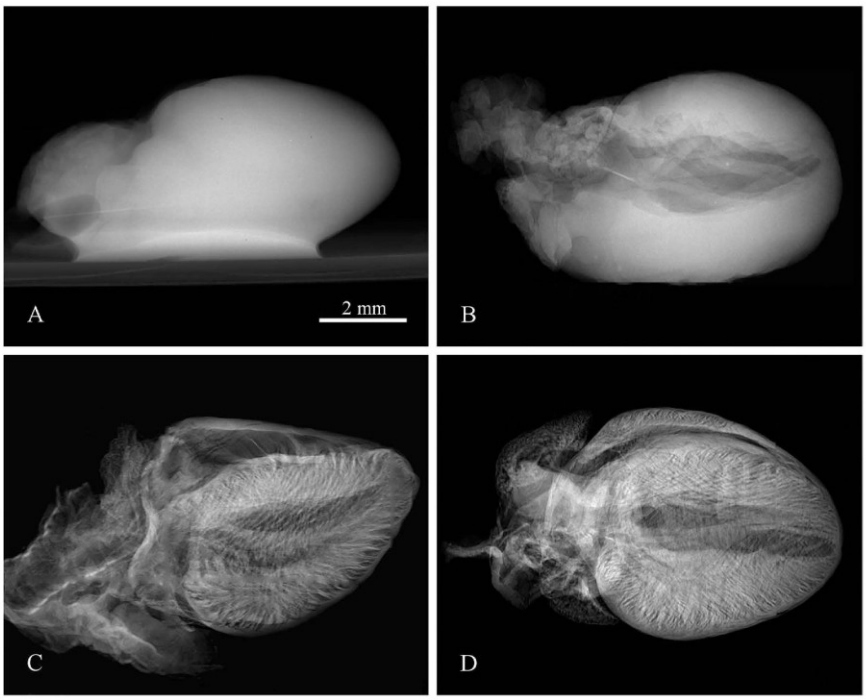

Figure 1. Demonstration of the contrast improvement in X-ray micro-radiography between a native sample and ethanol preserved samples. X-ray radiography of a native mouse heart (**A**) and samples preserved in 50% ethanol solution (**B**), 97% ethanol solution (**C**) and the ethanol series of increasing concentrations (**D**). Acquisition parameters: Tube voltage 60 kV, current 120 μA, acquisition time 40 s.

however, after 7 days in ethanol solution the contrast becomes stable without further changes. All samples presented in this work were preserved for at least 7 days.

From three different ways of ethanol fixation which were tested (50% solution, 97% solution, and series of increasing concentration 50–97%), we evaluated as most appropriate the approach based on the series of increasing ethanol concentration. The 50% ethanol solution has maintained the native look of the tissue, but it did not stiffen and improved the contrast of samples sufficiently. On the other hand, the use of the high ethanol concentration (97%) directly to a native tissue sample has resulted in severe tissue deformation or even occurrence of ruptures.

Experimental measurements indicate that the contrast develops with respect to the degree of drying of the sample. The ethanol evaporation is the fastest from the surface of the sample and from larger cavities. Contrast in radiographic images changes consequently as a function of resting time (the time delay between sample removal from the ethanol solution and the measurement) within the same type of tissue, as demonstrated for the case of lungs in Fig. 2. Different lung samples A, B and C were extracted from the ethanol solution and rested on paper towel in air for varying time periods. While sample A rested for just 10 minutes, it shows mostly the trachea and its bifurcations. At longer rest time, finer structures start appearing (see Fig. 2B). Finally the contrast of trachea and bronchial tree is almost completely shadowed by pronounced alveolar structure (see Fig. 2C).

In a similar manner also other hollow systems like veins, arteries and various ventricles provide extensive contrast enhancement following alcohol staining. Contrast enhancement in a murine kidney is demonstrated in Fig. 3. High contrast was obtained in the case of liver, where the vessel system is clearly pronounced down to the 15 μm thick venules, see Fig. 4. The dehydration also improves the detectability of tissue structures such as muscle fibres as the muscle tissue reacts differently than the surrounding fascial layer of muscle (visible in Fig. 1C,D). In the case of micro-tomography of the heart this effect can be used for visualization of the heart vortex – heart wall with helically shaped muscle fibres (see Fig. 5 and supplementary files 1 and 2). The data for the presented tomographic reconstruction was acquired using the high resolution setup equipped with the large area PCD. Thanks to the magnifying geometry used for the scan, the spatial resolution of projections is 7.2 μm. The transversal slices of the reconstructed 3-D model (see right part of Fig. 5) clearly reveal the helical structure of the heart vortex. Beside that it is possible to observe inner structures like heart chambers or valves, and to perform various distance, surface and volume measurements and other common analyses.

Discussion

The proposed approach provides enhanced CNR imaging with 3D information about investigated soft tissue structures at the micrometre scale without physical sectioning of the sample. Quick, non-destructive and non-distorted 3D visualisation of soft tissue structures with spatial resolution approaching the cellular level opens new possibilities in so-called virtual histology[8,9]. The spatial resolution, in our case limited to 5 μm by the focal

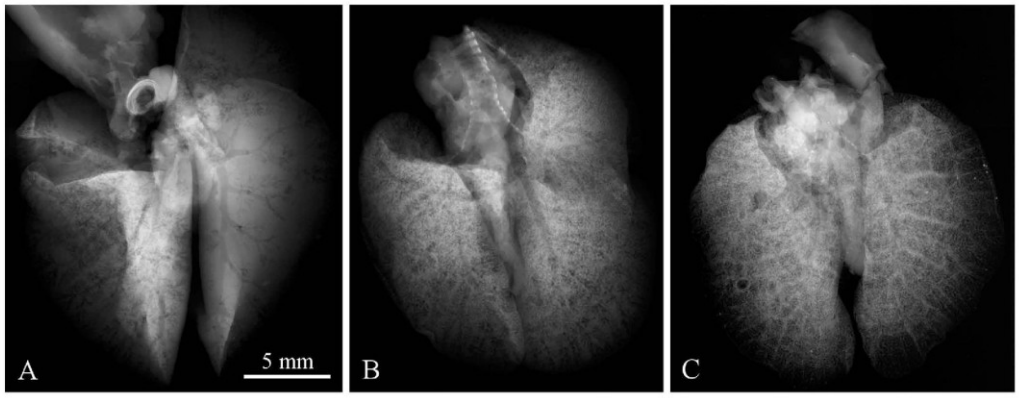

Figure 2. Demonstration of contrast development in X-ray micro-radiography of ethanol-preserved mouse lungs as a function of resting time. Three different samples scanned after 10, 20 and 40 minutes of relaxation, respectively, are shown. Short resting time makes the trachea and bronchial tree being visible (**A**), while longer resting time leads to discernment of the alveolar structures of lungs. In (**B**) a superposition of bronchial and alveolar structures are visible, in (**C**) the alveolar structures hinder the visibility of the trachea and bronchial tree. Acquisition parameters: Tube voltage 60 kV, current 120 μA, acquisition time 40 s.

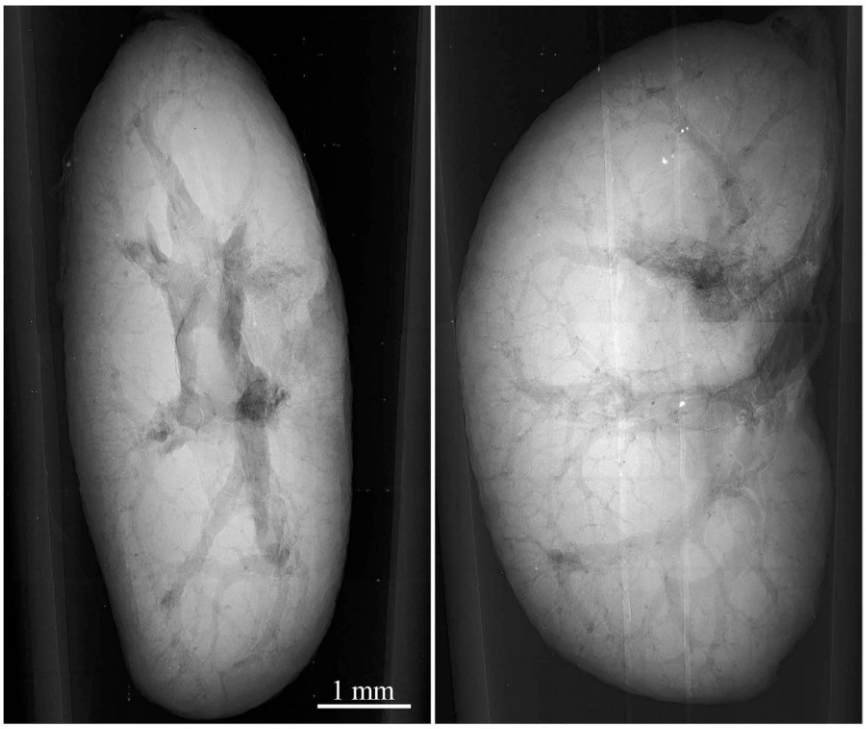

Figure 3. Selected projections from a tomographic dataset of ethanol-preserved murine kidney acquired using the high resolution micro-tomography setup equipped with the large-area PCD. The images demonstrate possibility to visualise various inner structures with superb image quality just based on the ethanol preservation. Acquisition parameters: Accelerating voltage 60 kV, current 90 μA, acquisition time 10 s.

spot size of the X-ray source used, can be further improved by new table-top laboratory sources with focal spots size well below 1 μm.

Very good soft tissue contrast together with non-destructive volumetric information can be provided also by highly sophisticated methods such as X-ray phase-contrast[23–28], dark-field imaging[29,30] or X-ray microscopy[31,32]. These methods, however, require an advanced setup and very special X-ray beam characteristics, which in most of the cases can be found only at large scale synchrotron facilities. These requirements crucially limit further widespread application of these techniques, e.g. in biology.

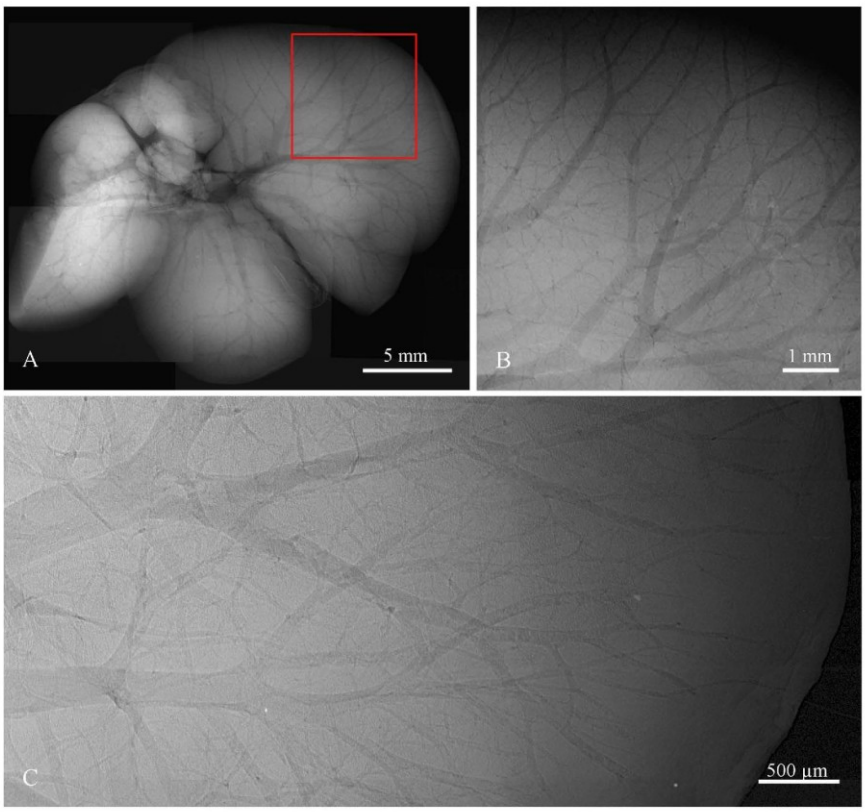

Figure 4. High resolution X-ray radiography of ethanol preserved mouse liver scanned using the compact micro-CT scanner with Quad detector assembly (**A,B**) and the high resolution setup (**C**). Due to the limited FOV the presented micro-radiographic image (**A**) is merged from 9 individual tiles. The selected ROI (**B**) shows the fine vascular structure of the liver lobe with venules diameter down to 40 µm. ROI of liver with 5 µm spatial resolution acquired using the large area Timepix detector (**C**) enables revealing venular structures down to 15 µm. Note also a white brim along the outer border of capillaries formed by phase effects enhancing further the final contrast. Acquisition parameters: Tube voltage 60 kV, current 120 µA, acquisition time 40 s.

Currently used X-ray micro-CT staining techniques for *ex-vivo* soft tissue absorption imaging utilize high-Z contrast agents which are delivered to the specific structure by elaborate, time demanding and irreversible staining techniques which depend also on the knowledge of skilled staff. Using the proposed method, high quality micro-radiographs and micro-CT scans of basically all murine organs can be acquired just after simple ethanol preservation of tissue. The method, moreover, keeps the samples fully usable for further measurements and research. The significant simplification of the sample preparation protocol and compatibility with established techniques makes consequently the method easily accessible to the general scientific community and opens the use of micro-CT as a new standard tool for inspection of soft tissue biological samples.

A set of comparative measurements was performed using a commercially available micro-CT scanner Bruker 1172 equipped with 11 Mpixel CCD detector (9 um pixel pitch) and micro-focus X-ray tube. The comparison has showed that the contrast improvement of soft tissue structures based on the ethanol staining is detectable even with state-of-the-art conventional X-ray cameras. Nevertheless, the profit of a noiseless PCD lies in the possibility to detect even extremely small variation in density/thickness formed, for example, by few micron thin veins. For charge-integrating devices such sensitivity is a difficult task due to various intrinsic sources of noise (dark current, leakage current, read-out noise) negatively affecting the CNR of radiographic images. Results of comparison between the large area PCD and CCD camera are demonstrated for the case of ethanol-preserved murine liver in Fig. 6. The pixel resolution of micro-radiographic systems was set to 4.3 µm in both cases and comparable detected open beam intensity was used. The comparison shows that PCD clearly provides better results in terms of CNR which provides significantly improved visualisation of many faintly attenuation object features. Moreover, CNR of the PCD radiograph can be further improved just by exposure time prolongation. The detail visibility in radiographs acquired using PCD is also partially positively affected by their steep point spread function.

Another important advantage of the approach based on the large-area photon counting detector is the capability to image whole murine organs with very high magnification. The sensitive area of state-of-the-art Charge-Coupled-Devices (CCDs) which are a promising detector technology currently used in micro-CT scanners is still limited to few square centimetres and their use is therefore limited to imaging of small objects. Thanks to development of large area photon counting detectors even larger organs, such as human, can be also visualized with moderate spatial resolution given basically by the pixel size of the detector (55 µm). The approach therefore

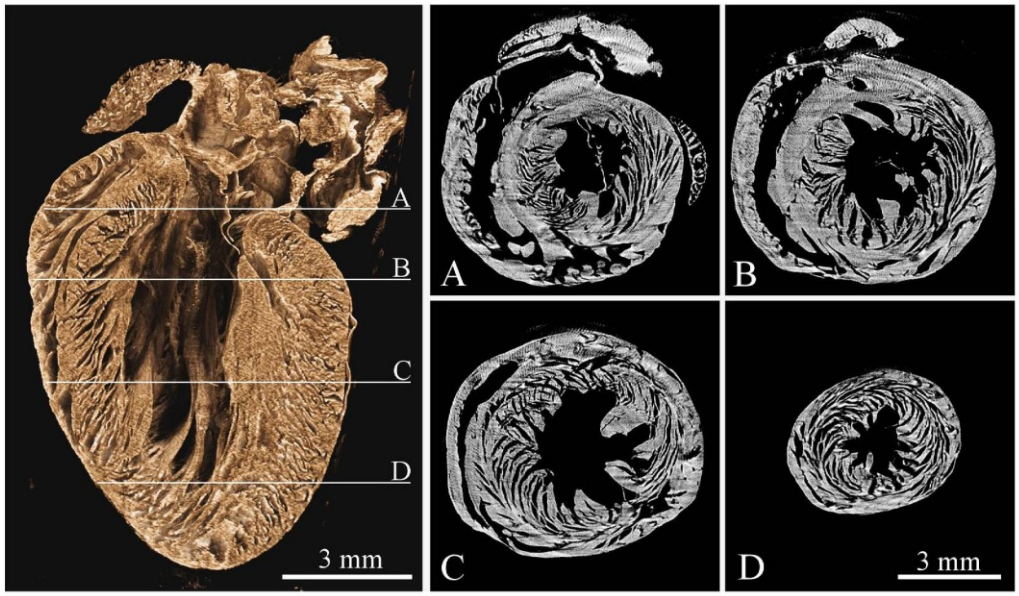

Figure 5. Tomographic reconstruction of a mouse heart acquired using the high resolution setup and large area Timepix detector. The left image shows the volume rendering of reconstructed dataset visualized using the false-colour system. The right part of the figure shows four different transversal slices (see labels A thru D) across the reconstructed volume demonstrating the heart vortex – helical structure of the muscle fibres. See supplementary files 1 and 2 providing animations of the reconstructed data in two different planes. Acquisition parameters: Tube voltage 70 kV, current 100 μA, 720 projections, acquisition time 5 s. per projection. Spatial resolution 7.2 μm.

provides from a single tomographic scan very complex 3-D model of relatively large tissue volume. This feature together with the high contrast provided by the ethanol staining opens new possibilities in understanding of the structure and functionality of soft tissue organs.

Conclusions

We have developed and demonstrated a flexible imaging method for 3D imaging of *ex-vivo* soft tissue samples based on the use of the large area photon-counting detector and simple ethanol preservation. The method provides substantial improvement of image quality of various soft tissue structures in absorption X-ray micro-radiography and micro-tomography applied without the use of higher-Z contrast agents. The achieved contrast provides different type of information compared to conventionally used contrast agents. Moreover, ethanol preservation stabilizes the samples structurally and improves the stability of sample imaging during long lasting tomographic scans. As ethanol preservation is one of standard steps of tissue fixation for histology, the presented approach can open a way for widespread use of micro-CT with all its advantages for routine 3D non-destructive soft tissue visualisation.

Methods

Sample processing. A set of measurements with *ex-vivo* mouse organs was performed. Use of laboratory animals was approved by Ethical Committee of the Third Faculty of Medicine, Charles University in Prague. The animals were treated with accordance to guidelines defined by Ethical Committee in decisions no. 246/1992 and no. 419/2012. Genetically modified mice C57BL/6 (weight 17 g) were terminated by ether inhalation overdose and their organs (brain, heart, kidney, liver and lungs) were extracted out for purposes of this study. All samples were inserted into ethanol solution immediately after extraction. As fixative we used 50% and 97% ethanol solutions and an ethanol series with gradually increasing concentration (50–97%). The samples were scanned after 24 hours, 72 hours, 1 week and 2 weeks after inserting into the fixative. Before data acquisition each sample was rested on the air for certain time (5–60 minutes) to let the redundant ethanol evaporate from the surface of the sample and from cavities. For the purposes of 2D projection imaging the sample was placed in a sample holder keeping the sample in place between two thin self-adhesive stretch foils which minimised the occurrence of motion artefacts and slowed down the further drying-out of the tissue (see Fig. 7 right). In the case of tomographic acquisition, samples were fit into the properly-sized cylindrical double-compartment sample holder with an ethanol reservoir that fixed the sample mechanically and kept saturated gaseous atmosphere preventing structural changes of the samples[33].

X-ray micro-CT s3etup and measurements. For the first evaluation, samples were scanned using a compact small animal X-ray micro-CT scanner[34]. The scanner provides spatial resolution ca. 28 μm and limited field of view given by the detector size (photon counting Timepix Quad detector[16] with 300 μm thick Si sensor, 512 × 512 pixels, 55 μm pixel pitch, sensitive area 7.92 cm^2). Thanks to the rotating gantry construction with a

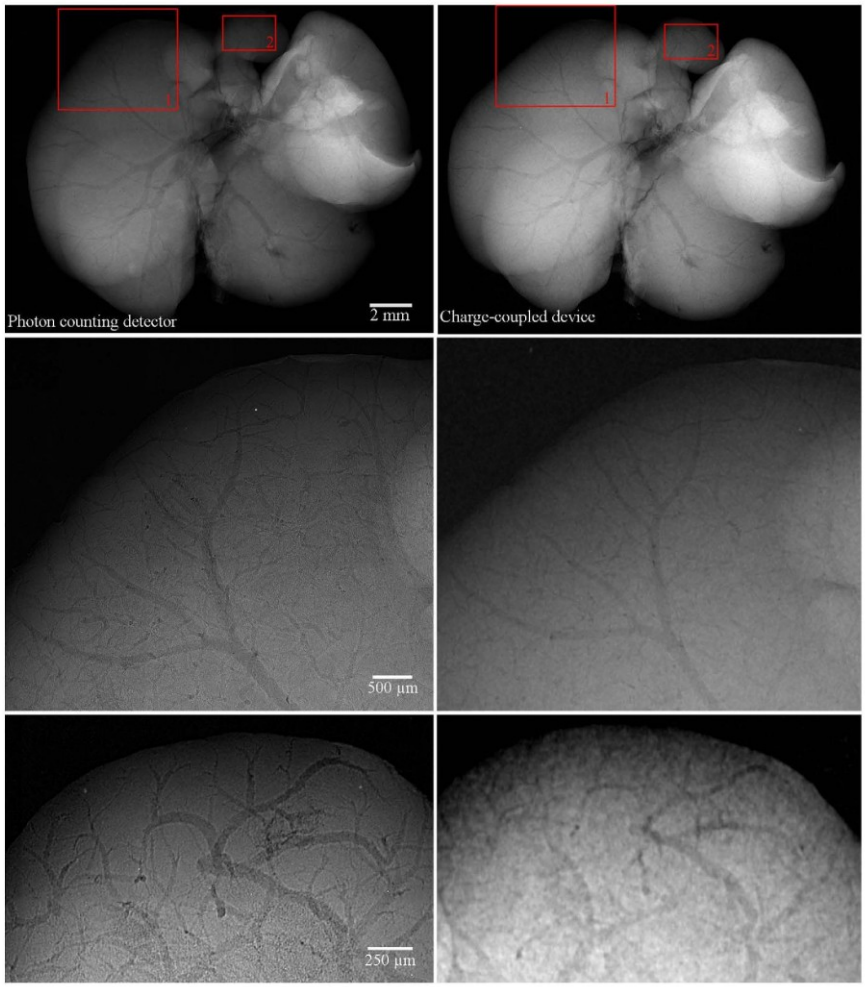

Figure 6. Comparison of X-ray micro-radiography of the ethanol-preserved mouse liver acquired using the PCD (left column) and CCD (right column). The pixel resolution of both setups was set to 4.3 μm. While globally both images look very similar, when observing a small region of interest (lower rows) the PCD reveals finer structures thanks to much higher CNR. Acquisition parameters were 60 kV, 100 in the case of the high resolution set-up with PCD and 40 kV, 260 μA in the case of the CCD-based setup. Acquisition time of each imaging system was set individually to provide comparable detected intensity of the open beam. While the PCD clearly visualizes venules smaller than 15 μm, in the case of the CCD detector only structures larger than ca. 60 μm are visible.

short source-to-detector distance and high beam intensity, rapid measurements of unstable samples and acquiring of tomographic datasets consisting of many projections are feasible. The gantry housing the X-ray source and detector rotates around the sample laying stationary on the holder in the horizontal direction. The configuration minimises the possibility of changes within the soft biological sample during the scan.

In order to obtain high-resolution radiographs and micro-CT scans of whole murine organs the upgraded high-resolution X-ray imaging setup[35] at IEAP CTU in Prague has been used. The high-resolution setup is equipped with the Hamamatsu L8601-01 X-ray tube with 5 μm focal spot and the large area photon counting detector WidePIX$_{10\times5}$ composed of 50 Timepix chips[22] providing the total pixel resolution of 2560 by 1280 pixels (see Fig. 7 left). The basic detector assembly (a single detector tile) consists of an edgeless 300 μm thick silicon sensor bump-bonded to a CMOS pixelated Timepix read-out chip (256 by 256 pixels, 55 μm pixel pitch)[16]. The high-resolution system is placed inside of a shielded vault enabling the use of imaging geometry with high magnification factor. The precise motorised positioning system allows scanning large samples in multiple sub-acquisitions that virtually increase the detector sensitive area. The best achievable spatial resolution is slightly below 5 μm (limited by the penumbral effect of the tube spot size).

The detected intensity in acquired data was over 10^5 and $1.5{\cdot}10^4$ events per pixel behind the object for 2D radiography and tomographic projection, respectively. All presented 2D radiographies and the projections used for tomographic reconstruction were processed by beam hardening correction[36]. The X-ray spectrum used for measurements corresponded to a tungsten anode with thin beryllium output window operated at 50–70 kVp. No filtration

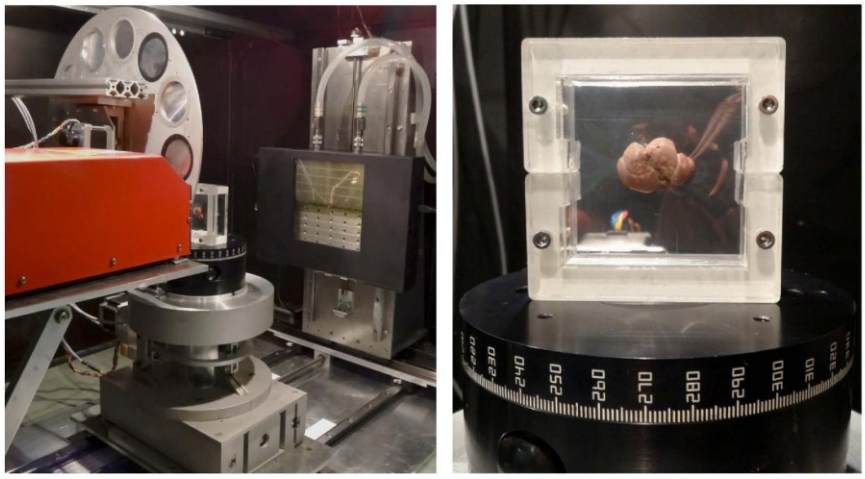

Figure 7. High-resolution table-top X-ray imaging setup. The system is equipped with a micro-focus X-ray tube, rotating carrousel with calibrating foils, precise sample positioning stage and the large area photon counting detector with sensitive area $14.3 \times 7.15\,cm^2$ (left). Detail view of a sample holder used for 2D high-resolution X-ray imaging of soft biological samples (right).

was used to maintain maximal content of soft X-rays providing the highest contrast in faintly attenuating soft tissue organs. The 2D radiographies were acquired with the highest possible magnification and resolution: ca. 28 μm and 5 μm in the case of the compact micro-CT scanner and the high resolution setup, respectively. The magnification used for tomographic measurements was set with respect to the dimensions of the sample to optimally cover the detector area. The tomographic data was reconstructed using the Volex reconstruction engine based on the filtered back-projection (Fraunhofer-Allianz Vision, Germany), alternatively an in-house implemented OSEM based iterative reconstruction algorithm was used also. Ring filtering was performed as a part of data pre-processing in sinogram domain using combined wavelet-Fourier filtering[37]. The reconstructed volumetric data was visualized using open source volume renderers AMIDE[38] and CTVox[39].

References

1. Suvarna, S. K., Layton, C. & Bancroft, J. D. *Bancroft's Theory and Practice of Histological Techniques*, *7th Edition*. Churchill Livingstone Elsevier, Oxford (2013).
2. Geyer, S. H., Mohun, T. J. & Weninger, J. W. Visualizing Vertebrae Embryos with Episcopic 3D Imaging Techniques. *ScientificWorldJournal* **16,** 1423–1437, doi: 10.1038/nphys265 (2009).
3. Mohun, J. T. & Weninger W. J. Imaging heart development using high-resolution episcopic microscopy. *Curr. Opin. Genetics. Dev.* **21,** 573–578, doi: 10.1016/j.gde.2011.07.004 (2011).
4. Gerneke, D. A. *et al.* Surface imaging microscopy using an ultramiller for large volume 3D reconstruction of wax- and resin-embedded tissues. *Microsc. Res. Tech.* **70,** 886–894, doi: 10.1002/jemt.20491 (2007).
5. Rosenthal, J. *et al.* Rapid High Resolution Three Dimensional Reconstruction of Embryos with Episcopic Fluorescence Image Capture. *Birth Defects Res. C Embryo Today* **72,** 213–223, doi: 10.1002/bdrc.20023 (2004).
6. Withers, P. J. X-ray nanotomography. *Mater. Today* **10,** 26–34, doi: 0.1016/S1369-7021(07)70305-X (2007).
7. Landis, E. N. & Keane, D. T. X-ray microtomography. *Mater. Charact.* **61,** 1305–1316, doi: 10.1016/j.matchar.2010.09.012 (2010).
8. Silva, J. M. S. *et al.* Three-dimensional non-destructive soft-tissue visualization with X-ray staining micro-tomography. *Sci. Rep.* **5,** 14088, doi: 10.1038/srep14088 (2015).
9. Metschner, B. D. MicroCT for Developmental Biology: A Versatile Tool for High-Contrast 3D Imaging at Histological Resolutions. *Dev. Dyn.* **238,** 632–640, doi: 10.1002/dvdy.21857 (2009).
10. Sharir, A., Ramniceanu, G. & Brumfeld, V. High Resolution 3D Imaging of *Ex-Vivo* Biological Samples by Micro CT. *J. Vis. Exp.* **52,** 2699, doi: 10.3791/2688 (2011).
11. Jeffery, N. S., Stephenson, R. S., Gallagher, J. A. & Cox, P. G. Micro-computed tomography with iodine staining resolves the arrangement of muscle fibres. *J. Biomech.* **44,** 189–192, doi: 10.1016/j.jbiomech.2010.08.027 (2011).
12. Johnson, J. T. *et al.* Virtual Histology of Transgenic Mouse Embryos for High-Throughput Phenotyping. *PLoS Genet.* **2,** e61, doi: 10.1371/journal.pgen.0020061 (2006).
13. Li, X., Anton, N., Zuber, G. & Vandamme, T. Contrast agents for preclinical targeted X-ray imaging. *Adv. Drug Deliv.* **76,** 116–133, doi:10.1016/j.addr.2014.07.013 (2014).
14. Mizutani, R. & Suzuki, Y. X-ray microtomography in biology. *Micron* **43,** 104–115, doi: 10.1016/j.micron.2011.10.002 (2012).
15. Pai, V. M. *et al.* Coronary artery wall imaging in mice using osmium tetroxide and micro-computed tomography (micro-CT). *J. Anat.* **220,** 514–524, doi: 10.1111/j.1469-7580.2012.01483.x (2012).
16. Llopart, X., Ballabriga, R., Campbell, M., Tlustos, L. & Wong, W. Timepix, a 65k programmable pixel readout chip for arrival time, energy and/or photon counting measurements. *Nucl. Instr. Meth.* A **581,** 485–484, doi: 0.1016/j.nima.2007.08.079 (2007).
17. Henrich, B. *et al.* PILATUS: A single photon counting pixel detector for X-ray applications. *Nucl. Instr. Meth. A* **607,** 247–249, doi: 10.1016/j.nima.2009.03.200 (2009).
18. Dinapoli, R. *et al.* EIGER: Next generation single photon counting detector for X-ray applications. *Nucl. Instr. Meth. A* **650,** 79–83, doi: doi:10.1016/j.nima.2010.12.005 (2011).
19. Berar, J. F. *et al.* XPAD3 hybrid pixel detector application. *Nucl. Instr. Meth. A* **607,** 23 –235, doi: 10.1016/j.nima.2009.03.208 (2009).
20. Bellazzini, R. *et al.* Chromatic X-ray imaging with a fine pitch CdTe sensor coupled to a large area photon counting pixel ASIC. *J. Instrum.* **8,** C02028, doi: 10.1088/1748-0221/8/02/C022028 (2013).

21. Jakubek, J. Data processing and image reconstruction methods for pixel detectors. *Nucl. Instr. Meth. A* **576,** 223–234, doi: 10.1016/j.nima.2007.01.157 (2007).
22. Jakubek, J. *et al.* Large area pixel detector WidePIX with full area sensitivity composed of 100 Timepix assemblies with edgeless sensors. *J. Instrum.* **9,** C04018, doi: 10.1088/1748-0221/9/04/C04018 (2014).
23. Shirai, R. *et al.* Enhanced renal image contrast by ethanol fixation in phase-contrast X-ray computed tomography. *J. Synchrotron Radiat.* **21,** 795–800, doi: 0.1107/S1600577514010558 (2014).
24. Takeda, T. *et al.* Ethanol fixed brain imaging by phase-contrast X-ray technique. *J. Phys. Conf. Ser.* **425,** 022004, doi: 10.1088/1742-6596/425/2/022004 (2013).
25. Momose, A., Takeda, T., Itai, Y. & Hirano, K. Phase-contrast x-ray computed tomography for observing biological soft tissues. *Nat. Med.* **2,** 473–475, doi: 10.1038/nm0496-473 (1996).
26. Pfeiffer, F., Weitkamp, T., Bunk, O. & David, C. Phase retrieval and differential phase-contrast imaging with lowbrilliance x-ray sources. *Nat. Phys.* **2,** 258–261, doi: 10.1038/nphys265 (2006).
27. Schulz, G. *et al.* Multimodal imaging of human cerebellum - merging X-ray phase microtomography, magnetic resonance microscopy and histology. *Sci. Rep.* **2,** 826, doi: 10.1038/srep00826 (2012).
28. Hagen, C. K. *et al.* High contrast microstructural visualization of natural acellular matrices by means of phase-based x-ray tomography. *Sci. Rep.* **5,** 18156, doi: 10.1038/srep18156 (2015).
29. Schleede, S. *et al.* Emphysema diagnosis using X-ray dark-field imaging at a laser-driven compact synchrotron light source. *Proc. Natl. Acad. Sci. USA* **44,** 17880–17882, doi: 10.1073/pnas.1206684109 (2012).
30. Bech, M. *et al. In-vivo* dark-field and phase-contrast x-ray imaging. *Sci. Rep.* **3,** 3209, doi: 10.1038/srep03209 (2013).
31. Lai, B. *et al.* Development of a hard x-ray imaging microscope. *Rev. Sci. Instrum.* **66,** 2287–2289, doi: 10.1063/1.1145666 (1995).
32. Wilhein, T. *et al.* Differential interference contrast x-ray microscopy with submicron resolution. *Appl. Phys. Lett.* **78,** 2082–2084, doi: 10.1063/1.1360776 (2001).
33. Dudak, J. *et al.* Evaluation of sample holders designed for long-lasting X-ray micro-tomographic scans of *ex-vivo* soft tissue samples. *J. Instrum.* **11,** C03005, doi: 10.1088/1748-0221/11/03/C03005 (2016).
34. Dudak, J. *et al.* X-ray micro-CT scanner for small animal imaging based on Timepix detector technology. *Nucl. Instr. Meth. A* **773,** 81–86, doi: 10.1016/j.nima.2014.10.076 (2015).
35. Jakubek, J., Holy, T., Jakubek, M., Vavrik, D. & Vykydal, Z. Experimental system for high resolution X-ray transmission radiography. *Nucl. Instr. Meth. A* **563,** 278–281, doi: doi:10.1016/j.nima.2006.01.033 (2006).
36. Vavrik, D. & Jakubek, J. Radiogram enhancement and linearization using the beam hardening correction method. *Nucl. Instr. Meth. A* **607,** 212–214, doi: 10.1016/j.nima.2009.03.156 (2009).
37. Münch, B., Trtik, P., Marone, F. & Stampanoni, M. Stripe and ring artefact removal with combined wavelet-Fourier filtering. *Opt. Express* **17,** 8567–8591 (2009).
38. Loening, A. M. & Gambhir, S. S. AMIDE: a free software tool for multimodality medical image analysis. *Mol. Imaging* **2,** 131–137, doi: 10.1162/153535003322556877 (2003).
39. Bruker MicroCT. Volume rendering. (2016) Available at: http://bruker-microct.com/products/ctvox.htm (Accessed: 14th March 2016).

Acknowledgements

Work funded by grant TA04011329 of the Technology agency of the Czech Republic. The authors thank Carlos Granja for remarks and reading the manuscript. Research performed in frame of the Medipix Collaboration. Use of laboratory animals was approved by Ethical Committee of the Third Faculty of Medicine, Charles University in Prague. The animals were treated with accordance to guidelines defined by Ethical Committee in decisions no. 246/1992 and no. 419/2012.

Author Contributions

J.D., J.Z. and F.K. conceived the experiments and developed the imaging methodology. J.D. and J.Ka. carried out micro-CT measurements. M.P., P.Z. and J.M. prepared biologic samples including the staining procedures. J.D. processed the acquired data including tomographic reconstructions and final visualizations. J.Z. implemented the OSEM-based tomographic reconstruction algorithm used. J.D. and F.K. prepared the manuscript. Z.H., J.Kv., J.D. and J.Ka. performed comparative scans of mouse organs and processed the data. All authors analysed the results and contributed to the manuscript.

Additional Information

Supplementary information accompanies this paper at http://www.nature.com/srep

Competing financial interests: The authors declare no competing financial interests.

How to cite this article: Dudak, J. *et al.* High-contrast X-ray micro-radiography and micro-CT of ex-vivo soft tissue murine organs utilizing ethanol fixation and large area photon-counting detector. *Sci. Rep.* **6**, 30385; doi: 10.1038/srep30385 (2016).

5.4. Ethanol fixation method for heart and lung imaging in micro-CT

Citace: **PATZELT, Matěj**; MRZÍLKOVÁ, Jana; DUDÁK, Jan; KREJČÍ, František; ŽEMLIČKA, Jan; KARCH, Jakub; MUSIL, Vladimír; ROSINA, Jozef; SÝKORA, Viktor; HOREHLEĎOVÁ, Barbora; ZACH, Petr. Ethanol fixation method for heart and lung imaging in micro-CT. *Japanese Journal of Radiology*. 2019, **37**(6), 500-510. ISSN 1867-1071. DOI: 10.1007/s11604-019-00830-6. **IF: 1.5/2018.**

5.4.1. Úvod a metodika

Zobrazení měkkých tkání v mikro-CT je náročné hlavně z důvodu jejich nízkého vnitřního kontrastu. Pro zvýšení jejich kontrastu bylo během posledních let vyvinuto velké množství kontrastních látek. Ty jsou však velmi často drahé, náročné na přípravu či odborný personál, časově náročné nebo dokonce toxické. Cílem této studie bylo vytvořit metodiku jednoduché a levné fixace ex-vivo měkkých tkání etanolem a výsledky porovnat s nativními kontrolami. Jako vhodné fixační činidlo byl zvolen etanol. Ve studii bylo použito 30 geneticky modifikovaných myší C57BL/6, kterým byly posmrtně odebrány plíce a srdce. Pro fixaci v etanolu byly vytvořeny tři protokoly – fixace v 97% etanolu, 50% etanolu a ve vzestupné řadě etanolu o koncentracích 25%, 50%, 75% a 97%, kdy v každé lázni byl vzorek fixován po dobu 12 hodin. Srdce a plíce ze tří myší promyté ve fyziologickém roztoku sloužily jako nativní kontroly. Vzorky byly snímány po 72, 168 a 336 hodinách fixace a každý vzorek byl snímán pouze jednou. Před snímáním se na 40 minut nechal každý vzorek při pokojové teplotě vyschnout, tak aby v dutých systémech vzorků nezůstala žádaná kapalina. Dostatečné vyschnutí se ukázalo jako klíčové, tak aby se všechen etanol vypařil a dutiny zůstaly naplněné vzduchem a bylo možné využít přirozeného kontrastu mezi vzduchem a tkání. Všechny vzorky byly během snímání umístěny v dvojkomorovém držáku, který byl popsán v předchozí publikaci. Pro snímání byly použity dva protokoly – jednodušší protokol, jehož výsledkem byly 2D snímky - mikroradiografie vzniklé sumací, druhým protokolem bylo klasické tomografické zobrazení s následnou 3D rekonstrukcí. Po snímání byly vzorky dále zpracovány histologicky a vzniklé řezy byly barveny Heatoxylin-Eosin a Weigert van Gieson. Dále se ve studii zkoumal vliv etanolu na objem vzorku, kdy při

fixaci v etanolu dochází k nevyhnutelnému smršťování vzorku. Před a po fixaci byly měřeny rozměry vzorků a také jejich objem. Zvýšení kontrastu bylo měřeno výpočtem relativního rozdílu kontrastu s výsledným kontrastním číslem (Pauwels et al. 2013), pro subjektivní hodnocení snímků byla použita Likertova škála.

5.4.2. Výsledky, diskuze a závěr

Etanol funguje jako skvělé fixační činidlo, žádný ze zkoumaných orgánů nejevil známky hniloby či rozpadu. V případě srdce všechny 2D snímky (mikroradiografie) srdcí fixovaných v etanolu zobrazily více detailů vnitřní struktury než snímky nativních srdcí, konkrétně se jednalo o svalová vlákna, levou a pravou komoru, levé a pravé ouško a jejich trámčitá svalovina či papilární svaly. Topografie a následná 3D rekonstrukce dále zobrazila srdeční chlopně, šlašinky, svalové trámce a jimi vytvořený srdeční vír. U fixace srdce v 97% etanolu bylo pozorováno výrazné ztvrdnutí vzorků, u dvou vzorků se dokonce objevily ruptury. Nejlepšího zobrazení detailů vnitřní struktury srdce bylo dosaženo po fixaci po dobu 168 hodin. U fixace srdce v 50% etanolu byly vzorky výrazně měkčí než při fixaci v 97%, také nebyly zpozorovány žádné ruptury. Nicméně zobrazení detailů vnitřní struktury nedosahovalo kvalit 97% fixace, a to ani po dvoutýdenní fixaci. V případě fixace srdce ve vzestupné řadě koncentrací etanolu bylo pozorováno ztvrdnutí vzorků podobné jako u 97% etanolu, nicméně nebyly pozorovány žádné ruptury. Zvýšení kontrastu se již po 72hodinách vyrovnala nejlepším výsledkům 97% etanolu, po 168 hodinové fixaci bylo zvýšení kontrastu nejlepší v rámci všech sledovaných koncentrací. Při srovnání tomografie s histologickým řezem, bylo na tomografii dokonce patrné více struktur než na histologickém preparátu.

V případě plic snímky nativních vzorků zobrazily, díky přirozenému kontrastu vzduch-tkáň, část vnitřní struktury – tracheu, primární bronchus a jeho první dělení. Mikroradiografie vzorků fixované v etanolu však zobrazily vnitřní struktury plic podstatně lépe. Zobrazeny byly navíc lobární bronchy a alveoly. Tomografie a následná 3D rekonstrukce dále zobrazila karinu průdušnice, okraje jednotlivých laloků a lalůčků a periferní větvení bronchů. Při fixaci v 97% byly účinky etanolu na vzorek téměř identické jako na vzorek srdce, nejlepších výsledků bylo dosaženo po 168 hodinové fixaci. U fixace plic v 50% etanolu došlo k výraznému zvýšení kontrastu až po 168, respektive po 336 hodinové fixaci, nicméně ani dvoutýdenní

fixace nedosáhla zvýšení kontrastu lepšího než u 97% etanolu. Výhodou fixace v 50% etanolu bylo, stejně jako u srdce, menší ztvrdnutí vzorků a nepřítomnost ruptur. V případě fixace plic ve vzestupné řadě koncentrací etanolu bylo pozorováno ztvrdnutí vzorků podobné jako u 97% etanolu, nicméně nebyly pozorovány žádné ruptury. Nejlepší zvýšení kontrastu bylo dosaženo po 336 hodinové fixaci. Při srovnání tomografie s histologickým řezem, bylo na tomografii patrné více struktur než na histologickém preparátu.

Etanolová metoda fixace ex-vivo měkkých tkání je levná a jednoduchá metoda, která může být použita jednak jako fixační činidlo měkkých tkání, tak i jako kontrastní látka. Velkou výhodou této metody je, že neničí vzorky a ty jsou tudíž dále k dispozici k dalším vyšetřením, jako je klasická histologie či imunohistochemie. Další nespornou výhodou je její jednoduchost, není k ní potřeba speciálně proškolený personál a navíc lze použít i v případě klinického výzkumu, kdy stačí například chirurgovi, aby daný vzorek vložit do zkumavky s etanolem a zapsal čas. Další výzkum bude probíhat se zaměřením na snížení doby fixace vzorků.

Obr. 7 Mikroradiografie srdce myši. Srdce bylo fixováno ve vzestupné řadě koncentrací etanolu po dobu 168 hodin.

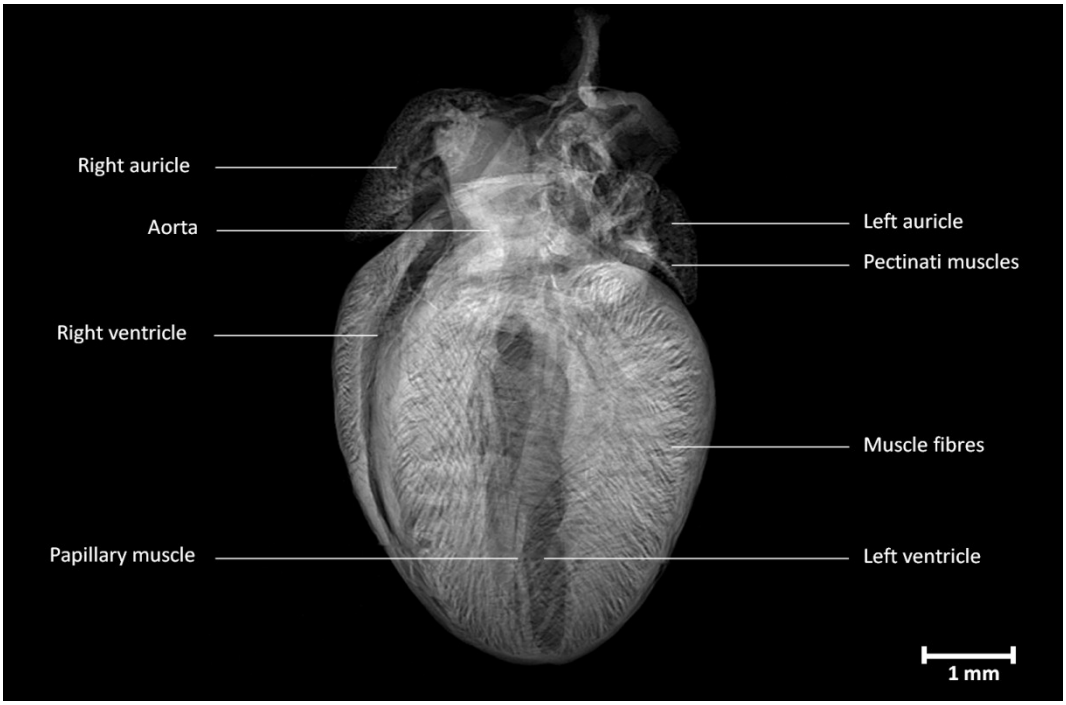

Obr. 8 Mikroradiografie srdce myši. Porovnání nativního srdce (vlevo) s fixovanými srdci. A – srdce fixovaná v 97% etanolu, B – srdce fixovaná v 50% etanolu, C – srdce fixovaná ve vzestupné řadě koncentrací etanolu

Obr. 9 Srovnání tomografie a klasické histologie u srdce fixovaného ve vzestupné řadě koncentrací etanolu. A, C – 3D rekonstrukce, B – klasická histologie, barvení Hematoxylin-eosin.

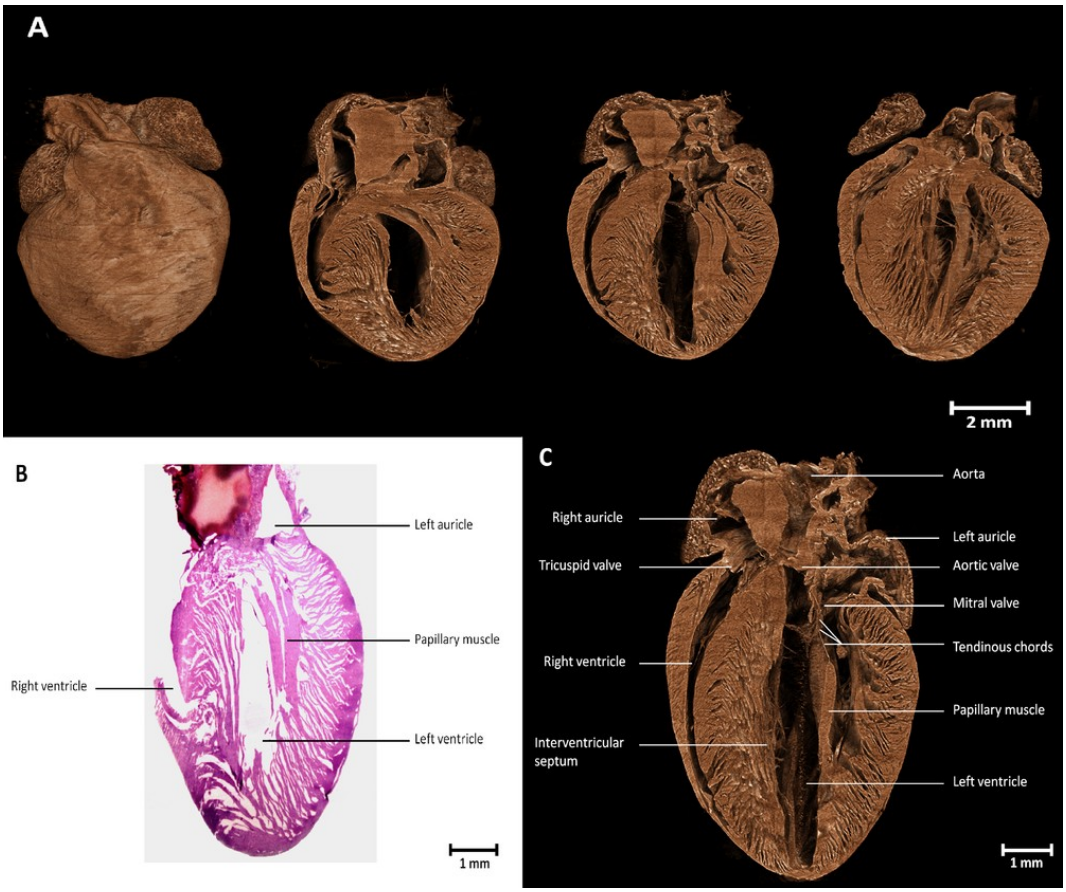

Obr. 10 Mikroradiografie plic myši. Plíce byly fixovány ve vzestupné řadě koncentrací etanolu po dobu 336 hodin.

Obr. 11 Mikroradiografie plic myši. Porovnání nativních plic (vlevo) s fixovanými plícemi. A – plíce fixované v 97% etanolu, B – plíce fixované v 50% etanolu, C – plíce fixované ve vzestupné řadě koncentrací etanolu

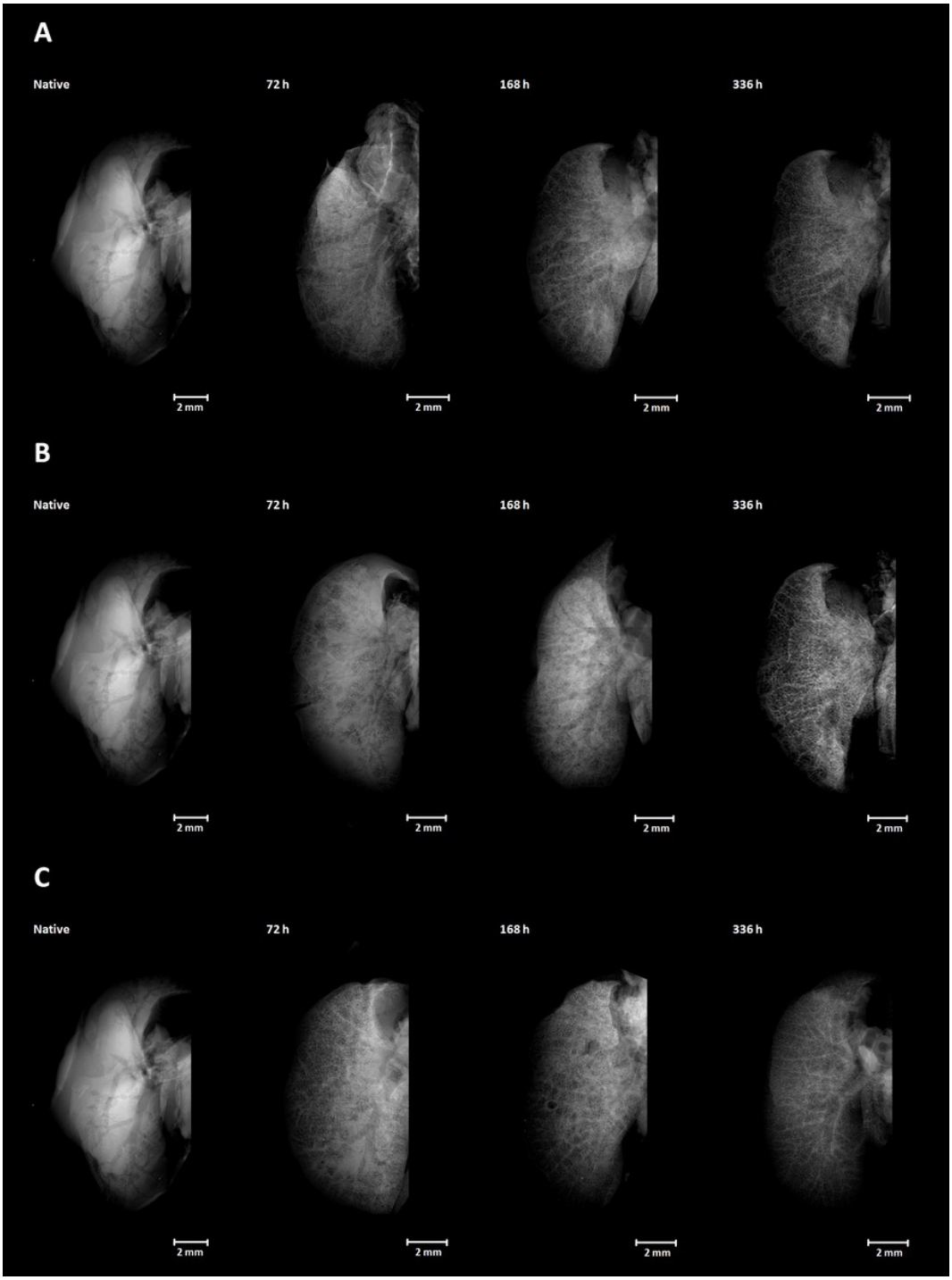

Obr. 12 Srovnání tomografie a klasické histologie u plic myši fixovaných ve vzestupné řadě koncentrací etanolu. A, C – 3D rekonstrukce, B – klasická histologie, barvení Weigert van Gieson.

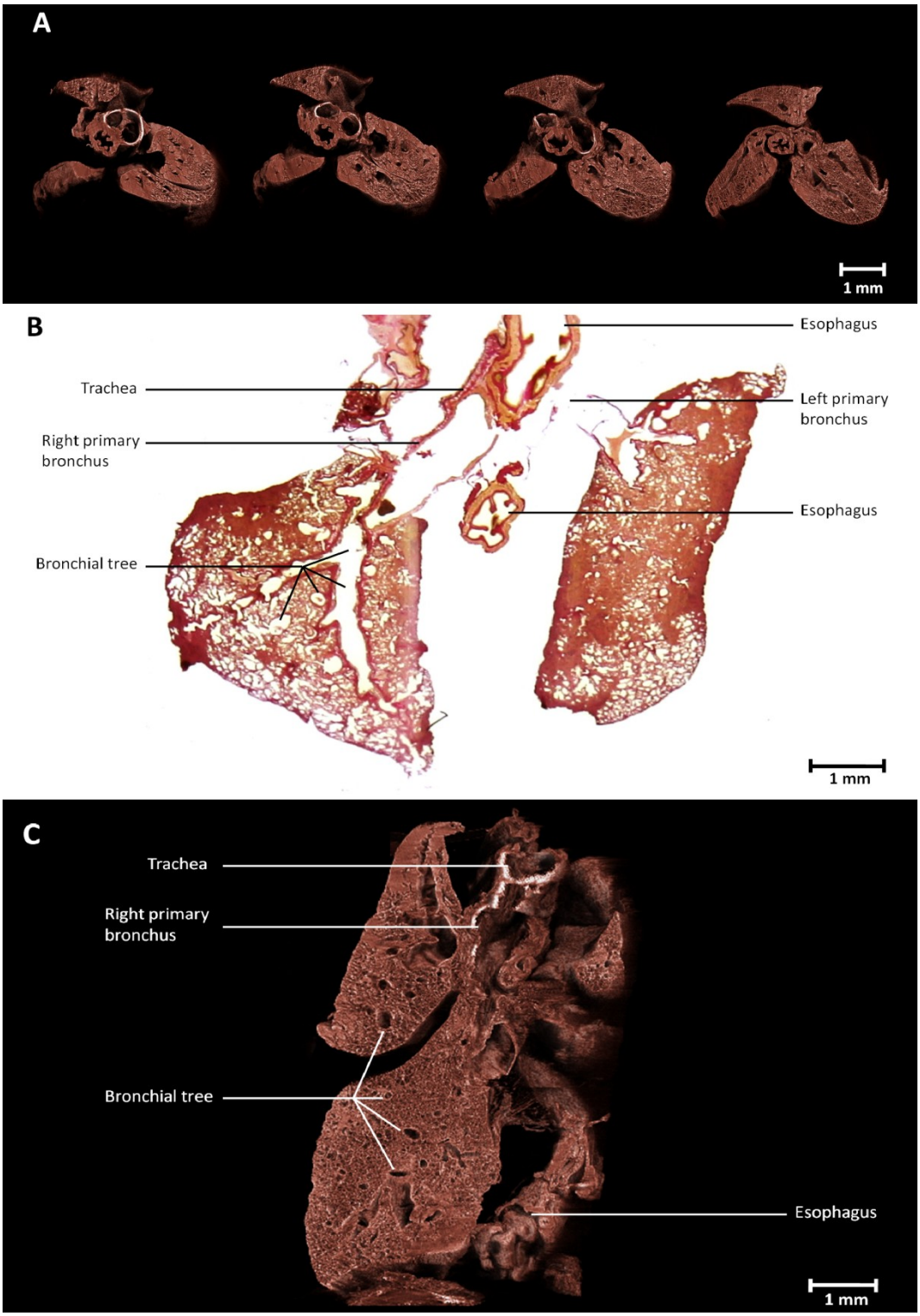

Japanese Journal of Radiology
https://doi.org/10.1007/s11604-019-00830-6

ORIGINAL ARTICLE

Ethanol fixation method for heart and lung imaging in micro-CT

Matej Patzelt[1,2,3] · Jana Mrzilkova[1,2,3] · Jan Dudak[1,2,4,5] · Frantisek Krejci[1,2,4] · Jan Zemlicka[1,2,4] · Jakub Karch[1,2,4,5] · Vladimir Musil[1,2,3,6] · Jozef Rosina[1,2,5,7] · Viktor Sykora[8] · Barbora Horehledova[9] · Petr Zach[1,2,3]

Received: 21 November 2018 / Accepted: 8 March 2019

Abstract

Purpose The soft tissue imaging in micro-CT remains challenging due to its low intrinsic contrast. The aim of this study was to create a simple staining method omitting the usage of contrast agents for ex vivo soft tissue imaging in micro-CT.

Materials and methods Hearts and lungs from 30 mice were used. Twenty-seven organs were either fixed in 97% or 50% ethanol solution or in a series of ascending ethanol concentrations. Images were acquired after 72, 168 and 336 h on a custom-built micro-CT machine and compared to scans of three native samples.

Results Ethanol provided contrast enhancement in all evaluated fixations. Fixation in 97% ethanol resulted in contrast enhancement after 72 h; however, it caused hardening of the samples. Fixation in 50% ethanol provided contrast enhancement after 336 h, with milder hardening, compared to the 97% ethanol fixation, but the visualization of details was worse. The fixation in a series of ascending ethanol concentrations provided the most satisfactory results; all organs were visualized in great detail without tissue damage.

Conclusions Simple ethanol fixation improves the tissue contrast enhancement in micro-CT. The best results can be obtained with fixation of the soft tissue samples in a series of ascending ethanol concentrations.

Keywords Ethanol · Micro-CT · Mice · Heart · Lungs

✉ Jana Mrzilkova
jana.mrzilkova@lf3.cuni.cz

1 Specialized Laboratory of Experimental Imaging, Third Faculty of Medicine, Charles University, Prague, Czech Republic

2 Institute of Experimental and Applied Physics and Faculty of Biomedical Engineering, Czech Technical University in Prague, Prague, Czech Republic

3 Department of Anatomy, Third Faculty of Medicine, Charles University, Ruska 87, 100 34 Prague, Czech Republic

4 Institute of Experimental and Applied Physics, Czech Technical University in Prague, Prague, Czech Republic

5 Faculty of Biomedical Engineering, Czech Technical University in Prague, Kladno, Czech Republic

6 Centre of Scientific Information, Third Faculty of Medicine, Charles University, Prague, Czech Republic

7 Department of Medical Biophysics and Informatics, Third Faculty of Medicine, Charles University, Prague, Czech Republic

8 Center for Experimental Biomodels, First Faculty of Medicine, Charles University, Prague, Czech Republic

9 Department of Radiology and Nuclear Medicine, Maastricht University Medical Center, Maastricht, The Netherlands

Introduction

Microcomputed tomography (micro-CT) is identical in its basic principles to a medical CT [1]. It uses X-ray attenuation data acquired from multiple projection angles and provides non-destructive 3D information of the inner structures of the investigated organs or tissues [2, 3]. Although it is nowadays possible to perform in vivo micro-CT scans of small animals, ex vivo scans of individual inner organs achieve still much higher spatial resolution and, therefore, provide better information on fine anatomical structures. State-of-the-art micro-CT systems provide spatial resolution down to several micrometers or even with sub-micron resolution in the case of laboratory-scale devices or using synchrotron radiation, respectively. The contrast in micro-CT arises from the attenuation of X-rays by absorption or scattering processes in examined objects [4]. Typically, highly mineralized structures, such as bones or teeth, which contain calcium phosphate minerals, give very good contrast in micro-CT.

Conversely, imaging of soft tissues such as nerves, muscles, adipose tissue or ligaments is quite challenging [5].

Published online: 14 March 2019

It is mainly due to low intrinsic X-ray contrast of soft tissues, which contain mainly low-atomic-number elements (carbon, hydrogen, oxygen), so it is necessary to use X-ray-absorbing contrast agents [1]. During the past years, several staining methods have been developed to increase the contrast of soft tissue structures [6]. However, most of these methods are complicated, time-consuming and some even use toxic contrast agents. One of the best and most widely used contrast agents for soft tissue contrast enhancement is aqueous solutions of osmium tetroxide (OsO_4), phosphomolybdic acid (PMA) or phosphotungstic acid (PTA) [5]. OsO_4 is very toxic, does not stain well if samples have been in alcohol and also its penetration is relatively slow. PTA also penetrates the tissues slowly, but it is less toxic, simpler to use and stains effectively alcohol-stored samples [1]. PMA gives better contrast among different tissues, but requires longer incubation [6].

Currently, micro-CT imaging of the heart mainly focuses on depicting healthy or damaged coronary arteries. For ex vivo imaging, a radio-opaque polymer blend (Microfil) is injected into the heart vasculature [7] or the OsO_4 fixation of the heart is used [8]. In vivo studies of the vascular system of mice usually apply intravenous iodine contrast agent [9]. The heart was also visualized in studies of embryos, where either iodine staining [10, 11] or OsO_4 fixation was used [6].

Regarding lungs, current studies mainly focus on in vivo imaging of pathologically changed mice lungs, to capture longitudinal information about the progression of the illness in preclinical models [12, 13]. These studies mainly aim to image lung tumors, using contrast agents such as gold nanoparticles or liposomal iodine [14] or lung fibrosis [15]. The imaging of healthy lungs was performed in studies evaluating structural differences between different mouse phenotypes [16].

Regardless of the assessed organ, an ideal contrast agent should be easily administered and have the ability to equally penetrate through the thick tissue layers [17]. Ethanol, currently used as a medium for a conservation of the samples or as a liquid medium for samples during scanning, showed potential to fulfill these criteria [1]. Takeda et al. [18] used 100% ethanol perfusion in rat brain for contrast enhancement during micro-CT acquisition with phase-contrast X-ray technique. A 100% ethanol solution was also used in the study by Shirai et al. [19], for kidney imaging in phase-contrast X-ray computed tomography. To our best knowledge, there is no study using only pure ethanol as a contrast medium for X-ray imaging of soft tissue based on absorption contrast.

The aim of this study was to evaluate whether ethanol would be a suitable contrast agent for ex vivo staining of the heart and lungs prior to micro-CT imaging based on absorption contrast.

Materials and methods

Tissue sample origins

The organs of 30 C57BL/6 genetically modified male mice (weight 17–20 g) were harvested for the purpose of this study. Mice were killed by cervical dislocation under the halothane anesthesia. Use of laboratory animals was approved by the local Ethical Committee of First and Third Faculty of Medicine, Charles University, Prague, Czech Republic. The animals were treated in accordance with the guidelines defined by the ethical committee, which follows The National Advisory Committee for Laboratory Animal Research (NAC LAR) guidelines.

Tissue sample fixation

Three different ethanol fixation protocols were used. Nine specimens were fixed with either protocol A, B or C. Protocol A and B used ethanol solution with a fixed concentration of 97% or 50%, respectively. Protocol C consisted of four consequent ethanol baths, each with increasing ethanol concentrations in the solution. Samples were fixed in 12-h steps, using ethanol solutions with ascending concentrations of 25%, 50%, 75% and 97%, respectively. The expected outcome after immersion in ethanol was shrinkage of the specimens [2], which was supposed to be different in various types of fixations.

After the scanning was complete, we stored the samples for 6 months at a 4 °C environment to evaluate the long-term fixation effect on the specimens.

Hearts and lungs from 3 mice were carefully harvested and then put into phosphate-buffered saline (PBS solution) for 2 h and then scanned as native specimens. These organs served as a reference set of samples to the examined ethanol fixation protocols.

Tissue sample imaging

Each sample was scanned just once, to avoid distortion of the results due to changes of the specimen volume during scanning. The imaging was performed systematically after 72 h, 168 h and 336 h of fixation. The 72-h time point was chosen according to an experiment based on the basic protocols for histological processing of the samples. To investigate the effect of long-term ethanol fixation on the specimens, additional scans were performed at the 168- and 336-h time points.

Before the scanning, the fixed organs were placed on a gauze at an air temperature of 23 °C to dry. The optimal length of tissue drying period was determined with the

previous experiment, where the organs were scanned in 2 min intervals during the drying period. With increasing drying time, more details became visible in distal parts of the organ. A period of 40 min provided the best visualization of details in both heart and lungs, as it allowed the redundant ethanol to vaporize from the whole organ including the vessels, ventricles, and other cavities. These structures, normally filled with liquid, became hollow during this time, and, due to ethanol that caused tissue stiffness, the cavities did not collapse. The air-tissue transition then produces a detectable absorption contrast. When the drying period was completed, the organs were positioned in a dedicated plastic holder with an ethanol reservoir. This device provided a stable environment with ethanol vapor and thus prevented structural changes of the organs during imaging [20].

The imaging protocol was identical for the ethanol fixed and native specimens.

Two different consecutive imaging protocols were used. First, X-ray micro-radiography of each sample using 60 kVp unfiltered tungsten spectrum and with 22 µm effective pixel size (EPS) was performed. This acquisition resulted in a 2D projection. Second, a micro-CT acquisition using the same X-ray spectrum but with a resolution higher than 10 µm delivered a 3D reconstruction of the specimen.

The data were acquired with an emphasis on high CNR. Therefore, the acquisition time was individually adjusted to achieve at least 10^5 or 10^4 detected photons per pixel behind the object in the case of a micro-radiography or a micro-CT projection, respectively. Micro-CT datasets were acquired with a total of 720 projections with 0.25° angle step. The data were transformed from the intensity domain to equivalent material thickness using a beam hardening correction designed for photon-counting detectors (PCDs) [21]. CT reconstructions were performed using the Volex reconstruction engine (courtesy of Fraunhofer ISS and Technology, Germany).

All CT data were evaluated in CTVox software [22].

Volume and shrinkage measurements

The shrinkage of the specimens was counted from the measurements of the three dimensions (height, length, depth) of the specimens with a sliding scale. Additionally, the volume of the specimen was assessed following the methodology used by Vickerton et al. [2]. Briefly, the volume of the specimen was measured in the water-filled tube, according to the rise in the level of water. The native dimensions of the specimens were assessed immediately after explantation. Dimensions of the fixed samples were assessed at the end of the fixation period. Each measurement was repeated five times. The percentage of shrinkage was calculated from the change of the volume and the dimensions between native and fixed sample.

Histological processing

Each organ was also processed histologically, to compare non-destructive soft tissue visualization obtained from micro-CT with conventional histology.

Samples originally fixed with one of the ethanol fixation protocols were first put in a 10% formalin solution for 2 h at 37 °C. Second, a dehydration process in six baths of alcohol (97% alcohol–benzene) for a total of 6 h at 37 °C was carried out. Third, the samples were fixed with alcohol–xylene 1:1 solution for 1 h at 45 °C, followed by two baths in xylene, in total for 2 h at 45 °C. Fourth, the samples were put in three paraffin baths for 5 h at a temperature of 60 °C and embedded in paraffin blocks. Fifth, after cutting paraffin blocks into slices, these were rehydrated again. Lastly, slices were stained with hematoxylin–eosin and Weigert van Gieson staining method, before they could be evaluated under a standard light microscope and binocular magnifying glass.

Scoring of the contrast enhancement

For a quantitative comparison of the microradiographies, the contrast number was adopted from Pauwels et al. [17]. In hearts, the relative contrast difference between the right ventricle of the heart and its wall was calculated from the mean gray value in Pixelman Software (IEAP CTU Prague) [23]. It was calculated with a formula $C = (G_1 - G_2)/G_1$, where G_1 represents the mean gray value of the right ventricle and G_2 is the mean gray value of the wall of the right ventricle.

The same process was done in the lungs, where contrast was calculated between the alveolar sac and its wall. The same formula was used, where G_1 is the mean gray value of the cavity of the alveolar sac and G_2 represents the mean gray value of the wall of the alveolar sac.

The mean gray values of all microradiographies were measured in raw data before BH corrections, selecting the region of interest (ROI). The contrast was then expressed in percentages.

In the scans of both the studied organs, monitored structures were set, in order to compare the quality of scans. Muscle fibers, left and right ventricle, left and right auricle, pectinate muscles, papillary muscles and aorta were set as monitored structures in the heart samples. Trachea, primary bronchus, lobar bronchus and alveolar sacs were set as monitored structures in lungs.

The subjective image quality was evaluated using a 4-point Likert scale: grade 1 = no monitored structures differentiation (contrast enhancement not sufficient for evaluation), grade 2 = possible to differentiate monitored structures (image sufficient for structure differentiation, although contrast enhancement is unsatisfactory), grade 3 = good (image with satisfactory contrast enhancement), grade 4 = excellent (image with optimal contrast enhancement).

Table 1 Summary of the shrinkage, calculated contrast and ruptures of the heart specimens

	Heart									
	Native	A (97%) 72 h	A (97%) 168 h	A (97%) 336 h	B (50%) 72 h	B (50%) 168 h	B (50%) 336 h	C (Asc.) 72 h	C (Asc.) 168 h	C (Asc.) 336 h
Shrinkage	No	21 ± 2%	21 ± 2%	21 ± 2%	14 ± 2%	14 ± 2%	14 ± 2%	18 ± 2%	18 ± 2%	18 ± 2%
Rupture of at least 1 specimen	No	Yes	Yes	Yes	No	No	No	No	No	No
Contrast between ventricle and muscles	12 ± 1%	29 ± 2%	34 ± 2%	31 ± 1%	14 ± 1%	20 ± 2%	24 ± 2%	30 ± 2%	36 ± 1%	33 ± 2%

Table 2 Summary of the shrinkage, contrast and ruptures of the lung specimens

	Lungs									
	Native	A (97%) 72 h	A (97%) 168 h	A (97%) 336 h	B (50%) 72 h	B (50%) 168 h	B (50%) 336 h	C (Asc.) 72 h	C (Asc.) 168 h	C (Asc.) 336 h
Shrinkage	No	18 ± 2%	18 ± 2%	18 ± 2%	12 ± 2%	12 ± 2%	12 ± 2%	15 ± 2%	15 ± 2%	15 ± 2%
Rupture of at least 1 specimen	No	Yes	Yes	Yes	No	No	No	No	No	No
Contrast between ventricle and muscles	15 ± 1%	18 ± 1%	23 ± 1%	20 ± 1%	16 ± 1%	20 ± 2%	24 ± 1%	28 ± 2%	33 ± 1%	36 ± 2%

Micro-CT apparatus

Two different custom-built micro-CT systems were used for purposes of this study. Both of them use cone-beam imaging geometry and a unique detector technology—Timepix photon-counting detectors (PCD) [24].

The basic Timepix assembly consists of a semiconductor sensor bump bonded to an electronic read-out chip composed of an array of 256 × 256 pixels with 55 µm pixel pitch. The significant advantage of the used PCD technology for low-contrast objects lies in a dark-current-free quantum-counting operation allowed by an adjustable energy threshold in each individual pixel. Thanks to these features, PCDs acquire noiseless data with virtually unlimited dynamic range. Therefore, an enormously high contrast-to-noise ratio (CNR) can be achieved. High CNR improves the detectability of low-contrast detail within the scanned object [25]. Although the pixel size of a Timepix device is 55 µm, it is possible to achieve much higher spatial resolution thanks to the cone-beam imaging geometry; point-like source of radiation produces a divergent beam of X-rays that magnifies the projection of a sample by a factor $M = \mathrm{SDD/SOD}$, where SDD is source–detector distance and SOD is source–object distance. In such case, ESP is commonly used to characterize the sampling density of the radiographic image. EPS is defined as the ratio between actual pixel size of the used detector and magnification factor M. Such an approach is generally used in the field of micro-CT for improving spatial resolution and detail detectability of the acquired data.

The first used system is equipped with a Kevex™ PXS-11 X-ray tube with focal spot size 28 µm and Timepix detector in Quad configuration (four read-out chips with a common silicon sensor providing a sensitive area 28 × 28 mm). The highest achievable spatial resolution is approx. 28 µm in this case. All presented 2D micro-radiographic images were acquired using the introduced setup [26].

The second system has been designed to provide a much higher spatial resolution and wide field of view. Thanks to a high-quality micro-focus X-ray tube Hamamatsu L8601-01 with focal spot size down to 5 µm, the setup achieves spatial resolution down to 5 µm [27]. It was recently upgraded by a large area Timepix detector built using WidePIX technology—a newly developed technique for assembling large area PCD arrays [28]. The used detector $\mathrm{WidePIX}_{10\times5}$ consists of 50 individual Timepix tiles and provides a field of view approx. 140 × 70 mm. The high-resolution setup was used for the presented micro-CT scans.

Statistical analysis

Statistical analysis was conducted using Statistical Package for Social Sciences version 23.0 (SPSS Inc., Chicago, IL, USA). One sample t test with a 2-sided α of 5% was used in this study. Continuous variables were expressed using mean values ± standard deviations (SD).

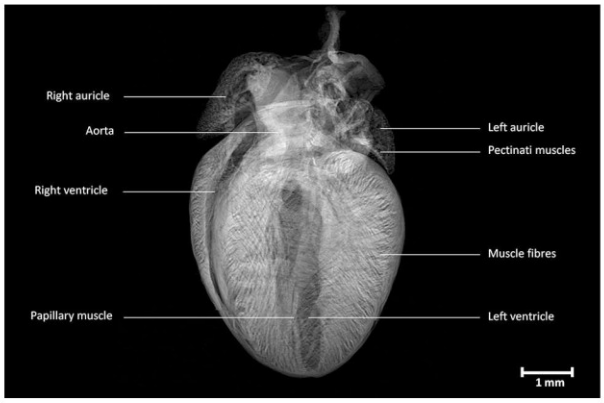

Fig. 1 High-resolution micro-radiography of a mouse heart. The heart was fixed in a series of ascending ethanol concentrations and scanned after 168 h

Results

All specimens were well fixed in ethanol; there was no sign of decomposition or rot. The quality of the tissue was not changed even after 6 months of fixation.

No scans were presented with *no monitored structures differentiation* (grade 1) or *possible to differentiate monitored structures* (grade 2). Scans of hearts and lungs fixed in 50% ethanol were scored as good (grade 3), and the rest of the scans were scored as excellent (grade 4).

The level of shrinkage, calculated contrast and also eventual rupture of the specimen are summarized in Tables 1 and 2.

Heart

Micro-radiography of a native specimen showed only the contour of the organ and no details of muscles, vessels or any other structures. As for the ethanol fixation, all evaluated fixation protocols yielded visualization of the heart in X-ray scan better compared to the native specimen. Micro-radiographs of fixed hearts depicted all monitored structures—muscle fibers, left and right ventricle, left and right auricle, pectinate muscles, papillary muscles and aorta (Fig. 1). The 3D reconstruction visualized the valves, tendinous cords and course of the muscles as heart's vortex and trabeculae, in addition to the basic structures visible on 2D micro-radiography.

In 97% ethanol fixation, the highest level of stiffness and shrinkage of the samples was observed. Due to very fast dehydration, small ruptures of the samples were observed in

two cases. Figure 2a shows a comparison of scans assessed after 72, 168 and 336 h of fixation and a native specimen.

Already after 72 h fixation, there was a significant contrast enhancement and all monitored structures were visible. The best visualization details within this ethanol concentration were, however, obtained after 168 h of fixation. Fixation for 336 h did not provide better visualization of the monitored structures or higher calculated contrast than 168 h of fixation.

With 50% ethanol fixation, all monitored structures were visualized. The sample was softer compared to the 97% ethanol protocol with no signs of rupture. Figure 2b shows a comparison of scans assessed after 72, 168 and 336 h of fixation and a native specimen.

The contrast enhancement after 72 h of fixation was only slightly better than in a native specimen. The best detailed visualization was observed after 336 h of fixation. However, fixation in 50% ethanol proved to be inferior to the 97% ethanol fixation protocol, in regard to sharp detail visualization.

The fixation in a series of ascending ethanol concentrations presented with a sample stiffness comparable to the 97% fixation protocol, but with no signs of specimen rupture. In all observed time points, a significant contrast enhancement was observed. According to calculated contrast, the best detailed visualization was reached after 168 h of fixation (Fig. 2c); however, the quality of visualization of the monitored structures was proportionate to the 72 h

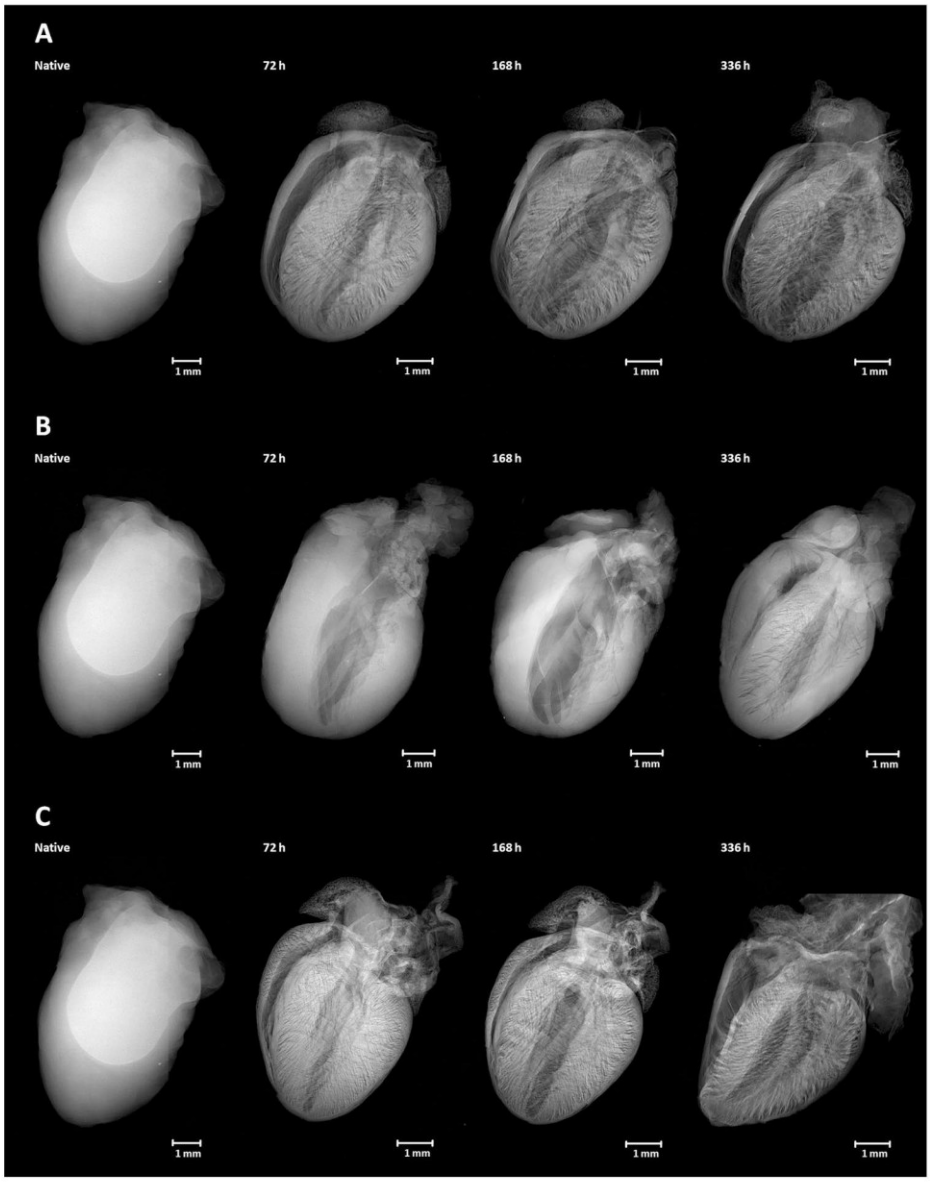

Fig. 2 X-ray micro-radiography of a mouse heart, comparing a native heart (left) to the fixed hearts (the rest). **a** Fixed in 97% ethanol for 72, 168 and 336 h, **b** fixed in 50% ethanol for 72, 168 and 336 h, **c** fixed in a series of ascending ethanol concentrations for 72, 168 and 336 h

fixation protocol. Fixation for 336 h did not provide better contrast enhancement than 168 h of fixation.

Fixation in a series of ascending ethanol concentrations provided the best detailed morphological imaging of all monitored structures of the heart.

3D reconstruction in comparison to histological samples of the heart is shown in Fig. 3. It shows the comparison between 3D micro-CT reconstruction and histological processing of a mouse heart fixed in a series of ascending ethanol concentrations and scanned after 168 h of fixation. 3D reconstructions from micro-CT scans show more of inner structures of the heart in comparison to histological processing, which, however, yielded a better resolution.

Lungs

High-resolution X-ray radiography of a native specimen showed, due to natural air-tissue contrast, not only the contour of the organ, but also a primary bronchus and its first branching. X-ray micro-radiography of fixed lungs revealed all monitored structures—trachea, primary bronchus, lobar bronchus and alveolar sacs (Fig. 4). The 3D reconstruction visualized the carina of the trachea, margins of pulmonary lobes and peripheral branching of the primary bronchus, in addition to the basic structures visualized on X-ray micro-radiography images.

The 97% ethanol fixation protocol caused significant stiffness, shrinkage and even tissue deformation of all samples. Figure 5a shows a comparison of contrast improvement in organs fixed in ethanol (72, 168 and 336 h) and in the native specimen.

After 72 h fixation, the contrast between the alveolar sac and its wall was 18 ± 1%. All monitored structured were visible. After 168 h of fixation, the best detailed visualization of all monitored structures was achieved, even with sharp details of the peripheral alveolar sacs. The fixation for 336 h provided a comparable visualization of the monitored structures as 168 h fixation protocol.

In 50% ethanol fixation, all monitored structures were visible. There was also a stiffness and shrinkage of the samples, although not that severe as with 97% concentration. There were no signs of specimen rupture. The 72 h fixation did not significantly increase the contrast between the alveolar sac and its wall compared to the native specimen.

The best detailed visualization was according to calculated contrast after 336 h of fixation; however, the contrast was only 24 ± 1%, which was essentially the same as after 168 h of fixation with 97% ethanol fixation protocol. The depiction of sharp details was inferior compared to the 97% fixation protocol (Fig. 5b).

The fixation in a series of ascending ethanol concentrations presented with a stiffness of the sample, similar to the 97% ethanol fixation protocol. In all assessed time points,

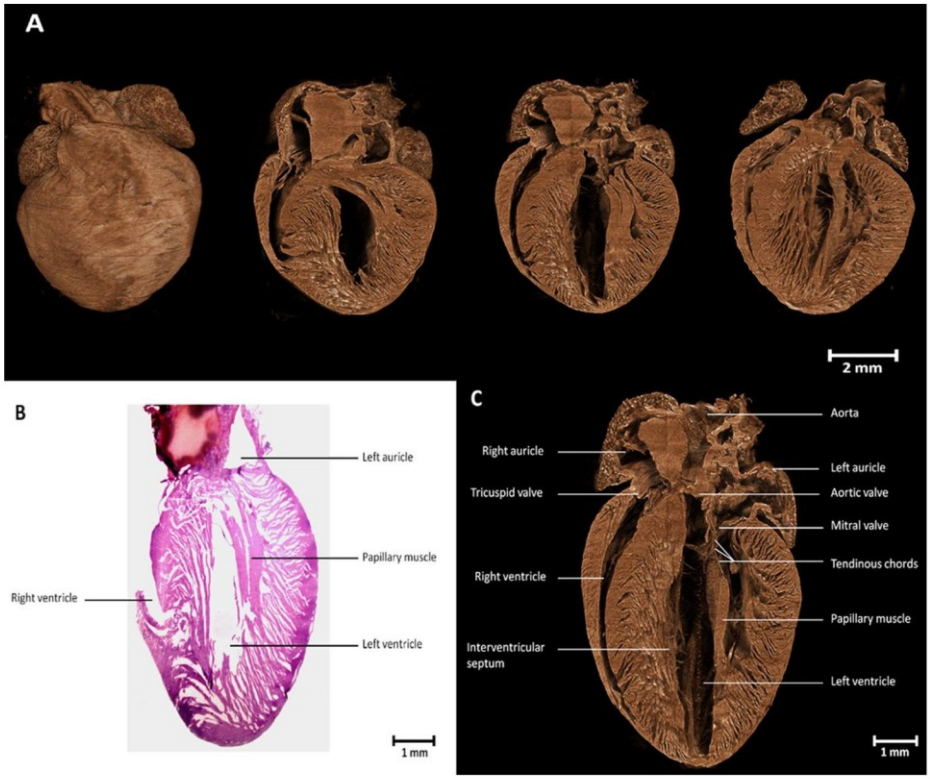

Fig. 3 Comparison between micro-CT imaging and histological processing of a mouse heart. **a** 3D micro-CT reconstruction of a mouse heart fixed in a series of ascending ethanol concentrations and scanned after 168 h; data acquired with 7.2 µm EPS. **b** Histological sample of the same mouse heart, performed after scanning in micro-CT; the sample was stained with hematoxylin–eosin. **c** 3D reconstruction of a mouse heart fixed in a series of ascending ethanol concentrations and scanned after 168 h

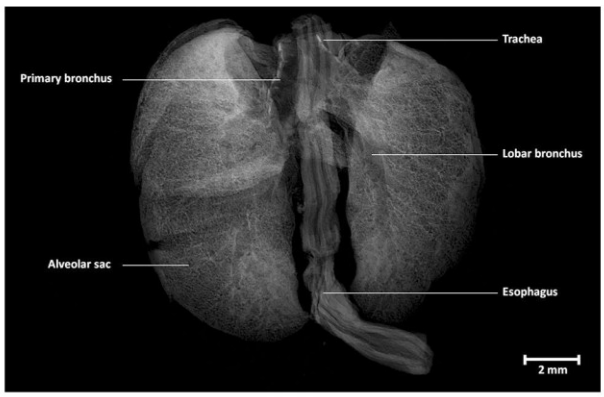

Fig. 4 X-ray micro-radiography of mouse lungs. The lungs were fixed in a series of ascending ethanol concentrations and scanned after 336 h

there was a significant contrast enhancement and adequate visualization of all monitored structures. The best detailed visualization was depicted after 336 h of fixation (Fig. 5c).

The 336 h fixation in a series of ascending ethanol concentrations provided the best detailed morphological imaging of lung structures compared to other fixation protocols.

3D reconstruction in comparison to the histological samples of the lungs is shown in Fig. 6. It has a quality between 3D X-ray micro-CT reconstruction and histological processing of mouse lungs. 3D reconstruction from micro-CT scan shows more of its inner structure; conversely, histological processing reached a better resolution.

Discussion

Soft tissue imaging with micro-CT is generally challenging due to the low intrinsic contrast of soft tissue in organs. Although several staining techniques for ex vivo use were introduced in the past years, most of these methods proved to be complicated, time-consuming and in some cases even toxic. This study clearly shows that ethanol solution can be used as a simple, cheap and stable fixation method dedicated to ex vivo soft tissue fixation prior to micro-CT imaging, while delivering improved contrast enhancement of soft tissues in organs.

We compared ethanol fixation protocols, which vary in ethanol concentration of the ethanol and in the duration of fixation. All ethanol fixation protocols used in the current study enhanced the contrast in mouse heart and lungs and provided detailed morphological information about the inner structure of these organs. Within the mouse heart, we were able to distinguish delicate structures such as the valves or tendinous cords. In the mouse lungs, even the alveoli structures were well visualized. The inner structure visualization was the main imaging drawback in the methods introduced by Descamps et al. [6], who tested OsO_4, PMA and PTA for discrimination between tissue types and organs. They managed to beautifully distinguish individual organs in embryos; however, a detailed inner structure of these organs was missing. Besides other disadvantages, OsO_4 and PTA are toxic agents and PMA requires long incubation.

PTA and OsO_4 together with inorganic iodine were also evaluated in the study by Metscher et al. [1]. Inorganic iodine is a well-known staining agent for micro-CT; it provides very good contrast among the tissues and rapidly diffuses into the specimen. The results of our current study raise question whether the ethanol solution has effect on inorganic iodine contrast enhancement or not. This is a topic for a next study.

The principle of our method is quite simple. Ethanol causes protein denaturation through the removal of the water molecule from the free carboxyl, hydroxyl, amino,

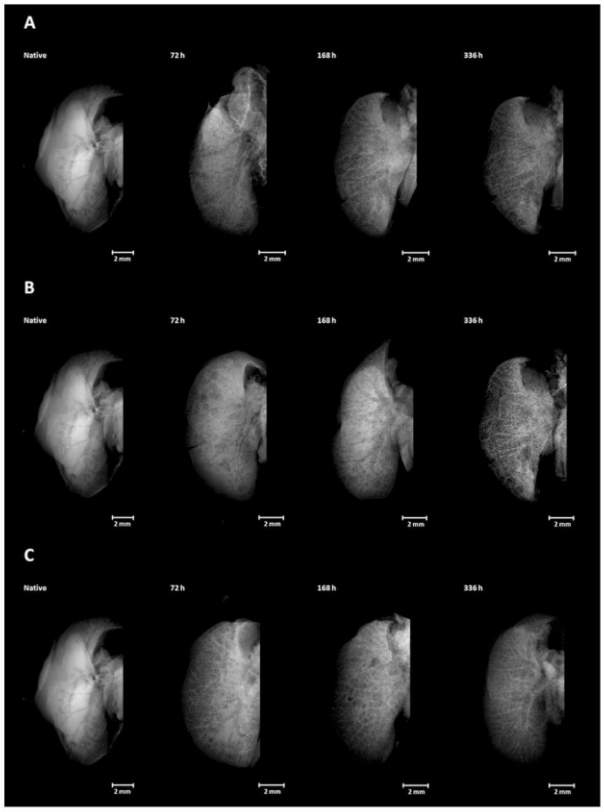

Fig. 5 X-ray micro-radiography of a mouse right lung, comparing a native right lung (left) to the fixed right lungs (the rest). **a** Fixed in 97% ethanol for 72, 168 and 336 h, **b** fixed in 50% ethanol for 72, 168 and 336 h, **c** fixed in a series of ascending ethanol concentrations and scanned after 72, 168 and 336 h

amido and imino groups of the proteins, resulting in protein coagulation and tissue shrinkage [29]. Additionally, ethanol also increases the organs' stiffness. The organ cavities and hollow spaces, therefore, do not collapse, and the air-tissue transition then produces a detectable contrast. For that reason, ethanol fixation together with a photon-counting detector provides a detailed soft tissue discrimination in the studied organs.

The great advantage lies in the noninvasive nature of this method. After the scanning is completed, tissues are still available for further staining, histochemical procedures, or classical histology. Compared to histology, our method is much simpler and also does not require slicing of the sample and consequently its destruction.

Long-term fixation of the samples in ethanol, in this study 6 months, does not have any effect on the quality of the specimens. It is, therefore, possible to scan them on several occasions, also on different micro-CT machines or in various laboratories. Owing to the simplicity of this method, there are no special requirements for qualification

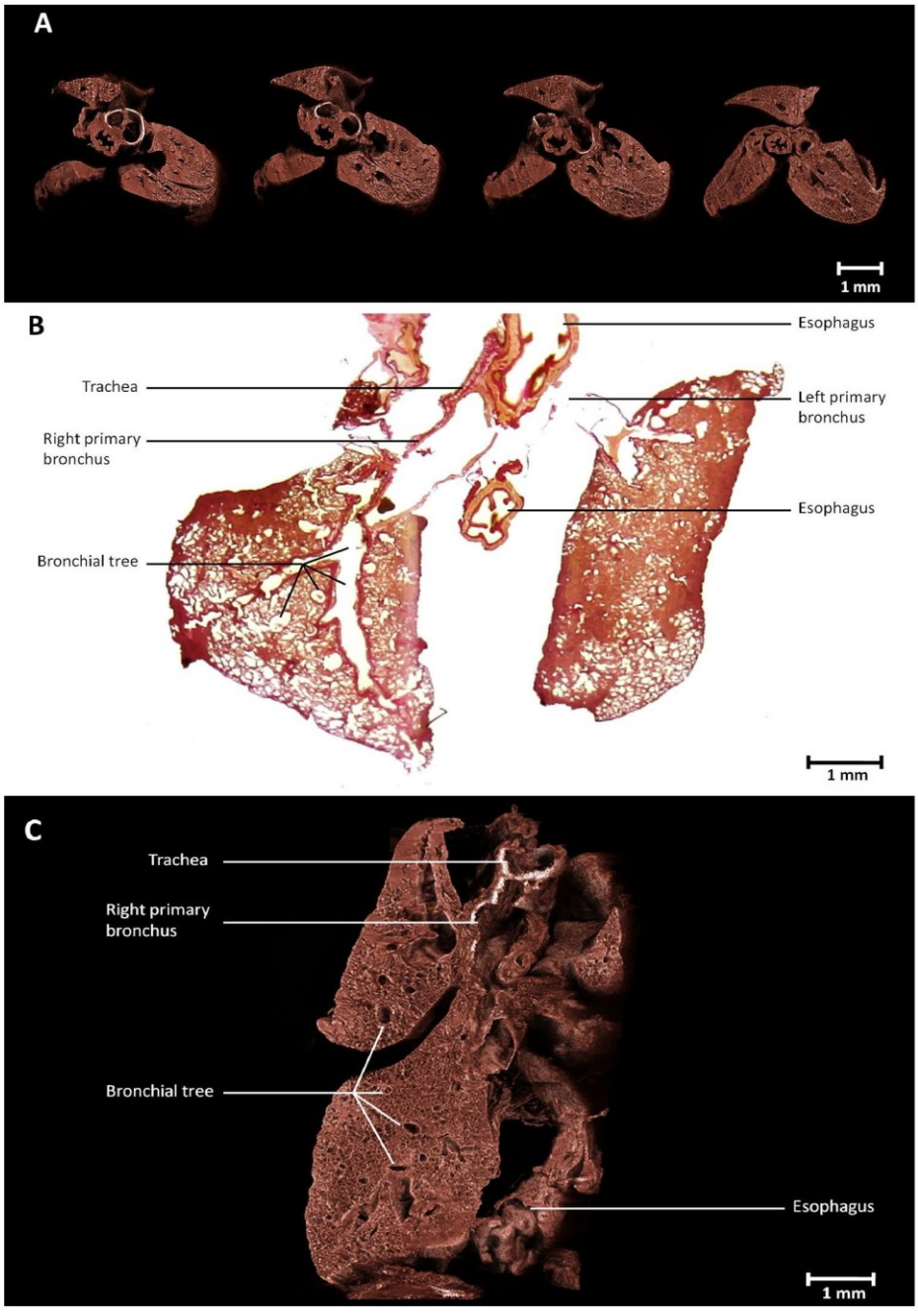

Fig. 6 Comparison between micro-CT imaging and histological processing of a mouse lung. **a** Transversal craniocaudal sections of 3D reconstruction of mouse lungs fixed in a series of ascending ethanol concentrations and scanned after 336 h, showing bifurcation of the trachea to primary bronchi and their topographical relationship to the esophagus, **b** histological sample of mouse lungs stained by Weigert van Gieson, **c** 3D reconstruction of mouse right lung, sagittal view; data acquired with EPS 3.55 µm

of laboratory personnel or laboratory equipment. This allows closer cooperation between researchers and laboratory personnel with different fields of expertise, or even use of this method by clinicians, who can collect the samples and simply fix them in a cartridge with the selected ethanol solution.

Furthermore, the 3D reconstructions can be easily and expeditiously analyzed in any cross sections with multiple post-procedural options, such as creating of rotational images or animations.

Possibly the fixation in 25% ethanol could be avoided, which could also reduce the duration of fixation time in each bath. However, optimal fixation times, number of baths and their concentrations in an ascending ethanol concentration protocol need to be determined with further study.

We believe that even more detailed structure imaging of tissue structures is possible with our ethanol protocol; however, it is currently limited by the spatial resolution of micro-CT machines. Although this research did not focus on pathological specimens, our protocol can be equally applied to pathological samples to depict morphological changes in organs.

The major limitation of this method is shrinkage of the soft tissue specimens, which was due to the properties of ethanol and it is technically unavoidable.

A relatively small number of specimens was evaluated per group. Only ethanol fixation methods were carried out in the current study, and comparison to conventional methods is therefore not available. However, a gold standard staining method is non-existent and a correlation to a reference measurement is not possible.

Conclusions

Ethanol fixation is a cheap and simple method, which can be used not only for the fixation of the soft tissue specimens, but also for tissue contrast enhancement in micro-CT imaging. The best results can be achieved when soft tissue fixation in a series of ascending ethanol concentrations is carried out.

Funding The work was supported by the Charles University Grant Agency [GAUK 130 717] and from European Regional Development Fund-Project "Engineering applications of microworld physics" [No. CZ.02.1.01/0.0/0.0/16_019/0000766].

Compliance with ethical standards

Conflicts of interest The authors declare that there is no conflict of interest regarding the publication of this paper.

Ethical statement All applicable institutional and national guidelines for the care and use of animals were followed.

References

1. Metscher BD. MicroCT for comparative morphology: simple staining methods allow high-contrast 3D imaging of diverse non-mineralized animal tissues. BMC Physiol. 2009;9:11. https://doi.org/10.1186/1472-6793-9-11.
2. Vickerton P, Jarvis J, Jeffery N. Concentration-dependent specimen shrinkage in iodine-enhanced microCT. J Anat. 2013;223(2):185–93. https://doi.org/10.1111/joa.12068.
3. Silva JMDE, Zanette I, Noel PB, Cardoso MB, Kimm MA, Pfeiffer F. Three-dimensional non-destructive soft-tissue visualization with X-ray staining micro-tomography. Sci Rep-UK. 2015;5:Artn 14088. https://doi.org/10.1038/srep14088.
4. Donath T, Pfeiffer F, Bunk O, Grunzweig C, Hempel E, Popescu S, et al. Toward clinical X-ray phase-contrast CT demonstration of enhanced soft-tissue contrast in human specimen. Invest Radiol. 2010;45(7):445–52. https://doi.org/10.1097/RLI.0b013e3181e21866.
5. Mizutani R, Suzuki Y. X-ray microtomography in biology. Micron. 2012;43(2–3):104–15. https://doi.org/10.1016/j.micron.2011.10.002.
6. Descamps E, Sochacka A, De Kegel B, Van Loo D, Van Hoorebeke L, Adriaens D. Soft tissue discrimination with contrast agents using micro-CT scanning. Belg J Zool. 2014;144(1):20–40.
7. Clauss SB, Walker DL, Kirby ML, Schimel D, Lo CW. Patterning of coronary arteries in wildtype and connexin43 knockout mice. Dev Dyn. 2006;235(10):2786–94. https://doi.org/10.1002/dvdy.20887.
8. Pai VM, Kozlowski M, Donahue D, Miller E, Xiao XH, Chen MY, et al. Coronary artery wall imaging in mice using osmium tetroxide and micro-computed tomography (micro-CT). J Anat. 2012;220(5):514–24. https://doi.org/10.1111/j.1469-7580.2012.01483.x.
9. Yamashita T, Kawashima S, Ozaki M, Namiki M, Hirase T, Inoue N, et al. Mouse coronary angiograph using synchrotron radiation microangiography. Circulation. 2002;105(2):E3–4. https://doi.org/10.1161/hc0202.100423.
10. Degenhardt K, Wright AC, Horng D, Padmanabhan A, Epstein JA. Rapid 3D phenotyping of cardiovascular development in mouse embryos by micro-CT with iodine staining. Circ Cardiovasc Imaging. 2010;3(3):314–22. https://doi.org/10.1161/Circimaging.109.918482.
11. Wong MD, Spring S, Henkelman RM. Structural stabilization of tissue for embryo phenotyping using micro-CT with iodine staining. PLoS ONE. 2013;8(12):e84321. https://doi.org/10.1371/journal.pone.0084321.
12. Gammon ST, Foje N, Brewer EM, Owers E, Downs CA, Budde MD, et al. Preclinical anatomical, molecular, and functional imaging of the lung with multiple modalities. Am J Physiol Lung C. 2014;306(10):L897–914. https://doi.org/10.1152/ajplung.00007.2014.
13. Vande Velde G, Poelmans J, De Langhe E, Hillen A, Vanoirbeek J, Himmelreich U, et al. Longitudinal micro-CT provides biomarkers of lung disease that can be used to assess the effect of therapy in preclinical mouse models, and reveal compensatory changes in lung volume. Dis Model Mech. 2016;9(1):91–8. https://doi.org/10.1242/dmm.020321.

14. Ashton JR, Clark DP, Moding EJ, Ghaghada K, Kirsch DG, West JL, et al. Dual-energy micro-CT functional imaging of primary lung cancer in mice using gold and iodine nanoparticle contrast agents: a validation study. PLoS ONE. 2014;9(2):e88129. https://doi.org/10.1371/journal.pone.0088129.
15. Rodt T, von Falck C, Dettmer S, Halter R, Maus R, Ask K, et al. Micro-computed tomography of pulmonary fibrosis in mice induced by adenoviral gene transfer of biologically active transforming growth factor-beta 1. Resp Res. 2010;11:181. https://doi.org/10.1186/1465-9921-11-181.
16. Thiesse J, Namati E, Sieren JC, Smith AR, Reinhardt JM, Hoffman EA, et al. Lung structure phenotype variation in inbred mouse strains revealed through in vivo micro-CT imaging. J Appl Physiol. 2010;109(6):1960–8. https://doi.org/10.1152/japplphysiol.01322.2009.
17. Pauwels E, Van Loo D, Cornillie P, Brabant L, Van Hoorebeke L. An exploratory study of contrast agents for soft tissue visualization by means of high resolution X-ray computed tomography imaging. J Microsc-Oxf. 2013;250(1):21–31. https://doi.org/10.1111/jmi.12013.
18. Takeda T, Thet-Thet-Lwin Kunii T, Sirai R, Ohizumi T, Maruyama H, et al. Ethanol fixed brain imaging by phase-contrast X-ray technique. J Phys: Conf Ser. 2013;425:022004. https://doi.org/10.1088/1742-6596/425/2/022004.
19. Shirai R, Kunii T, Yoneyama A, Ooizumi T, Maruyama H, Lwin TT, et al. Enhanced renal image contrast by ethanol fixation in phase-contrast X-ray computed tomography. J Synchrotron Radiat. 2014;21(Pt 4):795–800. https://doi.org/10.1107/S1600577514010558.
20. Dudak J, Zemlicka J, Krejci F, Karch J, Patzelt M, Zach P, et al. Evaluation of sample holders designed for long-lasting X-ray micro-tomographic scans of ex vivo soft tissue samples. J Instrum. 2016;11:C03005. https://doi.org/10.1088/1748-0221/11/03/C03005.
21. Jakubek J. Data processing and image reconstruction methods for pixel detectors. Nucl Instrum Methods A. 2007;576(1):223–34. https://doi.org/10.1016/j.nima.2007.01.157.
22. Bruker. CTVox: Volume Rendering [computer software] http://bruker-microct.com/products/downloads.htm (2015).
23. Turecek D, Holy T, Jakubek J, Pospisil S, Vykydal Z. Pixelman: a multi-platform data acquisition and processing software package for Medipix2, Timepix and Medipix3 detectors. J Instrum. 2011;6:C01046. https://doi.org/10.1088/1748-0221/6/01/C01046.
24. Llopart X, Ballabriga R, Campbell M, Tlustos L, Wong W. Timepix, a 65k programmable pixel readout chip for arrival time, energy and/or photon counting measurements. Nucl Instrum Methods A. 2007;581(1–2):485–94. https://doi.org/10.1016/j.nima.2007.08.079.
25. Dudak J, Zemlicka J, Karch J, Patzelt M, Mrzilkova J, Zach P, et al. High-contrast X-ray micro-radiography and micro-CT of ex vivo soft tissue murine organs utilizing ethanol fixation and large area photon-counting detector. Sci Rep-UK. 2016;6:30385. https://doi.org/10.1038/Srep30385.
26. Dudak J, Zemlicka J, Krejci F, Polansky S, Jakubek J, Mrzilkova J, et al. X-ray micro-CT scanner for small animal imaging based on Timepix detector technology. Nucl Instrum Methods A. 2015;773:81–6. https://doi.org/10.1016/j.nima.2014.10.076.
27. Jakubek J, Holy T, Jakubek M, Vavrik D, Vykydal Z. Experimental system for high resolution X-ray transmission radiography. Nucl Instrum Methods A. 2006;563(1):278–81. https://doi.org/10.1016/j.nima.2006.01.033.
28. Jakubek J, Jakubek M, Platkevic M, Soukup P, Turecek D, Sykora V, et al. Large area pixel detector WIDEPIX with full area sensitivity composed of 100 Timepix assemblies with edgeless sensors. J Instrum. 2014;9:C04018. https://doi.org/10.1088/1748-0221/9/04/C04018.
29. Howat WJ, Wilson BA. Tissue fixation and the effect of molecular fixatives on downstream staining procedures. Methods. 2014;70(1):12–9. https://doi.org/10.1016/j.ymeth.2014.01.022.

5.5. Imaging of Mouse Brain Fixated in Ethanol in Micro-CT

Citace: MRZÍLKOVÁ, Jana; **PATZELT, Matěj**; GALLINA, Pasquale; WURST, Zdeněk; ŠEREMETA, Martin; DUDÁK, Jan; KREJČÍ, František; ŽEMLIČKA, Jan; MUSIL, Vladimír; KARCH, Jakub; ROSINA, Jozef; ZACH, Petr. Imaging of Mouse Brain Fixated in Ethanol in Micro-CT. *BioMed Research International*. 2019, **2019**, 1-7. ISSN 2314-6133. DOI: 10.1155/2019/2054262. **IF: 2.197/2018.**

5.5.1. Úvod a metodika

Pro experimentální zobrazení centrální nervové soustavy je nejvhodnější mikro-magnetická rezonance, která je však velmi nákladná a v porovnání s mikro-CT má také horší rozlišení. Limitací mikro-CT je na druhou stranu nízký vnitřní kontrast mezi strukturami CNS. Cílem této práce bylo otestovat etanolovou fixační metodu na zdravém myším mozku ex-vivo a na vzniklých snímcích popsat co nejvíce klinicky důležitých anatomických struktur. Ve studii bylo použito 5 mozků geneticky modifikovaných myší C57BL/6, které byly fixované dle protokolu vzestupné řady etanolové koncentrace, popsané v předchozí publikaci. Vzorky byly snímané po 168 hodin fixace a vzniklé tomografie byly následně srovnány s již existujícími atlasy mozku myši a jednotlivé anatomické struktury byly popsány.

5.5.2. Výsledky, diskuze a závěr

V pěti koronárních, čtyřech sagitálních a třech horizontálních řezech bylo identifikováno celkově 42 struktur bílé hmoty a 53 struktur šedé hmoty. Koronární řezy byly vedeny v úrovni přední komisury, ventrální části dorzálního gyrus dentatus, dorzální části dorzálního gyrus dentatus a v úrovni mozkového kmene. Sagitální řezy byly vedeny v úrovni pallidum internum, kaudoputamen, laterálního septa a medálního septa. Horizontální řezy byly vedeny v horní části paraventrikálárních jader thalamu, v úrovni přední hypotalamické oblasti a v dolní části paraventrikulárních jader thalamu. Podařilo se identifikovat i velmi malé struktury bílé hmoty – medální lemniscus, stria terminalis nebo cingulum. V porovnání s mikro-MRI je mikro-CT levnější a dostupnější zařízení s jednodušším protokolem použití kontrastních látek a vyšším rozlišením.

Díky výzkumu zdravého mozku mohou na tuto práci navázat další práce zaměřené na patologie mozku, například studie na animálních modelech tumorů mozku, ischemických příhod či traumatech. Tato studie jasně prokázala, že mikro-CT v kombinaci s etanolovou metodou fixace je vhodné pro ex-vivo studium animálního mozku.

Hindawi
BioMed Research International
Volume 2019, Article ID 2054262, 7 pages
https://doi.org/10.1155/2019/2054262

Research Article

Imaging of Mouse Brain Fixated in Ethanol in Micro-CT

Jana Mrzílková,[1,2] Matěj Patzelt,[1,2] Pasquale Gallina,[3] Zdeněk Wurst,[2] Martin Šeremeta,[2] Jan Dudák,[4,5] František Krejčí,[4] Jan Žemlička,[4] Vladimír Musil,[1,2,6] Jakub Karch,[4] Jozef Rosina,[5,7] and Petr Zach[1,2]

[1]*Specialized Laboratory of Experimental Imaging Third Faculty of Medicine, Charles University, Institute of Experimental and Applied Physics and Faculty of Biomedical Engineering, Czech Technical University in Prague, Prague, Czech Republic*
[2]*Department of Anatomy, Third Faculty of Medicine, Charles University, Prague, Czech Republic*
[3]*Department of Surgery and Translational Medicine, Neurosurgery Unit, Florence School of Neurosurgery, University of Florence, Florence, Italy*
[4]*Institute of Experimental and Applied Physics, Czech Technical University, Prague, Czech Republic*
[5]*Czech Technical University in Prague, Faculty of Biomedical Engineering, Kladno, Czech Republic*
[6]*Centre of Scientific Information, Third Faculty of Medicine, Charles University, Prague, Czech Republic*
[7]*Department of Medical Biophysics and Informatics, Third Faculty of Medicine, Charles University, Prague, Czech Republic*

Correspondence should be addressed to Matěj Patzelt; matej.patzelt@centrum.cz

Received 30 November 2018; Revised 7 June 2019; Accepted 20 June 2019; Published 14 July 2019

Academic Editor: Gelin Xu

Micro-CT imaging is a well-established morphological method for the visualization of animal models. We used ethanol fixation of the mouse brains to perform high-resolution micro-CT scans showing in great details brain grey and white matters. It was possible to identify more than 50 neuroanatomical structures on the 5 selected coronal sections. Among white matter structures, we identified fornix, medial lemniscus, crossed tectospinal pathway, mammillothalamic tract, and the sensory root of the trigeminal ganglion. Among grey matter structures, we identified basal nuclei, habenular complex, thalamic nuclei, amygdala, subparts of hippocampal formation, superior colliculi, Edinger–Westphal nucleus, and others. We suggest that micro-CT of the mouse brain could be used for neurohistological lesions evaluation as an alternative to classical neurohistology because it does not destroy brain tissue.

1. Introduction

Microcomputed tomography (micro-CT) scanning provides nondestructive imaging of tissues and has potential to produce 3D images. Highly mineralized structures, such as bones and teeth, give very good contrast in micro-CT [1]. On the other hand imaging of soft tissues such as nerve, muscle, adipose tissue, or ligaments is very problematic [2]. Interestingly, alcohol fixation works well with the neuronal tissue and specifically with the brain but together with the iodine and phosphotungstic acid [3]. Brain tissue has several distinguishing characteristics compared to other soft tissues. It is composed of white matter that contains relatively high amount of phospholipid molecules forming myelin sheaths around axons of neurons that behave on the micro-CT simply as fat (mostly visualized on micro-CT darker compared to grey matter) and from grey matter containing bodies of neurons (appear on micro-CT lighter compared to white matter bundles) that share basic common cellular characteristics (biophysical, biochemical, and biological) of other soft tissues. Micro-CT studies visualizing neuronal tissue usually focus on peripheral nerves and their lesions [4], overall brain atrophy [5], freeze-dried human acellular nerve allografting (hANA) [6], and brain tumor models in mice [7]. Generally there are more micro-CT studies on pathological neuronal tissues than on the healthy ones.

Behavioral studies on the mice model often require precise analysis of the brain area selected for the experiment. For example, in animal models of ischemia exact place of the neuronal lesion has to be verified and quantified [8]. Evaluation of exact lesion site needs different kinds of structural/histological atlases ([9, 10]; Allen Mouse Brain

Atlas, 2014) based on various staining procedures (Nissl, parvalbumin, calbindin, etc.). Besides classical neurohistological lesion verification, combination of 7T Bruker MRI with magnetic particle analysis (MPI) of the brain tissue in real time becomes popular [11]. Micro-CT imaging of the brain could be considered as a new attempt to visualize neuronal tissue for the experimental purposes. Micro-CT imaging with phase contrast of the ethanol fixated rat brain was successfully described in [12], although only gross neuroanatomical structures were observed. Soaking the brains in nonionic iodinated contrast agent resulted in clear differences in signal between the grey matter, the white matter, and the ventricular spaces [13], but without possibility to distinguish neuroanatomical borders of individual brain nuclei or cortical regions. Diffusible iodine-based contrast-enhanced computed tomography (diceCT) in female mouse was suggested to be effective for gross differences in the overall brain shape in large numbers of samples [14]. Combined MRI-CT atlases of developing and adult mouse brains fixed with paraformaldehyde and subsequent PBS wash-out are unique for coregistration of brain areas but without detailed neuroanatomical structures delineation [15]. We tried to visualize and identify on micro-CT as much as possible neuroanatomical structures on coronal, sagittal, and horizontal sections of the healthy mouse brain.

2. Materials and Methods

2.1. Tissue Sample Origins. We evaluated 5 brains from C57BL/6 genetically modified male mice (weight 17-20 g) from the Institute of Experimental Imaging, First Faculty of Medicine, Charles University, Prague, Czech Republic. This mouse strain was selected because it is commonly used in neurosciences and other research fields [16]. Mice were euthanized by cervical dislocation and their brains were harvested for purpose of this study; this method did not affect mice brain distortion at all. Study was approved by Ethical Committee of the Third Faculty of Medicine, Charles University, Czech Republic.

2.2. Tissue Sample Processing. Brains from 5 mice were carefully extracted from the skulls by the following steps. Cervical spinal cord and brain stem were released by small tongs as disruption of cervical vertebras. Then temporal bones and vestibulocochlear, oculomotor, optic, and olfactory nerves were dissected. After extraction of the brain from skull, any remnants of bone fragments on the brain surface were carefully checked and cleaned before scanning. The brain samples were put into Eppendorf tubes with ethanol-soaked gauze at the bottom for the purpose of the scan. The conical shape of Eppendorf tubes very efficiently supports the samples and avoids undesirable movements. The wet gauze maintains a saturated gaseous atmosphere preventing further drying out and shrinkage of sample. After the extraction, brains were fixated subsequently in 25%, 50%, 75%, and 97% ethanol for 12 hours. This type of ethanol fixation is also known as graded dehydration series of ethanol (GEHC) and has been documented as promising in undistorted soft tissue fixation [17]. Micro-CT scanning was performed after 168 hours of fixation.

2.3. Tissue Sample Scanning. Brains were left prior to scanning on the gauze for 40 minutes in air temperature 23°C. This allowed vaporization of redundant ethanol from the whole brain, including the ventricles and other cavities. After the period of drying, brains were positioned in the special plastic holder with an ethanol reservoir, which made an atmosphere of gas, which prevented structural changes of the brains during scanning [18, 19]. Two different scanning techniques were performed. First, just X-ray radiography was performed followed by a microtomography and final 3D reconstruction [18, 19]. The data were reconstructed into the final 3D dataset using Volex reconstruction software and visualized using program CTVox in standard PC [20]. On the sagittal projection some processing artifacts are often seen: flattening of the whole brain craniocaudally, artificial space between the hippocampal formation and thalamus, fimbria fornicis separated from the white matter nearby stria terminalis and ventriculus lateralis, and cerebellar fissure behind inferior colliculi.

2.4. Micro-CT Apparatus. The used micro-CT set-up was described in detail in our previous publications [18, 19, 21]. Briefly, apparatus consisted of two different custom-built micro-CT systems; routine detection system was equipped with a Kevex™ PXS-11 X-ray tube and Timepix detector in Quad configuration (four read-out chips with a common silicon sensor providing sensitive area 28 × 28 mm, 512 × 512 pixels, 55 μm pixel pitch). The highest achievable spatial resolution was approximately 28 μm. Presented 2D microradiographic images were acquired with the introduced setup. The other high-resolution system was equipped with a large area photon counting detector WidePIX$_{10\times5}$. WidePIX is a recently introduced technology for tiling of large area PCD arrays from individual Timepix chips [22]. Specifically, detector WidePIX$_{10x5}$ is composed of 50 Timepix tiles and offers approximately 140 x 70 mm field view (2560 × 1280 pixels). High quality microfocus X-ray tube Hamamatsu L8601-01 enables spatial resolution down to 5 micrometers [23].

2.5. Scan Parameters. The high-resolution setup was used for the presented micro-CT scans. The data were acquired with an emphasis on high CNR. The acquisition time was adjusted in order to reach at least 10^5 or 10^4 detected photons per pixel in the background of the object in microradiography or a micro-CT projection, respectively. CT reconstructions were done by Volex reconstruction engine (courtesy of Fraunhofer IIS and Technology, Germany).

The detector as well as the whole CT scan was controlled using Pixelman software [24]. The CT scan was carried out with 4.4 μm EPS. The total number of 848 projections was acquired with 0.38 degree angle step. The acquisition time was 3.6 seconds per projection. The tube voltage was set to 60 kVp and it was operated with 6 W of output power. The projections were processed using a dedicated beam-hardening correction [25] and the slight image distortions

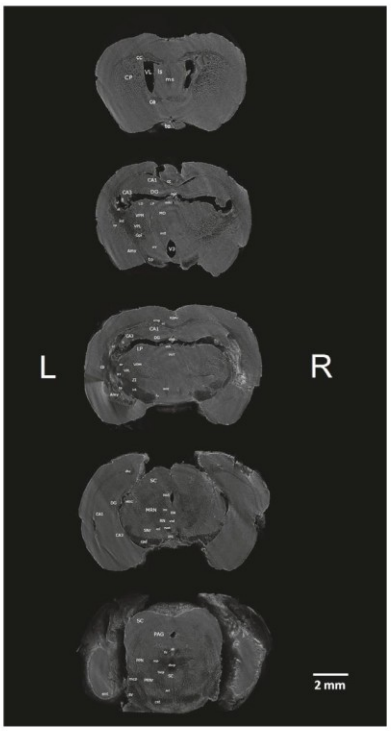

Figure 1: Micro-CT slices (program CTVox) of the 5 coronal sections of the mouse brain with labeled grey and white matter structures. Brain sections from top down are taken 1x at the level of anterior commissure, 2x at the dorsal hippocampus, 1x at the ventral hippocampus, and 1x at the brain stem (superior colliculi). Section orientation: L – left, R – right.

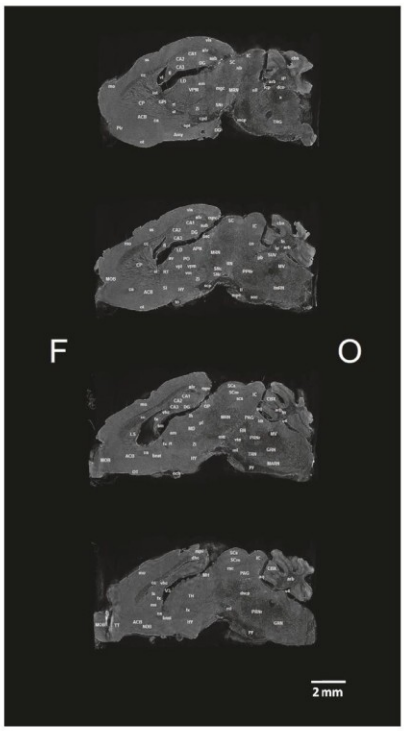

Figure 2: Micro-CT slices (program CTVox) of the 4 sagittal sections of the mouse brain with labeled grey and white matter structures. Brain sections from top down are taken 1x at the level of pallidum internum, 1x at the middle of caudatoputamen, 1x at the lateral septum, and 1x at the medial septum. Section orientation: F – frontal, O – occipital.

coming from the tiled detector construction were corrected [26]. The CT reconstruction was carried out using Volex reconstruction engine.

2.6. Gray and White Matter Labelling. For the frontal and sagittal sections Allen Mouse Atlas was used as reference [27]. For the horizontal sections C57BL/6J Atlas was used as reference (The Mouse Brain Library, http://www.mbl.org). Anatomical structures of digitalized brain sections were labeled in the environment of freeware program Xnview (https://www.xnview.com/en/). All depicted pictures of the labelled mouse brain are from one specimen only so that structures correspond between exactly three planes (horizontal, sagittal, and coronal), because of tiny morphological differences between various mouse brains.

3. Results

We identified 42 white matter and 53 grey matter brain structures (see Abbreviations) in five coronal (Figure 1), four sagittal (Figure 2), and three horizontal (Figure 3) brain sections of *ex vivo* healthy mouse brain using micro-CT. All structures were identified manually by two experienced neuroanatomists and registered in micro-CT scans using online Adult Mouse Brain Atlas [27] for coronal and sagittal sections and the online Mouse Brain Library (C57BL/6J Atlas) for horizontal sections.

3.1. Frontal Sections of the Mouse Brain. The positions of the five coronal sections of the mouse brain were selected because of their relevance to experimental neuropsychological studies in animal model. In frontodorsal order the sections were taken (a) in the frontal lobe at the level of the *anterior commissure*, (b) at the ventral part of the dorsal *dentate gyrus*, *dorsal hippocampus*, and the third ventricle, (c) at the dorsal part of the dorsal *dentate gyrus*, *dorsal hippocampus*, and the *paraventricular nucleus of the thalamus*, (d) at the level of the ventral *dentate gyrus*, *ventral hippocampus*, and *midbrain reticular nucleus*, and (e) at the level of the brain stem with *superior colliculi* and *dorsal raphe nucleus*. We were unable to identify hyperintensity in the brain stem between trigeminal nuclear complex, lateral lemniscal nuclei, and medial cerebellar peduncle. Another poorly visible area is located below superior and inferior colliculi, towards thalamic nuclei. Similarly, resolution of the bed nucleus striae terminalis and substantia innominata is poor. Opposite, there is good resolution for both zona incerta and reticular part of the substantia nigra. Although there is relatively big trigeminal nuclear complex that is easy to identify, separate subnuclei of the complex are hard to differentiate. The caudatoputamen is

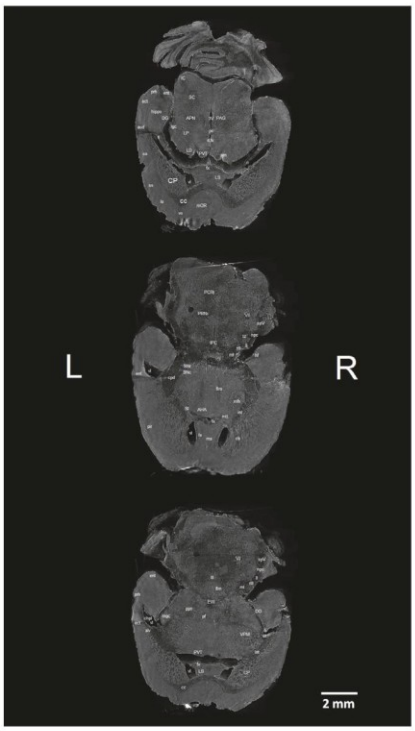

FIGURE 3: Micro-CT slices (program CTVox) of the 3 horizontal sections of the mouse brain with labeled grey and white matter structures. Brain sections from top down are taken 1x at the upper part of thalamic paraventricular nucleus, 1x at the anterior hypothalamic area, and 1x at the lower part of the thalamic paraventricular nucleus. Section orientation: L – left, R – right.

a very well visible structure and inside is rich system of the hypointensities that could be either white matter of the internal capsule or the Virchow-Robin spaces formed by capillary bed stream of thalamostriatal artery. Hypothalamic subparts are more difficult to discern compared to thalamic subnuclear groups. Stria medullaris thalami is normally found on the superior part of the thalamus; however here it is detached from it and bound to dorsal hippocampal commissure on the caudal surface of the fornix. While most of the thalamic nuclei are hyperdense, most midbrain structures (reticular nucleus, periaqueductal gray, etc.) are hypodense.

3.2. Sagittal Sections of the Mouse Brain. Within hippocampal formation dentate gyrus, CA1, Ca2, and CA3 subfields and subiculum were identified. Sagittal projection offers better visibility over frontal projection. Above cerebellar peduncle zona incerta, substantia nigra, and ventrally stria terminalis were visible. Within brain stem trigeminal nucleus, dorsal vagal nucleus, and nucleus interpeduncularis were visible. On the other hand, we have not seen well borders of the amygdaloid complex; it had the same gray color as nearby structures (olfactory tubercle or nucleus accumbens).

3.3. Horizontal Sections of the Mouse Brain. We identified in the ventral part of the sections clearly visible medial and lateral septum. Callosal body in contrast to online atlas was very well visible in all three sections and in front of it was well preserved medial frontal and/or orbital cortex. Also frontal part of the lateral ventricles clearly separated caudatoputamen from septal nuclei and internal capsule. Penetrations of the internal capsule into caudatoputamen are, especially, well visible. Dorsally to septal area structures of the thalamus (paraventricular nucleus and laterodorsal complex of nuclei) were located, and also stria medullaris thalami and lateral geniculate complex. On the other hand, detailed inner structure of the hippocampal formation (ventral part) was not very well visible as in the frontal sections. Besides reticular, pontine, or parvocellular nuclei, other brain stem nuclei were not visible compared to the frontal sections.

4. Discussion

Micro-CT imaging in mouse is often limited to the whole body scans, including skeleton, organs and blood vessels [28, 29], and brain blood supply changes in various experimental pathological conditions [30, 31], or to the brain tumors (for example glioblastoma) [32]. Scanning of the mouse brain gives better results when it is extracted from the skull. The reason is that the skull induces beam-hardening artifacts to adjacent soft tissue [15]. Our work provides comparable results as reported by [3]; nevertheless, in our case, any high-Z contrast agent was needed.

High-resolution MRI three-dimensional atlas of the mouse brain shows sixty-two structures at the resolution 32 μm with the habenular nuclear complex being the smallest visible structure [33]. In comparison our micro-CT ethanol fixated brain scans showed more than fifty structures within only 5 representative coronal sections. It seems that pure GEHC ethanol brain fixation shows better differences between white and gray matters on micro-CT compared to MRI. We identified small white matter structures like cingulum bundle, medial lemniscus, crossed tectospinal pathway, and stria terminalis which is a better result compared to the MRI.

Frontal and sagittal sections atlases of the mouse brain [27] are easier to find in the literature compared to the horizontal ones (for example MRI atlas of C57BL/6J, DBA/2J, or A/J mouse from The Mouse Brain Library). Some MRI atlases are without grey and white brain matter labels, for example, 8-week-old 129S1/SvImJ male mice atlas [34].

We did not attempt yet to create the whole atlas of the mouse brain on the micro-CT. Our goal was to visualize clinically important brain structures like hippocampal formation and its subfields, thalamic nuclei, fornix, medial and lateral septal nuclei, and others. We suggest as the next step manual or semiautomatic reconstruction of the whole mouse brain micro-CT atlas. Histological staining (Nissl) and optical microscopy are mostly used for brain lesion evaluation in experimental studies (insertions of cannulas, electrolesions, chemical lesions, electrode positions, polymer substance delivery, ischemia after carotid arteries ligations, etc.). The disadvantage of these approaches is altered brain tissue that cannot be used afterwards for other staining (for example immunostaining) or at the cost of complicated

protocols for sections storing and handling. With the micro-CT lesion verification, we can use intact brain tissue for further processing and thus replacing classical histological verification with virtual visual evaluation. Moreover, micro-CT lesion visualization can be enhanced by computer processing leading to volume rendering or providing virtual dissection of the brain in unorthodox planes unavailable in classical histology. Level of details in high-resolution micro-CT almost corresponds to the classical histology sections. Within destructive methodologies, it seems to be a choice for immunohistochemistry since the brains are processed only in ethanol.

5. Conclusion

We show that micro-CT could be used in neuroresearch alongside classical histology or magnetic resonance imaging. Besides higher price and lower resolution of the magnetic resonance imaging, it is not always available to all laboratories and micro-CT is easier to get access to. Even if one does not have micro-CT in the laboratory, it is possible to use fixation of the brain specimen and send it to micro-CT for analysis. This is not so simple for magnetic resonance imaging; we cannot use fixation or it would not be visualized properly. Fixation of the brain tissue should be done as soon as possible or the brain would decompose. Magnetic resonance imaging is better for living organisms while micro-CT for fixed brain tissue. Laboratories with micro-CT could offer services for others (sending fixated brain specimen) since acquisition time for micro-CT scanning is relatively short compared to magnetic resonance imaging. Immunohistochemistry or general staining histological protocols could then follow in a short time. The disadvantage of the micro-CT is still the relatively small Timepix detector area but with time we could expect an increase in its size. Ex vivo ethanol fixation of the brain tissue grants sufficient tissue contrast, but we trend to the situation where brain rotation could be highly contrasted even during in vivo scanning.

Abbreviations

ACB: Nucleus accumbens
AHA: Anterior hypothalamic area
alv: Alveus
Amy: Amygdala
APN: Anterior pretectal nucleus
aq: Cerebral aqueduct
arb: Arbor vitae
aud: Auditory cortex
av: Anteroventral nucleus of the thalamus
bnst: Bed nucleus striae terminalis
bsc: Brachium of superior colliculus
bsRN: Brain stem reticular nuclei
ca: Anterior commissure
CA1: Field of CA1
CA3: Field of CA3
cb: Cell bridges of ventral striatum
cbx: Cerebellar cortex
cc: Corpus callosum
cing: Cingulum bundle
cn: Cuneiform nucleus
CP: Caudatoputamen
cpd: Cerebral peduncle
cst: Corticospinal tract
d3v: Dorsal third ventricle
dco: Dorsal cochlear nucleus
DG: Dentate gyrus
dhc: Dorsal hippocampal commissure
dr: Dorsal nucleus raphe
dscp: Superior cerebellar peduncle decussation
ect: Ectorhinal cortex
em: External medullary lamina of the thalamus
ent: Entorhinal area
EW: Edinger-Westphal nucleus
fi: Fimbria fornicis
flm: Medial longitudinal fascicle
fn: Fastigial nucleus
fx: Fornix
Gpi: Globus pallidus, internal segment
GRN: Gigantocellular reticular nucleus
hf: Hippocampal fimbria
hippo: Hippocampal formation
HY: Hypothalamus
chpl: Choroid plexus
IC: Inferior colliculus
icp: Inferior cerebellar peduncle
III: Oculomotor nucleus
inc: Interstitial nucleus of Cajal
int: Internal capsule
IP: Interposed nucleus of cerebellum
IPC: Interpeduncular nucleus
iv: Trochlear nucleus
LAV: Lateral vestibular nucleus
LD: Lateral dorsal nucleus of the thalamus
ldt: Laterodorsal tegmental nucleus
lgc: Lateral geniculate complex
lh: Lateral habenula
LHA: Lateral hypothalamic area
ll: Lateral lemniscus
lo: Lateral orbital cortex
LP: Lateral posterior nucleus of the thalamus
LPO: Lateral preoptic area
ls: Lateral septal nucleus
MARN: Magnocellular reticular nucleus
mcp: Middle cerebellar peduncle
MD: Mediodorsal nucleus of the thalamus
mfb: Medial forebrain bundle
MGC/mgc: Medial geniculate complex
mh: Medial habenula
ml: Medial lemniscus
mo: Somatomotor cortical areas
MOB: Main olfactory bulb
mOR: Medial orbital cortex
mpc: Medial cerebellar peduncle
MRN: Midbrain reticular nucleus
ms: Medial septal nucleus
mtt: Mammillothalamic tract
MV: Medial vestibular nucleus

MV:	Medial vestibular nucleus
nb:	Nucleus of the brachium of the inferior colliculus
NDB:	Nucleus of the diagonal band
nll:	Nucleus of the lateral lemniscus
not:	Nucleus of the optic tract
och:	Optic chiasma
OP:	Olivary pretectal nucleus
or:	Optic radiation
ot:	Olfactory tubercle
PAG:	Periaqueductal gray
pb:	Parabrachial nucleus
pc:	Posterior commissure
PCRt:	Parvicellular reticular nucleus
pf:	Parafascicular nucleus
Pir:	Piriform cortical area
Po:	Posterior thalamic complex
PPN/ppn:	Pedunculopontine nucleus
ppt:	Posterior pretectal nucleus
prh:	Perirhinal cortex
PRNr:	Pontine reticular nucleus
PVT:	Paraventricular nucleus of the thalamus
py:	Pyramid
RN:	Red nucleus
RSPv/rspv:	Retrosplenial area, ventral part
RT/rt:	Reticular nucleus of the thalamus
rust:	Rubrospinal tract
SC:	Superior colliculus
SCm:	Motor part of superior colliculus
scp:	Superior cerebellar peduncles
SCs:	Sensory part of superior colliculus
scs:	Superior colliculus commissure
SI:	Substantia innominata
sm:	Stria medullaris thalami
SNc:	Substantia nigra, compact part
SNr:	Substantia nigra, reticular part
soc:	Superior olivary complex
spV:	Spinal tegmental tract
ss:	Somatosensory cortical areas
st:	Stria terminalis
stn:	Subthalamic nucleus
sub:	Subiculum
SUV:	Superior vestibular nucleus
SV:	Sensory root of the trigeminal nerve
TH:	Thalamus
to:	Tractus opticus
TRG:	Trigeminal nuclei
TRN:	Tegmental reticular nucleus
tscp:	Crossed tectospinal pathway
TT:	Taenia tecta
tz:	Trapezoid body
V3:	Third ventricle
v4:	Fourth ventricle
vhc:	Ventral hippocampal commissure
VII:	Motor nucleus of the facial nerve
vIIIn:	Vestibulocochlear nerve
vis:	Visual cortical areas
VL/vl:	Lateral ventricle
vm:	Ventral medial nucleus of the thalamus
vo:	Ventral orbital cortex
VPL:	Ventral posterolateral nucleus of the thalamus
VPM/vpm:	Ventral posteromedial nucleus of the thalamus
vta:	Ventral tegmental area
vtd:	Ventral tegmental decussation
x:	Nucleus X
Zi/zi:	Zona incerta.

Data Availability

Pictures of the mouse brain are available on request in our laboratory. The data used to support the findings of this study are available from the corresponding author upon request.

Conflicts of Interest

The authors declare that they have no conflicts of interest.

Acknowledgments

Project was supported by Charles University [Grants nos. Q35, Q41, and 260388/SVV/2019]; European Regional Development Fund-Project "Engineering applications of micro world physics" [Grants nos. CZ.02.1.01/0.0/0.0/16_019/0000766]; the Charles University Grant Agency [Grant no. GAUK 130717]; Czech Science Foundation [Grant no. P30412G069]; National Institute of Mental Health (NIMH-CZ) [Grant no. ED2.1.00/03.0078]; and the European Regional Development Fund [Grant no. RVO67985823].

References

[1] C. Jud, F. Schaff, I. Zanette, J. Wolf, A. Fehringer, and F. Pfeiffer, "Dentinal tubules revealed with X-ray tensor tomography," *Dental Materials*, vol. 32, no. 9, pp. 1189–1195, 2016.

[2] G. R. Naveh, V. Brumfeld, M. Dean, R. Shahar, and S. Weiner, "Direct MicroCT imaging of non-mineralized connective tissues at high resolution," *Connective Tissue Research*, vol. 55, no. 1, pp. 52–60, 2014.

[3] T. Zikmund, M. Novotná, M. Kavková et al., "High-contrast differentiation resolution 3D imaging of rodent brain by X-ray computed microtomography," *Journal of Instrumentation*, vol. 13, article C02039, pp. 1–12, 2018.

[4] T. M. Hopkins, A. M. Heilman, J. A. Liggett et al., "Combining micro-computed tomography with histology to analyze biomedical implants for periphera nerve repair," *Journal of Neuroscience Methods*, vol. 30, no. 255, pp. 122–130, 2015.

[5] J. Buytaert, J. Goyens, D. De Greef, P. Aerts, and J. Dirckx, "Volume shrinkage of bone, brain and muscle tissue in sample preparation for micro-ct and light sheet fluorescence microscopy (LSFM)," *Microscopy and Microanalysis*, vol. 20, no. 4, pp. 1208–1217, 2014.

[6] S. Zhu, Q. Zhu, X. Liu et al., "Three-dimensional reconstruction of the microstructure of human acellular nerve allograft," *Scientific Reports*, vol. 1, no. 6, article 30694, 2016.

[7] S. Yahyanejad, P. V. Granton, N. G. Lieuwes et al., "Complementary use of bioluminescence imaging and contrast-enhanced

micro-computed tomography in an orthotopic brain tumor model," *Molecular Imaging*, vol. 13, 2014.

[8] F. Fluri, M. K. Schuhmann, and C. Kleinschnitz, "Animal models of ischemic stroke and their application in clinical research," *Drug Design, Development and Therapy*, vol. 2, no. 9, pp. 3445–3454, 2015.

[9] *Paxinos and Franklin's the Mouse Brain in Stereotaxic Coordinates*, Academic Press, Cambridge, Mass, USA, 4th edition, 2012.

[10] D. M. Jacobowitz and L. C. Abbot, *Chemoarchitectonic Atlas of the Developing Mouse Brain*, CRC Press, Boca Raton, Fla, USA, 1st edition, 1997.

[11] B. Zheng, T. Vazin, P. W. Goodwill et al., "Magnetic particle imaging tracks the long-term fate of in vivo neural cell implants with high image contrast," *Scientific Reports*, vol. 5, article 14055, 2015.

[12] T. Takeda, T. Thet-Lwin, T. Kunii et al., "Ethanol fixed brain imaging by phase-contrast X-ray technice," *Journal of Physics: Conference Series*, vol. 425, no. 2, article 022004, 2013.

[13] S. Saito and K. Murase, "Ex vivo imaging of mouse brain using micro-CT with non-ionic iodinated contrast agent: a comparison with myelin staining," *British Journal of Radiology*, vol. 85, no. 1019, pp. e973–e978, 2012.

[14] R. Anderson and A. M. Maga, "A novel procedure for rapid imaging of adult mouse brains with microCT using iodine-based contrast," *PLoS ONE*, vol. 10, no. 11, article e0142974, 2015.

[15] M. Aggarwal, J. Zhang, M. Miller, R. Sidman, and S. Mori, "Magnetic resonance imaging and micro-computed tomography combined atlas of developing and adult mouse brains for stereotaxic surgery," *Neuroscience*, vol. 162, no. 4, pp. 1339–1350, 2009.

[16] H. W. Dong, *The Allen Reference Atlas: A Digital Color Brain Atlas of the C57Bl/6J Male Mouse*, John Wiley and Sons Inc, New Jersey, NJ, USA, 2008.

[17] B. D. Metscher, "MicroCT for comparative morphology: simple staining methods allow high-contrast 3D imaging of diverse non-mineralized animal tissues," *BMC Physiology*, vol. 9, no. 11, 2009.

[18] J. Dudak, J. Zemlicka, J. Karch et al., "High-contrast X-ray micro-radiography and micro-CT of ex-vivo soft tissue murine organs utilizing ethanol fixation and large area photon-counting detector," *Scientific Reports*, vol. 27, no. 6, article 30385, 2016.

[19] J. Dudak, J. Zemlicka, F. Krejci et al., "Evaluation of sample holders designed for long-lasting X-ray micro-tomographic scans of ex-vivo soft tissue samples," *Journal of Instrumentation*, vol. 11, article C03005, 2016.

[20] Bruker MicroCT, "Volume rendering," 2016, http://bruker-microct.com/products/ctvox.htm.

[21] J. Dudak, J. Zemlicka, F. Krejci et al., "X-ray micro-CT scanner for small animal imaging based on Timepix detector technology," *Nuclear Instruments and Methods in Physics Research Section A: Accelerators, Spectrometers, Detectors and Associated Equipment*, vol. 773, pp. 81–86, 2015.

[22] J. Jakubek, M. Jakubek, M. Platkevic et al., "Large area pixel detector WIDEPIX with full area sensitivity composed of 100 Timepix assemblies with edgeless sensors," *Journal of Instrumentation*, vol. 9, no. 4, article C04018, 2014.

[23] Hamatsu datasheet, https://www.hamamatsu.com/resources/pdf/etd/L9181-02_TXPR1015E.pdf.

[24] D. Turecek, T. Holy, J. Jakubek, S. Pospisil, and Z. Vykydal, "Pixelman: a multi-platform data acquisition and processing software package for Medipix2, Timepix and Medipix3 detectors," *Journal of Instrumentation*, vol. 6, no. 1, 2011, C01046-C01046.

[25] J. Jakubek, "Data processing and image reconstruction methods for pixel detectors," *Nuclear Instruments and Methods in Physics Research Section A: Accelerators, Spectrometers, Detectors and Associated Equipment*, vol. 576, no. 1, pp. 223–234, 2007.

[26] J. Zemlicka, J. Dudak, J. Karch, and F. Krejci, "Geometric correction methods for Timepix based large area detectors," *Journal of Instrumentation*, vol. 12, no. 1, 2017, C01021-C01021.

[27] Allen Brain Reference Atlases, "Adult mouse," 2004, http://atlas.brain-map.org/.

[28] H. Wang, D. B. Stout, R. Taschereau et al., "MARS: A mouse atlas registration system based on a planar x-ray projector and an optical camera," *Physics in Medicine and Biology*, vol. 57, no. 19, pp. 6063–6077, 2012.

[29] M. Baiker, J. Milles, J. Dijkstra et al., "Atlas-based whole-body segmentation of mice from low-contrast Micro-CT data," *Medical Image Analysis*, vol. 14, no. 6, pp. 723–737, 2010.

[30] S. Ghanavati, L. X. Yu, J. P. Lerch, and J. G. Sled, "A perfusion procedure for imaging of the mouse cerebral vasculature by X-ray micro-CT," *Journal of Neuroscience Methods*, vol. 221, pp. 70–77, 2014.

[31] J. Y. Park, S. K. Lee, J. Y. Kim et al., "A new micro-computed tomography-based high-resolution blood-brain barrier imaging technique to study ischemic stroke," *Stroke*, vol. 45, no. 8, pp. 2480–2484, 2014.

[32] S. Kirschner, B. Mürle, M. Felix et al., "Imaging of orthotopic glioblastoma xenografts in mice using a clinical CT scanner: comparison with micro-CT and histology," *PLoS ONE*, vol. 9, no. 11, article e0165994, p. 11, 2016.

[33] A. Dorr, J. Lerch, S. Spring, N. Kabani, and R. Henkelman, "High resolution three-dimensional brain atlas using an average magnetic resonance image of 40 adult C57Bl/6J mice," *NeuroImage*, vol. 42, no. 1, pp. 60–69, 2008.

[34] N. Kovacević, J. T. Henderson, E. Chan et al., "A three-dimensional MRI atlas of the mouse brain with estimates of the average and variability," *Cerebral Cortex*, vol. 15, no. 5, pp. 639-45, 2005.

6. Závěry

Zobrazování měkkých tkání v mikro-CT je problematické z důvodu jejich velmi nízkého vnitřního kontrastu a pro kvalitní zobrazení jejich vnitřní struktury je tedy nutné použít kontrastní látky. Ty jsou však velmi často příliš drahé, komplikované, toxické a také často znehodnotí vzorek pro další diagnostické metody. Celosvětový výzkum v oblasti zobrazování měkkých tkání in-vivo a ex-vivo v mikro-CT se zaměřuje na hledání ideální kontrastní látky. Taková látka by měla být snadno použitelná, dostupná a měla by rovnoměrně pronikat i tlustými vrstvami tkáně (Pauwels et al. 2013).

Pro získání kvalitních tomografií je nezbytný kvalitní mikro-CT přístroj. V rámci spolupráce ve Specializované laboratoři experimentálního zobrazování 3. LF UK, ÚTEF ČVUT a FBMI ČVUT byl přepracován původní mikrotomograf MARS na zařízení schopné kvalitního zobrazení měkkých tkání. Srdcem modifikovaného přístroje se stal photon-counting detektor Timepix Quad s rozměry 2,8x2,8 cm, který vyniká schopností úspěšně potlačovat šum.

V práci byl vytvořen protokol pro fixaci měkkých tkání pro ex-vivo snímání v mikro-CT. Konkrétně se jednalo o myší srdce a plíce, které byly po explantaci okamžitě fixovány v etanolu. Jako nejlepší protokol vyšla fixace ve vzestupné řadě koncentrací etanolu 25%, 50%, 75% a 97%, kdy v každé lázni byl vzorek uchován po dobu 12 hodin. Vzorky srdce byly poté snímány za 168 hodin, v případě plic po 336 hodinách. Klíčovým krokem je nutnost nechat vzorky před snímáním vyschnout po dobu 40 minut při pokojové teplotě. Díky tomuto jednoduchému kroku dochází k vypaření etanolu ze všech dutin zkoumaného orgánu, které nekolabují a jsou následně vyplněné vzduchem. Při snímání je ve vnitřních strukturách orgánu primárně detekovaný kontrast vzduch-tkáň.

Pro další klinický výzkum v oblasti neurověd byla etanolová metoda aplikována na zobrazení ex-vivo zdravého myšího mozku v mikro-CT. V klinicky zajímavých oblastech mozku se provedly koronární, sagitální a horizontální řezy, na kterých bylo celkově identifikováno a popsáno 42 struktur bílé hmoty a 53 šedé hmoty mozkové.

Detailní zobrazení struktur zdravého mozku animálního modelu pomocí mikro-CT je klíčové pro další studium CNS na animálním modelu v preklinickém výzkumu.

Výstupy této dizertační práce prokázaly, že etanolová fixační metoda ex-vivo měkkých tkání je levná, jednoduchá a efektivní kontrastní látka pro zobrazování těchto tkání v mikro-CT. Díky své jednoduchosti není potřeba k fixaci vzorků speciálně vyškolený personál, a tak může být etanolová metoda aplikována ve spolupráci s kliniky v klinickém výzkumu. Zkoumané tkáně je následně možné podrobit dalšímu zkoumání, například klasické histologii.

Souhrn

Rentgenové snímkování je neinvazivní zobrazovací technika pro zobrazení vnitřní struktury zkoumaného objektu. V posledních letech získává na popularitě zobrazování biologických vzorků v mikro-CT. Nevýhodou této techniky je snížená schopnost zobrazovat měkké tkáně jako jsou například svaly, tuková tkáň nebo nervová tkáň, pro jejich nízký vnitřní kontrast. Cílem této práce bylo upravit komerční mikro-CT MARS, tak aby bylo schopné kvalitně zobrazovat měkké tkáně a vytvořit protokol jednoduché a levné fixace ex-vivo měkkých tkání pro zobrazování v mikro-CT.

V práci bylo použito modifikované mikro-CT MARS osazené photon counting detektorem Timepix Quad s rozlišením 30μm. Mikro-CT bylo následně otestováno na fantomu i reálných měkkých tkáních. Pro snímání ex-vivo měkkých tkání v mikro-CT byla vyvinuta etanolová metoda fixace. Srdce a plíce laboratorních myší byly fixovány buď v 97% etanolu, 50% etanolu nebo ve vzestupné řadě koncentrací etanolu. Vzorky byly snímané buď po 72 hodinách, 168 hodinách, nebo po 336 hodinách. Výsledné snímky byly porovnány navzájem a se snímky nativních vzorků. Dále byla tato metoda fixace vyzkoušena na zdravých mozcích laboratorních myší za účelem zhodnocení přínosu zobrazování mozku v mikro-CT ve výzkumu centrálního nervového systému.

Modifikované mikro-CT bylo úspěšně vyzkoušeno pro zobrazování měkkých tkání ex-vivo. V případě vyvinuté etanolové metody bylo nejlepších výsledků dosaženo u vzorku srdce po 168 hodinách fixace ve vzestupné řadě koncentrací etanolu, u plic po fixaci po dobu 336 hodin, také ve vzestupné řadě koncentrací etanolu. Při snímání mozku se podařilo zobrazit klinicky významných 42 struktur bílé hmoty a 53 struktur šedé hmoty.

V práci bylo prokázáno, že modifikované mikro-CT MARS je vhodné pro kvalitní zobrazování měkkých tkání. Etanolová metoda fixace měkkých tkání je levná a jednoduchá metoda zvýšení vnitřního kontrastu měkkých tkání, která mimo jiné umožňuje rozlišení klinicky významných struktur šedé a bílé hmoty mozku laboratorní myši.

Summary

X-ray radiography is a noninvasive imaging technique for a visualization of internal structures of investigated samples. In past years, imaging of biological samples in a micro-CT is gaining in popularity. The disadvantage of this technology is a low ability to display soft tissues like muscles, fat tissue or nerves due to their low intrinsic contrast. The aim of this study was to modify a conventional micro-CT MARS in order to improve the scanning of the soft tissues and to create a protocol for simple and cheap fixation of ex-vivo soft tissues for micro-CT scanning.

In the study, a modified micro-CT MARS was used together with a photon-counting detector Timepix Quad with the resolution 30μm. The micro-CT was afterward tested on the phantom and also on the real soft tissues. For scanning soft tissues in the micro-CT, the ethanol fixation method was invented. Hearts and lungs from laboratory mice were either fixated in 97%, 50% ethanol solution or in a series of ascending ethanol concentrations. Images were acquired after 72, 168 and 336 hours. The resulting images were compared among themselves and with the native specimens. This fixation method was also used in scanning healthy mice brains in order to evaluate the contribution of displaying of a brain in a micro-CT in the research of the central nervous system.

The modified micro-CT machine was successfully tested for displaying ex-vivo soft tissues. As for the ethanol method, the best results were obtained in case of a heart after 168 hours of fixation in a series of ascending ethanol concentrations and in case of lungs after 336 hours. In scans of the brain, it was possible to visualize 42 clinically important structures of white matter and 53 structures of grey matter.

In this study, it was proven, that the modified micro-CT MARS is suitable for high-quality scanning of ex-vivo soft tissues. The ethanol method of fixation of soft tissues is a cheap and simple method for increasing intrinsic contrast in soft tissues and therefore allows distinguishing clinically important structures of white and grey matter in the brain of a laboratory mouse.

Seznam použitých zkratek

3. LF	3. lékařská fakulta
CCDs	Charge-Coupled Devices
CMOS	Complementary Metal Oxide Semiconductor
CNS	Centrální nervový systém
CT	Computed Tomography (Výpočetní tomografie)
ČVUT	České vysoké učení technické
FBMI	Fakulta biomedicínského inženýrství
MARS	Medipix All Resolution System
MRI	Magnetic Resonance Imaging (Magnetická rezonance)
Mikro-CT	Micro-Computed tomography (Mikro-výpočetní tomografie)
Mikro-MRI	Micro-Magnetic Resonance Imaging (Mikro-magnetická rezonance)
PCXD	Photon Counting X-ray Detectors (Foton-počítající detektory rentgenového záření)
ROI	Region of Interest (Oblast zájmu)
UK	Univerzita Karlova
ÚTEF	Ústav technické a experimentální fyziky

Seznam použité literatury

ALBERS, Jonas, M. Andrea MARKUS, Frauke ALVES a Christian DULLIN, 2018. X-ray based virtual histology allows guided sectioning of heavy ion stained murine lungs for histological analysis. *Scientific Reports* [online]. B.m.: Springer US, **8**(1), 1–10. ISSN 20452322. Dostupné z: doi:10.1038/s41598-018-26086-0

BADEA, C. T., M. DRANGOVA, D. W. HOLDSWORTH a G. A. JOHNSON, 2008a. In vivo small-animal imaging using micro-CT and digital subtraction angiography. *Physics in Medicine and Biology* [online]. **53**(19). ISSN 00319155. Dostupné z: doi:10.1088/0031-9155/53/19/R01

BADEA, Cristian T, Boma FUBARA, Laurence W HEDLUND a G Allan JOHNSON, 2005. 4-D micro-CT of the mouse heart. *Molecular imaging*. **4**(2), 110–116. ISSN 1535-3508 (Print).

BADEA, Cristian T, Eduard SCHREIBMANN a Tim FOX, 2008b. A registration based approach for 4D cardiac micro-CT using combined prospective and retrospective gating. *Medical physics* [online]. **35**(4), 1170–1179. ISSN 0094-2405 (Print). Dostupné z: doi:10.1118/1.2868778

BALINT, Richard, Tristan LOWE a Tom SHEARER, 2016. Optimal contrast agent staining of ligaments and tendons for X-ray computed tomography. *PLoS ONE* [online]. **11**(4). ISSN 19326203. Dostupné z: doi:10.1371/journal.pone.0153552

BENTLEY, Michael D, Maria C ORTIZ, Erik L RITMAN a J Carlos ROMERO, 2002. The use of microcomputed tomography to study microvasculature in small rodents. *American journal of physiology. Regulatory, integrative and comparative physiology* [online]. **282**(5), R1267-79. ISSN 0363-6119 (Print). Dostupné z: doi:10.1152/ajpregu.00560.2001

BORAH, Babul, Gary J GROSS, Thomas E DUFRESNE, Tim S SMITH, Michael D COCKMAN, Paula A CHMIELEWSKI, Mark W LUNDY, James R HARTKE a Earl W SOD, 2001. Three-dimensional microimaging (MRμI and μCT), finite element modeling, and rapid prototyping provide unique insights into bone architecture in osteoporosis. *The Anatomical Record* [online]. B.m.: John Wiley & Sons, Ltd, **265**(2), 101–110. ISSN 0003-276X. Dostupné z: doi:10.1002/ar.1060

CHAFFEY, Nigel, 2001. Hayat MA. 2000. Principles and techniques of electron microscopy: biological applications. 4th edn. 543pp. Cambridge: Cambridge University Press. {pound}65 (hardback). *Annals of Botany* [online]. Dostupné z: doi:10.1006/anbo.2001.1367

CHOI, Jaesung P, Xi YANG, Matthew FOLEY, Xian WANG a Xiangjian ZHENG, 2017. Induction and Micro-CT Imaging of Cerebral Cavernous Malformations in Mouse Model. *Journal of visualized experiments : JoVE* [online]. (127). ISSN 1940-087X (Electronic). Dostupné z: doi:10.3791/56476

CHOU, Yu-fen, D PH, Benjamin WALDER, Xinli ZHANG, D PH, Chia SOO, Kang TING, D M SC, Benjamin WU a D PH, 2007. MicroCT Evaluation of Three-Dimensional Mineralization in Response to BMP-2 Doses In Vitro and in Critical Sized Rat Calvarial Defects [online]. **13**(3). Dostupné z: doi:10.1089/ten.2006.0141

CLARK, D P a C T BADEA, 2014. Micro-CT of rodents: state-of-the-art and future perspectives. *Physica medica : PM : an international journal devoted to the applications of physics to medicine and biology : official journal of the Italian Association of Biomedical Physics (AIFB)* [online]. **30**(6), 619–634. ISSN 1724-191X (Electronic). Dostupné z: doi:10.1016/j.ejmp.2014.05.011

CLAUSS, Sarah B, Diana L WALKER, Margaret L KIRBY, Dan SCHIMEL a Cecilia W LO, 2006. Patterning of coronary arteries in wildtype and connexin43 knockout mice. *Developmental dynamics : an official publication of the American Association of Anatomists* [online]. **235**(10), 2786–2794. ISSN 1058-8388 (Print). Dostupné z: doi:10.1002/dvdy.20887

DE CRESPIGNY, Alex, Hani BOU-RESLAN, Merry C. NISHIMURA, Heidi PHILLIPS, R. A D CARANO a Helen E. D'ARCEUIL, 2008. 3D micro-CT imaging of the postmortem brain. *Journal of Neuroscience Methods* [online]. **171**(2), 207–213. ISSN 01650270. Dostupné z: doi:10.1016/j.jneumeth.2008.03.006

DEGENHARDT, Karl, Alexander C. WRIGHT, Debra HORNG, Arun PADMANABHAN a Jonathan A. EPSTEIN, 2010. Rapid 3D phenotyping of cardiovascular development in mouse embryos by micro-CT with iodine staining. *Circulation: Cardiovascular Imaging* [online]. **3**(3), 314–322. ISSN 19419651. Dostupné z: doi:10.1161/CIRCIMAGING.109.918482

DESCAMPS, Emilie, Alicja SOCHACKA, Barbara DE KEGEL, Denis Van LOO, Lucvan HOOREBEKE a Dominique ADRIAENS, 2014. Soft tissue discrimination with contrast agents using micro-ct scanning. *Belgian Journal of Zoology*. **144**(1), 20–40. ISSN 07776276.

DETOMBE, Sarah A, Nancy L FORD, Fuli XIANG, Xiangru LU, Qingping FENG a Maria DRANGOVA, 2008. Longitudinal follow-up of cardiac structure and functional changes in an infarct mouse model using retrospectively gated micro-computed tomography. *Investigative radiology* [online]. **43**(7), 520–529. ISSN 1536-0210 (Electronic). Dostupné z: doi:10.1097/RLI.0b013e3181727519

DING, Ming, Anders ODGAARD a Ivan HVID, 1999. Accuracy of cancellous bone volume fraction measured by micro-CT scanning. *Journal of Biomechanics* [online]. **32**(3), 323–326. ISSN 0021-9290. Dostupné z: doi:https://doi.org/10.1016/S0021-9290(98)00176-6

DOI, A, T KATO a H TAKAHASHI, 2013. Measurement of density and granularity of archeological artifacts using industrial computed tomography. In: *2013 International Joint Conference on Awareness Science and Technology & Ubi-Media Computing (iCAST 2013 & UMEDIA 2013)* [online]. s. 334–338. ISBN null VO -. Dostupné z: doi:10.1109/ICAwST.2013.6765461

DRANGOVA, Maria, Nancy L FORD, Sarah A DETOMBE, Andrew R WHEATLEY a David W HOLDSWORTH, 2007. Fast retrospectively gated quantitative four-dimensional (4D) cardiac micro computed tomography imaging of free-breathing mice. *Investigative radiology* [online]. **42**(2), 85–94. ISSN 0020-9996 (Print). Dostupné z: doi:10.1097/01.rli.0000251572.56139.a3

DU PLESSIS, Anton, Stephan G LE ROUX, Johan ELS, Gerrie BOOYSEN a Deborah C BLAINE, 2015. Application of microCT to the non-destructive testing of

an additive manufactured titanium component. *Case Studies in Nondestructive Testing and Evaluation* [online]. **4**, 1–7. ISSN 2214-6571. Dostupné z: doi:https://doi.org/10.1016/j.csndt.2015.09.001

DU PLESSIS, Anton, Babatunde James OLAWUYI, William Peter BOSHOFF a Stephan Gerhard LE ROUX, 2016. Simple and fast porosity analysis of concrete using X-ray computed tomography. *Materials and Structures* [online]. **49**(1), 553–562. ISSN 1871-6873. Dostupné z: doi:10.1617/s11527-014-0519-9

DUDAK, Jan, Jan ZEMLICKA, Frantisek KREJCI, Stepan POLANSKY, Jan JAKUBEK, Jana MRZILKOVA, Matej PATZELT a Jan TRNKA, 2015. X-ray micro-CT scanner for small animal imaging based on Timepix detector technology. *Nuclear Instruments and Methods in Physics Research, Section A: Accelerators, Spectrometers, Detectors and Associated Equipment* [online]. B.m.: Elsevier, **773**, 81–86. ISSN 01689002. Dostupné z: doi:10.1016/j.nima.2014.10.076

ENGELHORN, Tobias, Ilker Y EYUPOGLU, Marc A SCHWARZ, Marek KAROLCZAK, Holger BRUENNER, Tobias STRUFFERT, Willi KALENDER a Arnd DOERFLER, 2009. In vivo micro-CT imaging of rat brain glioma: a comparison with 3T MRI and histology. *Neuroscience letters* [online]. **458**(1), 28–31. ISSN 1872-7972 (Electronic). Dostupné z: doi:10.1016/j.neulet.2009.04.033

ERJAVEC, Igor, 2013. Computed microtomography visualization and quantification of mouse ischemic brain lesion by nonionic radio contrast agents [online]. 3–11. Dostupné z: doi:10.3325/cmj.2013.54.3

FAIS, Paolo, Chiara GIRAUDO, Alessia VIERO, Alessandro AMAGLIANI, Guido VIEL, Massimo MONTISCI, Diego MIOTTO a Giovanni CECCHETTO, 2015. Identification of bullet entrance in different type of intermediate firearm wounds through micro-computed tomography analysis. *Journal of Forensic Radiology and Imaging* [online]. **3**(3), 147–152. ISSN 2212-4780. Dostupné z: doi:https://doi.org/10.1016/j.jofri.2015.07.004

FELDKAMP, L A, L C DAVIS a J W KRESS, 1984. Practical cone-beam algorithm. *J. Opt. Soc. Am. A* [online]. B.m.: OSA, **1**(6), 612–619. Dostupné z: doi:10.1364/JOSAA.1.000612

FORD, Nancy L, Ian LEE, Anthony TAM a Don D SIN, 2020. Micro-computed tomography imaging of a rodent model of Chronic Obstructive Pulmonary Disease (COPD). In: Andrzej KROL a Barjor S GIMI, ed. *Medical Imaging 2020: Biomedical Applications in Molecular, Structural, and Functional Imaging* [online]. B.m.: SPIE, s. 612–619. Dostupné z: doi:10.1117/12.2549805

GAMMON, Seth T, Nathan FOJE, Elizabeth M BREWER, Elizabeth OWERS, Charles A DOWNS, Matthew D BUDDE, W Matthew LEEVY a My N HELMS, 2014. Preclinical anatomical, molecular, and functional imaging of the lung with multiple modalities. *American journal of physiology. Lung cellular and molecular physiology* [online]. **306**(10), L897-914. ISSN 1522-1504 (Electronic). Dostupné z: doi:10.1152/ajplung.00007.2014

GHANAVATI, Sahar, Lisa X YU, Jason P LERCH a John G SLED, 2014. A perfusion procedure for imaging of the mouse cerebral vasculature by X-ray micro-CT. *Journal of Neuroscience Methods* [online]. **221**, 70–77. ISSN 0165-0270.

Dostupné z: doi:https://doi.org/10.1016/j.jneumeth.2013.09.002

GIGNAC, Paul M. a Nathan J. KLEY, 2014. Iodine-enhanced micro-CT imaging: Methodological refinements for the study of the soft-tissue anatomy of post-embryonic vertebrates. *Journal of Experimental Zoology Part B: Molecular and Developmental Evolution* [online]. **322**(3), 166–176. ISSN 15525015. Dostupné z: doi:10.1002/jez.b.22561

GIRARD, Romuald, Hussein A ZEINEDDINE, Courtney ORSBON, Huan TAN, Thomas MOORE, Nick HOBSON, Robert SHENKAR, Rhonda LIGHTLE, Changbin SHI, Maged D FAM, Ying CAO, Le SHEN, April I NEANDER, Autumn RORRER, Carol GALLIONE, Alan T TANG, Mark L KAHN, Douglas A MARCHUK, Zhe-Xi LUO a Issam A AWAD, 2016. Micro-computed tomography in murine models of cerebral cavernous malformations as a paradigm for brain disease. *Journal of neuroscience methods* [online]. **271**, 14–24. ISSN 1872-678X (Electronic). Dostupné z: doi:10.1016/j.jneumeth.2016.06.021

GREGOR, Tom, Petra KOCHOV, Lada EBERLOV, Luk NEDOROST, Eva PROSECK, Vclav LIKA, Hynek MRKA, David KACHLK, Ivan PIRNER, Petr ZIMMERMANN, Anna KRLKOV, Milena KRLKOV a Zbynk TONAR, 2012. Correlating Micro-CT Imaging with Quantitative Histology. *Injury and Skeletal Biomechanics* [online]. Dostupné z: doi:10.5772/48680

HAYASAKA, Naoto, Nobuo NAGAI, Naoyuki KAWAO, Atsuko NIWA, Yoshichika YOSHIOKA, Yuki MORI, Hiroshi SHIGETA, Nobuo KASHIWAGI, Masaaki MIYAZAWA, Takao SATOU, Hideaki HIGASHINO, Osamu MATSUO a Takamichi MURAKAMI, 2012. In Vivo Diagnostic Imaging Using Micro-CT: Sequential and Comparative Evaluation of Rodent Models for Hepatic/Brain Ischemia and Stroke. *PLOS ONE* [online]. B.m.: Public Library of Science, **7**(2), e32342. Dostupné z: https://doi.org/10.1371/journal.pone.0032342

HOPKINS, Tracy M, Alexander M HEILMAN, James A LIGGETT, Kathleen LASANCE, Kevin J LITTLE, David B HOM, Danielle M MINTEER, Kacey G MARRA a Sarah K PIXLEY, 2015. Combining micro-computed tomography with histology to analyze biomedical implants for peripheral nerve repair. *Journal of neuroscience methods* [online]. **255**, 122–130. ISSN 1872-678X (Electronic). Dostupné z: doi:10.1016/j.jneumeth.2015.08.016

HOUNSFIELD, G N, 1973. Computerized transverse axial scanning (tomography). 1. Description of system. *The British journal of radiology* [online]. **46**(552), 1016–1022. ISSN 0007-1285 (Print). Dostupné z: doi:10.1259/0007-1285-46-552-1016

HOUNSFIELD, G N, 1976. Picture quality of computed tomography. *AJR. American journal of roentgenology* [online]. **127**(1), 3–9. ISSN 0361-803X (Print). Dostupné z: doi:10.2214/ajr.127.1.3

HOUNSFIELD, G N, 1978. Potential uses of more accurate CT absorption values by filtering. *AJR. American journal of roentgenology* [online]. **131**(1), 103–106. ISSN 0361-803X (Print). Dostupné z: doi:10.2214/ajr.131.1.103

HUTCHINSON, E. F., G. FLORENTINO, J. HOFFMAN a B. KRAMER, 2017a. Micro-CT assessment of changes in the morphology and position of the immature mandibular canal during early growth. *Surgical and Radiologic Anatomy* [online].

B.m.: Springer Paris, **39**(2), 185–194. ISSN 12798517. Dostupné z: doi:10.1007/s00276-016-1694-x

HUTCHINSON, J Ciaran, Susan C SHELMERDINE, Ian C SIMCOCK, Neil J SEBIRE a Owen J ARTHURS, 2017b. Early clinical applications for imaging at microscopic detail: microfocus computed tomography (micro-CT). *The British journal of radiology* [online]. 2017/05/04. B.m.: The British Institute of Radiology., **90**(1075), 20170113. ISSN 1748-880X. Dostupné z: doi:10.1259/bjr.20170113

JEFFERY, Nathan S, Robert S STEPHENSON, James A GALLAGHER, Jonathan C JARVIS a Philip G COX, 2011. Micro-computed tomography with iodine staining resolves the arrangement of muscle fibres. *Journal of biomechanics* [online]. **44**(1), 189–192. ISSN 1873-2380 (Electronic). Dostupné z: doi:10.1016/j.jbiomech.2010.08.027

JIRIK, Miroslav, Zbynek TONAR, Anna KRALICKOVA, Lada EBERLOVA, Hynek MIRKA, Petra KOCHOVA, Tomas GREGOR, Petr HOSEK, Miroslava SVOBODOVA, Eduard ROHAN, Milena KRALICKOVA a Vaclav LISKA, 2016. Stereological quantification of microvessels using semiautomated evaluation of X-ray microtomography of hepatic vascular corrosion casts. *International journal of computer assisted radiology and surgery* [online]. **11**(10), 1803–1819. ISSN 1861-6429 (Electronic). Dostupné z: doi:10.1007/s11548-016-1378-3

JOHNSON, John T., Mark S. HANSEN, Isabel WU, Lindsey J. HEALY, Christopher R. JOHNSON, Greg M. JONES, Mario R. CAPECCHI a Charles KELLER, 2006. Virtual histology of transgenic mouse embryos for high-throughput phenotyping. *PLoS Genetics* [online]. **2**(4), 471–477. ISSN 15537390. Dostupné z: doi:10.1371/journal.pgen.0020061

KAPADIA, Rasesh D, George B STROUP, Alison M BADGER, Bruno KOLLER, Joshua M LEVIN, Robert W COATNEY, Robert A DODDS, Xiaguong LIANG, Michael W LARK a Maxine GOWEN, 1998. Applications of micro-CT and MR microscopy to study pre-clinical models of osteoporosis and osteoarthritis. **6**, 361–372.

KIM, J., S. PARK, M. HEGAZY a S. LEE, 2013. Comparison of a photon-counting-detector and a CMOS flat-panel-detector for a micro-CT. *IEEE Nuclear Science Symposium Conference Record* [online]. ISSN 10957863. Dostupné z: doi:10.1109/NSSMIC.2013.6829119

KOVACEVIC, N, J T HENDERSON, E CHAN, N LIFSHITZ, J BISHOP, A C EVANS, R M HENKELMAN a X J CHEN, 2005. A three-dimensional MRI atlas of the mouse brain with estimates of the average and variability. *Cerebral cortex (New York, N.Y. : 1991)* [online]. **15**(5), 639–645. ISSN 1047-3211 (Print). Dostupné z: doi:10.1093/cercor/bhh165

KURDZIEL, Michael D, Michael D NEWTON, Samantha HARTNER, Kevin C BAKER a Jerome Michael WIATER, 2018. Quantitative evaluation of retrieved reverse total shoulder arthroplasty liner surface deviation and volumetric wear. *Journal of orthopaedic research : official publication of the Orthopaedic Research Society* [online]. **36**(7), 2007–2014. ISSN 1554-527X (Electronic). Dostupné z: doi:10.1002/jor.23849

KWON, H M, G SANGIORGI, E L RITMAN, A LERMAN, C MCKENNA, R VIRMANI, W D EDWARDS, D R HOLMES a R S SCHWARTZ, 1998a. Adventitial vasa vasorum in balloon-injured coronary arteries: visualization and quantitation by a microscopic three-dimensional computed tomography technique. *Journal of the American College of Cardiology* [online]. **32**(7), 2072–2079. ISSN 0735-1097 (Print). Dostupné z: doi:10.1016/s0735-1097(98)00482-3

KWON, H M, G SANGIORGI, E L RITMAN, C MCKENNA, D R Jr HOLMES, R S SCHWARTZ a A LERMAN, 1998b. Enhanced coronary vasa vasorum neovascularization in experimental hypercholesterolemia. *The Journal of clinical investigation* [online]. **101**(8), 1551–1556. ISSN 0021-9738 (Print). Dostupné z: doi:10.1172/JCI1568

LAM, Wilfred W, David W HOLDSWORTH, Louise Y DU, Maria DRANGOVA, David G MCCORMACK a Giles E SANTYR, 2007. Micro-CT imaging of rat lung ventilation using continuous image acquisition during xenon gas contrast enhancement. *Journal of applied physiology (Bethesda, Md. : 1985)* [online]. **103**(5), 1848–1856. ISSN 8750-7587 (Print). Dostupné z: doi:10.1152/japplphysiol.00009.2007

LIN, Ming De, Lutao NING, Cristian T BADEA, Nilesh N MISTRY, Student MEMBER, Yi QI, G Allan JOHNSON a Associate MEMBER, 2008. A High-Precision Contrast Injector for Small Animal X-Ray Digital Subtraction Angiography. **55**(3), 1082–1091.

MAIRE, E a P J WITHERS, 2014. Quantitative X-ray tomography. *International Materials Reviews* [online]. B.m.: Taylor & Francis, **59**(1), 1–43. ISSN 0950-6608. Dostupné z: doi:10.1179/1743280413Y.0000000023

METSCHER, Brian D., 2009a. Micro CT for comparative morphology: Simple staining methods allow high-contrast 3D imaging of diverse non-mineralized animal tissues. *BMC Physiology* [online]. **9**(1). ISSN 14726793. Dostupné z: doi:10.1186/1472-6793-9-11

METSCHER, Brian D., 2009b. MicroCT for developmental biology: A versatile tool for high-contrast 3D imaging at histological resolutions. *Developmental Dynamics* [online]. **238**(3), 632–640. ISSN 10588388. Dostupné z: doi:10.1002/dvdy.21857

MISSBACH-GUENTNER, Jeannine, Diana PINKERT-LEETSCH, Christian DULLIN, Roser UFARTES, Daniel HORNUNG, Bjoern TAMPE, Michael ZEISBERG a Frauke ALVES, 2018. 3D virtual histology of murine kidneys -high resolution visualization of pathological alterations by micro computed tomography. *Scientific reports* [online]. **8**(1), 1407. ISSN 2045-2322 (Electronic). Dostupné z: doi:10.1038/s41598-018-19773-5

MIZUTANI, Ryuta, D PH, Akihisa TAKEUCHI, D PH, Kentaro UESUGI, M SC, Susumu TAKEKOSHI a D PH, 2008. X-Ray Microtomographic Imaging. **14**(4).

MIZUTANI, Ryuta a Yoshio SUZUKI, 2012. X-ray microtomography in biology. *Micron* [online]. B.m.: Elsevier Ltd, **43**(2–3), 104–115. ISSN 09684328. Dostupné z: doi:10.1016/j.micron.2011.10.002

NAHRENDORF, Matthias, Cristian BADEA, Laurence W HEDLUND, Jose-Luiz

FIGUEIREDO, David E SOSNOVIK, G Allan JOHNSON a Ralph WEISSLEDER, 2007. High-resolution imaging of murine myocardial infarction with delayed-enhancement cine micro-CT. *American journal of physiology. Heart and circulatory physiology* [online]. 2007/02/23. **292**(6), H3172–H3178. ISSN 0363-6135. Dostupné z: doi:10.1152/ajpheart.01307.2006

NAKASHIMA, Daisuke, Ken ISHII, Morio MATSUMOTO, Masaya NAKAMURA a Takeo NAGURA, 2018. A study on the use of the Osstell apparatus to evaluate pedicle screw stability: An in-vitro study using micro-CT. *PLOS ONE* [online]. B.m.: Public Library of Science, **13**(6), e0199362. Dostupné z: https://doi.org/10.1371/journal.pone.0199362

NAVRÁTIL, Leoš a Jozef ROSINA, 2019. *Medicínská biofyzika: 2., zcela přepracované a doplněné vydání*. 2. Praha: Grada Publishing a.s. ISBN 978-80-271-0209-9.

O'NEILL, Kevin R, Christopher M STUTZ, Nicholas A MIGNEMI, Michael C BURNS, Matthew R MURRY, Jeffry S NYMAN a Jonathan G SCHOENECKER, 2012. Micro-computed tomography assessment of the progression of fracture healing in mice. *Bone* [online]. **50**(6), 1357–1367. ISSN 8756-3282. Dostupné z: doi:https://doi.org/10.1016/j.bone.2012.03.008

OSES, Pierre, Marie-Ange RENAULT, Remi CHAUVEL, Lionel LEROUX, Cecile ALLIERES, Benjamin SEGUY, Jean-Marie Daniel LAMAZIERE, Pascale DUFOURCQ, Thierry COUFFINHAL a Cecile DUPLAA, 2009. Mapping 3-dimensional neovessel organization steps using micro-computed tomography in a murine model of hindlimb ischemia-brief report. *Arteriosclerosis, thrombosis, and vascular biology* [online]. **29**(12), 2090–2092. ISSN 1524-4636 (Electronic). Dostupné z: doi:10.1161/ATVBAHA.109.192732

PARAMESWARAN, Harikrishnan, Erzsebet BARTOLAK-SUKI, Hiroshi HAMAKAWA, Arnab MAJUMDAR, Philip G ALLEN a Bela SUKI, 2009. Three-dimensional measurement of alveolar airspace volumes in normal and emphysematous lungs using micro-CT. *Journal of applied physiology (Bethesda, Md.: 1985)* [online]. **107**(2), 583–592. ISSN 8750-7587 (Print). Dostupné z: doi:10.1152/japplphysiol.91227.2008

PAUWELS, E., D. VAN LOO, P. CORNILLIE, L. BRABANT a L. VAN HOOREBEKE, 2013. An exploratory study of contrast agents for soft tissue visualization by means of high resolution X-ray computed tomography imaging. *Journal of Microscopy* [online]. **250**(1), 21–31. ISSN 00222720. Dostupné z: doi:10.1111/jmi.12013

PERRIEN, Daniel S, Mohamed A SALEH, Keiko TAKAHASHI, Meena S MADHUR, David G HARRISON, Raymond C HARRIS a Takamune TAKAHASHI, 2016. Novel methods for microCT-based analyses of vasculature in the renal cortex reveal a loss of perfusable arterioles and glomeruli in eNOS-/- mice. *BMC nephrology* [online]. B.m.: BioMed Central, **17**, 24. ISSN 1471-2369. Dostupné z: doi:10.1186/s12882-016-0235-5

RANI, Laís, Sales OLIVEIRA, Stella SUELI, Lourenço BRAGA, Aline ARÊDES, Maria TEREZA, Hordones RIBEIRO, Richard BENGT a Carlos JOSÉ, 2018. Molar

cusp deformation evaluated by micro-CT and enamel crack formation to compare incremental and bulk- fi lling techniques. *Journal of Dentistry* [online]. B.m.: Elsevier, (April), 0–1. ISSN 0300-5712. Dostupné z: doi:10.1016/j.jdent.2018.04.015

REN, Liqiang, Bin ZHENG a Hong LIU, 2018. Tutorial on X-ray photon counting detector characterization. *Journal of X-ray science and technology* [online]. **26**(1), 1–28. ISSN 1095-9114 (Electronic). Dostupné z: doi:10.3233/XST-16210

RITMAN, Erik L., 2004. Micro-Computed Tomography—Current Status and Developments. *Annual Review of Biomedical Engineering* [online]. **6**(1), 185–208. ISSN 1523-9829. Dostupné z: doi:10.1146/annurev.bioeng.6.040803.140130

RUTTY, G N, A BROUGH, M J P BIGGS, C ROBINSON, S D A LAWES a S V HAINSWORTH, 2013. The role of micro-computed tomography in forensic investigations. *Forensic Science International* [online]. **225**(1), 60–66. ISSN 0379-0738. Dostupné z: doi:https://doi.org/10.1016/j.forsciint.2012.10.030

SAITO, S a K MURASE, 2012. Ex vivo imaging of mouse brain using micro-CT with non-ionic iodinated contrast agent: a comparison with myelin staining. *The British journal of radiology* [online]. **85**(1019), e973-8. ISSN 1748-880X (Electronic). Dostupné z: doi:10.1259/bjr/13040401

SALVO, L, P CLOETENS, E MAIRE, S ZABLER, J J BLANDIN, J Y BUFFIÈRE, W LUDWIG, E BOLLER, D BELLET a C JOSSEROND, 2003. X-ray micro-tomography an attractive characterisation technique in materials science. *Nuclear Instruments and Methods in Physics Research Section B: Beam Interactions with Materials and Atoms* [online]. **200**, 273–286. ISSN 0168-583X. Dostupné z: doi:https://doi.org/10.1016/S0168-583X(02)01689-0

SARRAJ, Wafa M, Rong TANG, Anas L NAJJAR, Molly GRIFFIN, Anthony H BUI, Alan ZAMBELI-LJEPOVIC, Mike SENTER-ZAPATA, Maya LEWIN-BERLIN, Leopoldo FERNANDEZ, Juliette BUCKLEY, Amy LY, Elena BRACHTEL, Owen AFTRETH, John GILBERTSON, Yukako YAGI, Michele GADD, Kevin S HUGHES, Barbara L SMITH a James S MICHAELSON, 2015. Prediction of primary breast cancer size and T-stage using micro-computed tomography in lumpectomy specimens. *Journal of pathology informatics* [online]. **6**, 60. ISSN 2229-5089 (Print). Dostupné z: doi:10.4103/2153-3539.170647

SCHAMBACH, Sebastian J., Simona BAG, Lothar SCHILLING, Christoph GRODEN a Marc A. BROCKMANN, 2010. Application of micro-CT in small animal imaging. *Methods* [online]. B.m.: Elsevier Inc., **50**(1), 2–13. ISSN 10462023. Dostupné z: doi:10.1016/j.ymeth.2009.08.007

SÉGUIN, Fredrick H, 1990. High-Resolution Computed Tomography and Digital Radiography of Archaeological and Art-Historical Objects. *MRS Proceedings* [online]. 2011/02/28. B.m.: Cambridge University Press, **185**, 65. ISSN 0272-9172. Dostupné z: doi:DOI: 10.1557/PROC-185-65

SHIRAI, Ryota, Takuya KUNII, Akio YONEYAMA, Takahito OOIZUMI, Hiroko MARUYAMA, Thet Thet LWIN, Kazuyuki HYODO a Tohoru TAKEDA, 2014. Enhanced renal image contrast by ethanol fixation in phase-contrast X-ray computed tomography. *Journal of Synchrotron Radiation* [online]. B.m.: International Union of Crystallography, **21**(4), 795–800. ISSN 16005775. Dostupné

z: doi:10.1107/S1600577514010558

SHOFER, Scott, Cristian BADEA, Scott AUERBACH, David A SCHWARTZ a G Allan JOHNSON, 2007. A micro-computed tomography-based method for the measurement of pulmonary compliance in healthy and bleomycin-exposed mice. *Experimental lung research* [online]. **33**(3–4), 169–183. ISSN 0190-2148 (Print). Dostupné z: doi:10.1080/01902140701364458

SWAIN, Michael a Jing XUE, 2009. State of the Art of Micro-CT Applications in Dental Research. *International journal of oral science* [online]. **1**, 177–188. Dostupné z: doi:10.4248/IJOS09031

TAKEDA, T, A MOMOSE, Y ITAI, J WU a K HIRANO, 1995. Phase-contrast imaging with synchrotron X-rays for detecting cancer lesions. *Academic radiology* [online]. **2**(9), 799–803. ISSN 1076-6332 (Print). Dostupné z: doi:10.1016/s1076-6332(05)80490-8

TAKEDA, T, A MOMOSE, Q YU, J WU, K HIRANO a Y ITAI, 2000. Phase-contrast X-ray imaging with a large monolithic X-ray interferometer. *Journal of synchrotron radiation* [online]. **7**(Pt 4), 280–282. ISSN 0909-0495 (Print). Dostupné z: doi:10.1107/S0909049500004295

TAKEDA, Tohoru, THET-THET-LWIN, Takuya KUNII, Ryota SIRAI, Takahito OHIZUMI, Hiroko MARUYAMA, Kazuyuki HYODO, Akio YONEYAMA a Kazuhiro UEDA, 2013. Ethanol fixed brain imaging by phase-contrast X-ray technique. *Journal of Physics: Conference Series* [online]. **425**(PART 2). ISSN 17426596. Dostupné z: doi:10.1088/1742-6596/425/2/022004

TANG, Rong, Julliette M BUCKLEY, Leopoldo FERNANDEZ, Suzanne COOPEY, Owen AFTRETH, James MICHAELSON, Mansi SAKSENA, Lan LEI, Michelle SPECHT, Michele GADD, Yukako YAGI, Elizabeth RAFFERTY, Elena BRACHTEL a Barbara L SMITH, 2013. Micro-computed tomography (Micro-CT): a novel approach for intraoperative breast cancer specimen imaging. *Breast cancer research and treatment* [online]. **139**(2), 311–316. ISSN 1573-7217 (Electronic). Dostupné z: doi:10.1007/s10549-013-2554-6

TANG, Rong, Mansi SAKSENA, Suzanne B COOPEY, Leopoldo FERNANDEZ, Julliette M BUCKLEY, Lan LEI, Owen AFTRETH, Frederick KOERNER, James MICHAELSON, Elizabeth RAFFERTY, Elena BRACHTEL a Barbara L SMITH, 2016. Intraoperative micro-computed tomography (micro-CT): a novel method for determination of primary tumour dimensions in breast cancer specimens. *The British journal of radiology* [online]. **89**(1058), 20150581. ISSN 1748-880X (Electronic). Dostupné z: doi:10.1259/bjr.20150581

VANDE VELDE, Greetje, Jennifer POELMANS, Ellen DE LANGHE, Amy HILLEN, Jeroen VANOIRBEEK, Uwe HIMMELREICH a Rik J LORIES, 2016. Longitudinal micro-CT provides biomarkers of lung disease that can be used to assess the effect of therapy in preclinical mouse models, and reveal compensatory changes in lung volume. *Disease models & mechanisms* [online]. **9**(1), 91–98. ISSN 1754-8411 (Electronic). Dostupné z: doi:10.1242/dmm.020321

VASCONCELOS, Karla De Faria, Bernardo MATTOS, Luis Eduardo PADOVAN a Paulo Henrique Luiz DE, 2016. with autogenous and xenogenous grafts : A pilot

study ıvia dos Santos Corpas MicroCT assessment of bone microarchitecture in implant sites reconstructed with autogenous and xenogenous grafts : a pilot study [online]. (March). Dostupné z: doi:10.1111/clr.12799

WILLEKENS, Inneke, Tony LAHOUTTE, Phil SALMON, Nico BULS, Vicky CAVELIERS, Rudi DEKLERCK, Axel BOSSUYT a Johan DE MEY, 2009. Aurovist contrast enhancement in healthy mice.

WILLEMINK, Martin, Mats PERSSON, Amir POURMORTEZA, Norbert PELC a Dominik FLEISCHMANN, 2018. Photon-counting CT: Technical Principles and Clinical Prospects. *Radiology* [online]. **289**, 172656. Dostupné z: doi:10.1148/radiol.2018172656

WONG, Michael D., Shoshana SPRING a R. Mark HENKELMAN, 2013. Structural stabilization of tissue for embryo phenotyping using micro-CT with iodine staining. *PLoS ONE* [online]. **8**(12), 1–7. ISSN 19326203. Dostupné z: doi:10.1371/journal.pone.0084321

ZAGORCHEV, Lyubomir, Pierre OSES, Zhen W. ZHUANG, Karen MOODIE, Mary Jo MULLIGAN-KEHOE, Michael SIMONS a Thierry COUFFINHAL, 2010. Micro computed tomography for vascular exploration. *Journal of Angiogenesis Research* [online]. **2**(1), 1–11. ISSN 20402384. Dostupné z: doi:10.1186/2040-2384-2-7

ZIKMUND, T, M NOVOTNÁ, M KAVKOVÁ, M TESAŘOVÁ, M KAUCKÁ, B SZAROWSKÁ, I ADAMEYKO, E HRUBÁ, M BUCHTOVÁ, E DRAŽANOVÁ, Z STARČUK a J KAISER, 2018. High-contrast differentiation resolution 3D imaging of rodent brain by X-ray computed microtomography. *Journal of Instrumentation* [online]. B.m.: IOP Publishing, **13**(02), C02039–C02039. ISSN 1748-0221. Dostupné z: doi:10.1088/1748-0221/13/02/c02039

Seznam obrázků

Seznam příloh

Příloha 1: DUDÁK, Jan; ŽEMLIČKA, Jan; KREJČÍ, František; POLANSKÝ, Štěpán; JAKUBEK, Jan; MRZÍLKOVÁ, Jana; **PATZELT, Matěj;** TRNKA, Jan. X-ray micro-CT scanner for small animal imaging based on Timepix detector technology.

Příloha 2: DUDÁK, Jan; ŽEMLIČKA, Jan; KREJČÍ, František; KARCH, Jakub; **PATZELT, Matěj;** ZACH, PETR; SÝKORA, VIKTOR, MRZÍLKOVÁ, Jana. Evaluation of sample holders designed for long-lasting X-ray micro-tomographic scans of ex-vivo soft tissue samples.

Příloha 3: DUDÁK, Jan; ŽEMLIČKA, Jan; KARCH, Jakub; **PATZELT, Matěj;** MRZÍLKOVÁ, Jana; ZACH, Petr; HERMANOVÁ, Zuzana; KVACEK, Jiří; KREJČÍ, František. High-contrast X-ray microradiography and micro-CT of ex-vivo soft tissue murine organs utilizing ethanol fixation and large area photon-counting detector.

Příloha 4: PATZELT, Matěj; MRZÍLKOVÁ, Jana; DUDÁK, Jan; KREJČÍ, František; ŽEMLIČKA, Jan; KARCH, Jakub; MUSIL, Vladimír; ROSINA, Jozef; SÝKORA, Viktor; HOREHLEĎOVÁ, Barbora; ZACH, Petr. Ethanol fixation method for heart and lung imaging in micro-CT.

Příloha 5: MRZÍLKOVÁ, Jana; **PATZELT, Matěj**; GALLINA, Pasquale; WURST, Zdeněk; ŠEREMETA, Martin; DUDÁK, Jan; KREJČÍ, František; ŽEMLIČKA, Jan; MUSIL, Vladimír; KARCH, Jakub; ROSINA, Jozef; ZACH, Petr. Imaging of Mouse Brain Fixated in Ethanol in Micro-CT.

Přehled publikací autora s impakt faktorem

Publikace in extenso ve vztahu k dizertační práci

DUDÁK, Jan; ŽEMLIČKA, Jan; KREJČÍ, František; POLANSKÝ, Štěpán; JAKUBEK, Jan; MRZÍLKOVÁ, Jana; **PATZELT, Matěj;** TRNKA, Jan. X-ray micro-CT scanner for small animal imaging based on Timepix detector technology. *Nuclear Instruments & Methods in Physics Research Section A - Accelerators Spectrometers Detectors and Associated Equipment*. 2015, **774**(11), 81-86. ISSN 0168-9002. DOI: 10.1016/j.nima.2014.10.076. **IF: 1.316/2013**.

DUDÁK, Jan; ŽEMLIČKA, Jan; KREJČÍ, František; KARCH, Jakub; **PATZELT, Matěj;** ZACH, PETR; SÝKORA, VIKTOR, MRZÍLKOVÁ, Jana. Evaluation of sample holders designed for long-lasting X-ray micro-tomographic scans of ex-vivo soft tissue samples. *Journal of Instrumentation* 2016, **11**(03), C03005-C03005. ISSN 1748-0221. DOI: 10.1088/1748-0221/11/03/C03005. **IF: 1.399/2015**.

DUDÁK, Jan; ŽEMLIČKA, Jan; KARCH, Jakub; **PATZELT, Matěj;** MRZÍLKOVÁ, Jana; ZACH, Petr; HERMANOVÁ, Zuzana; KVACEK, Jiří; KREJČÍ, František. High-contrast X-ray microradiography and micro-CT of ex-vivo soft tissue murine organs utilizing ethanol fixation and large area photon-counting detector. *Scientific Reports.* 2016, **6**, e30385;1-9. ISSN 2045-2322. DOI: 10.1038/srep30385 **IF: 5.228/2015**.

PATZELT, Matěj; MRZÍLKOVÁ, Jana; DUDÁK, Jan; KREJČÍ, František; ŽEMLIČKA, Jan; KARCH, Jakub; MUSIL, Vladimír; ROSINA, Jozef; SÝKORA, Viktor; HOREHLEĎOVÁ, Barbora; ZACH, Petr. Ethanol fixation method for heart and lung imaging in micro-CT. *Japanese Journal of Radiology*. 2019, **37**(6), 500-510. ISSN 1867-1071. DOI: 10.1007/s11604-019-00830-6. **IF: 1.5/2018.**

MRZÍLKOVÁ, Jana; **PATZELT, Matěj**; GALLINA, Pasquale; WURST, Zdeněk; ŠEREMETA, Martin; DUDÁK, Jan; KREJČÍ, František; ŽEMLIČKA, Jan; MUSIL, Vladimír; KARCH, Jakub; ROSINA, Jozef; ZACH, Petr. Imaging of Mouse Brain Fixated in Ethanol in Micro-CT. *BioMed Research International*. 2019, **2019**, 1-7. ISSN 2314-6133. DOI: 10.1155/2019/2054262. **IF: 2.197/2018.**

Publikace bez vztahu k dizertační práci

MRZÍLKOVÁ, Jana; KOUTELA, Antonella; KUTOVÁ, Martina; **PATZELT, Matěj**; IBRAHIM, Ibrahim; AL-KAYSSI, Dina; BARTOŠ, Aleš; ŘÍPOVÁ, Daniela; ČERMÁKOVÁ, Pavla a ZACH, Petr. Hippocampal spatial position evaluation on MRI for research and clinical practice. *PLoS One*. 2014, **9**(12), e115174; 1-15. ISSN 1932-6203. DOI: 10.1371/journal.pone.0115174. **IF: 3.534/2013**.

PATZELT, Matěj; ZÁRUBOVÁ, Lucie; KLENER, Pavel; BÁRTA Josef; BENKOVÁ Kamila; BRANDEJSOVÁ, Adrianna; TRNĚNÝ, Marek; GÜRLICH, Robert; SUKOP, Andrej. Anaplastic Large-Cell Lymphoma Associated with Breast Implants: A Case Report of a Transgender Female. *Aesthetic Plastic Surgery.* 2018, **42**(2), 451-455. ISSN: 0364-216X. DOI: 10.1007/s00266-017-1012-y **IF: 1.484/2017**.

STINGL, Josef; MUSIL, Vladimír; PIRK, Jan; STRAKA, Zdeněk; ŠETINA, Marek; ŠACH, Josef; KACHLÍK, David; **PATZELT, Matěj**. Vasa vasorum of the failed aorto-coronary venous grafts. *Surgical and Radiologic Anatomy*. 2018, **40**(7): 769–778. ISSN 0930-1038. DOI: 10.1007/s00276-018-2036-y **IF: 1.003/2017.**

MUSIL, Vladimír; ŠACH, Josef; KACHLÍK, David; **PATZELT, Matěj;** STINGL, Josef. Vasa vasorum: an old term with new problems. *Surgical and Radiologic Anatomy*. 2018, **40**(10), 1159-1164. ISSN 0930-1038 DOI: 10.1007/s00276-018-2068-3. **IF: 1.003/2017.**

SUKOP, Andrej; **PATZELT, Matěj**; KOZÁK, Jiří; LEŠKO, Robert. A Case Report: Reconstruction of the anterior skull base with free muscle flap after iatrogenic injury. Cesk Slov Neurol N 2018; **81**(6), 707-708. ISSN: 1210-7859. DOI: 10.14735/amcsnn2018707 **IF: 0.508/2017.**

MUSIL, Vladimír; ŠACH, Josef; **PATZELT, Matěj**; KACHLÍK, David; STINGL, Josef. Valves of the small coronary veins in porcine hearts. *Journal of Morphology*. 2019, **280**(5), 681-686. ISSN 0362-2525. DOI: 10.1002/jmor.20974. IF: **1.711/2018.**

PATZELT, Matěj; KACHLÍK, David; STINGL, Josef; ŠACH, Josef; STIBOR, Radek; BENADA, Oldrich; KOFRONOVA, Olga; MUSIL, Vladimír. Morphology of the vasa vasorum in coronary arterie sof the porcine heart: a new insight. *Annals of Anatomy - Anatomischer Anzeiger*. 2019, **223**, 119-126. ISSN 09409602. DOI: 10.1016/j.aanat.2019.02.006. **IF: 1.852/2018.**

Přehled publikací autora bez impakt faktoru

Publikace bez vztahu k dizertační práci

STINGL, Josef; RATAJOVÁ, Jana; SUCHOMEL, Zdeněk; MALINOVÁ, Petra; **PATZELT, Matěj**; MUSIL, Vladimír. Rok 1848 - významný mezník v historii české chirurgie. *Rozhledy v chirurgii*. 2019, **98**(11), 462-468. ISSN 0035-9351. DOI: 10.33699/PIS.2019.98.11.462–468